

UNIVERSITY OF BELGRADE  
FACULTY OF PHYSICS

Miloš M. Radonjić

INFLUENCE OF DISORDER ON  
CHARGE TRANSPORT IN STRONGLY  
CORRELATED MATERIALS NEAR THE  
METAL-INSULATOR TRANSITION

Doctoral Dissertation

Belgrade, 2014.

УНИВЕРЗИТЕТ У БЕОГРАДУ  
ФИЗИЧКИ ФАКУЛТЕТ

Милош М. Радоњић

**УТИЦАЈ НЕУРЕЂЕНОСТИ НА  
ЕЛЕКТРОНСКИ ТРАНСПОРТ У ЈАКО  
КОРЕЛИСАНИМ МАТЕРИЈАЛИМА  
БЛИЗУ МЕТАЛ-ИЗОЛАТОР ПРЕЛАЗА**

Докторска дисертација

Београд, 2014.

Thesis advisor, Committee member:

Dr. Darko Tanasković

Associate Research Professor

Institute of Physics Belgrade

University of Belgrade

Committee member:

Prof. Dr. Zoran Radović

Professor

Faculty of Physics

University of Belgrade

Committee member:

Prof. Dr. Đorđe Spasojević

Associate Professor

Faculty of Physics

University of Belgrade

Committee member:

Dr. Antun Balaž

Associate Research Professor

Institute of Physics Belgrade

University of Belgrade

*To my family*

## Захвалница

*На пруженој љубави, разумевању и подршци, као и на свему што се не би могло ни побројати, захваљујем се својој породици, оцу Миливоју, мајци Љиљани, брату Милану и сестри Миљани.*

*Хвала ментору др Дарку Танасковићу на одличној сарадњи, вођењу и великодушној помоћи у току истраживачког рада и израде докторске тезе. Хвала др Владимиру Добросављевићу на изврсној сарадњи, подршци и гостопримству које ми је указао. На пријатном и конструктивном заједничком раду захваљујем се колеги Јакши Вучичевићу. Посебно се захваљујем др Зорану Поповићу и др Ненаду Лазаревићу на успешној и веома плодотворној сарадњи.*

*Др Александру Белићу хвала на указаном поверењу и прилици да будем део Лабораторије за примену рачунара у науци, као и свим колегама на пријатној и радној атмосфери.*

*Хвала и свим пријатељима који су непосредно или посредно допринели овом постигнућу.*

*Ова дисертација је урађена у Лабораторији за примену рачунара у науци Института за физику Универзитета у Београду и финансирана је у оквиру пројеката ОН141035, ОН171017 и ИИИ45018 Министарства науке, односно Министарства просвете, науке и технолошког развоја Републике Србије.*

# Influence of disorder on charge transport in strongly correlated materials near the metal-insulator transition

## Abstract

The influence of disorder on transport properties in strongly correlated materials has remained unclear, so far. Strong Coulomb repulsion between the electrons in partially filled valence orbitals can lead to the localization of the wave functions - Mott insulating state. How these processes are modified by the presence of disorder is a very important question, specially having in mind that many strongly correlated compounds are non-stoichiometric and, therefore, intrinsically disordered.

In this thesis we study the disordered half-filled Hubbard model within the dynamical mean field theory (DMFT) and its extensions, this is a unique theoretical method that is reliable and controllable in a wide temperature, disorder and interaction range. The DMFT assumes the local (momentum independent) self-energy, but takes fully into the account temporal quantum fluctuations. In the clean case, this theory is exact in the limit of large coordination number. Technically, the DMFT solution reduces to the solution of the Anderson impurity model immersed in the self-consistently calculated conduction bath.

For the case of weak disorder we used the coherent potential approximation for solving the disordered half-filled Hubbard model, where the disorder is taken into account by the simple averaging of the local Green's functions. The ensemble of the impurity models is solved with the site-independent (averaged) conduction bath. For the constant interaction, the disorder effectively induces local doping, broadens the bands and moving the system away from the Mott transition. The resistivity curves have the same non-monotonic temperature dependence near the Mott transition as in the clean case. The maximal metallic resistivity exceeds the quasi-classical Mott-Ioffe-Regel limit by an order of magnitude. Interestingly, the Drude-like peak in the optical conductivity persists even for temperatures when the resistivity is comparable to the Mott-Ioffe-Regel limit.

We have determined a universal scaling for the resistivity of various correlated metals, which is based on the existence of the coherence temperature  $T^*$  inversely proportional to the effective mass. This scaling is shown to be valid also on the

metallic side of the metal-insulator transition of diluted two-dimensional electron gases, Si MOSFETs and GaAs/AlGaAs heterostructures. This gives strong evidence that the driving force for the unusual transport properties in these systems is strong electron-electron scattering, and not disorder.

To explore strongly disordered systems, we have implemented the Statistical DMFT, which takes into account spatial fluctuations in the conduction bath. We have successfully applied, for the first time, the Statistical DMFT method on the finite size cubic lattice. We determined that the finite size effects are negligible already on the lattice with  $6 \times 6 \times 6$  sites (except at the lowest temperatures, deep in the Fermi liquid regime). Then we concentrated on a single realization of disorder on the lattice of size  $6 \times 6 \times 6$  using the Continues Time Quantum Monte Carlo (CTQMC) as the impurity solver, and the analytical continuation by the maximum entropy method in order to obtain local quantities on the real frequency axis. We confirmed that the disorder is strongly screened on the metallic side of the Mott MIT and that the inelastic scattering is dominant at finite temperatures. We defined a local resistivity and proposed a resistor network method for calculating the dc resistivity. This approach is justified by the observation that the inter-site correlations are very weak and the incoherent scattering dominant. We identified two types of sites: strongly correlated - with the local occupation close to 1, and weakly correlated - away from local half-filling. Non-monotonic temperature dependence in the resistivity originates from strong temperature dependent local resistivity on strongly correlated sites.

**Keywords:** strong correlations, disorder, Mott metal-insulator transition, dynamical mean field theory

**Scientific field:** Physics

**Research area:** Condensed matter physics

**UDC number:** 538.9(043.3)

# Утицај неуређености на електронски транспорт у јако корелисаним материјалима близу метал-изолатор прелаза

## Сажетак

Утицај неуређености на транспортне особине јако корелисаних материјала је до сада остао неразјашњен. Јако Кулоново одбијање међу електронима на делимично попуњеним валентним орбиталама може довести до локализације таласне функције - Мотовог изолаторског стања. Како се Мотов метал-изолатор прелаз мења у присуству неуређености је веома важно питање, посебно имајући у виду да су многи јако корелисани материјали нестехиометријска једињења па је неуређеност, односно одступање од идеалне периодичности, неизбежно.

У овој тези је проучаван неуређени полупопуњени Хабардов модел у оквиру динамичке теорије средњег поља (ДМФТ) и њених уопштења. ДМФТ је јединствен теоријски метод који је поуздан и контролисан у широком интервалу температура, интеракција и јачине неуређености. ДМФТ третира само локалне интеракционе корелације, али у потпуности узима у обзир временске (квантне) флукуације кроз фреквентну зависност сопствене енергије  $\Sigma(\omega)$ . У чистом случају теорија је тачна у лимесу великог координационог броја. ДМФТ једначине се свде на решавање модела Андерсонове нечистоће урођеног у само-усаглашено израчунато поље проводних електрона.

У случају слабе неуређености користили смо апроксимацију кохерентног потенцијала при решавању једначина за неуређен полупопуњен Хабардов модел. У овом приступу неуређеност се урачунава једноставним усредњавањем локалне Гринове функције. Хибридизациона функција (динамичко средње поље проводних електрона) је при томе иста за сваки чвор решетке. При константној интеракцији, неуређеност ефективно шири проводну зону и систем удаљава од Мотовог прелаза. Криве отпорности имају сличну немонотону температурну зависност у близини Мотовог прелаза као и у чистом случају. Вредност за максималну металну отпорност прелази квази-класичну Мот-Јофе-Регел границу за ред величине. Друдеов пик у оптичкој проводности опстаје чак и када је отпорност упоредива са Мот-Јофе-Регел границом.

Утврдили смо универзално скалирање кривих отпорности у функцији тем-

пературе, за различите јако корелисане материјале, услед постојања температуре кохеренције  $T^*$  обрнуто пропорционалне ефективној маси у близини Мотовог прелаза. Ово скалирање важи и на металној страни метал-изолатор прелаза у разређеном дводимензионом електронском гасу у силицијум МОСФЕТ-има и GaAs хетероструктурама. Ово снажно указује да је транспорт у широком интервалу температура одређен јаким електрон-електрон расејањем, а не последицом неуређености.

За проучавање јако неуређеног система, применили смо статистичку ДМФТ, која узима у обзир просторне флукуације у хибридизационој функцији. По први пут смо применили овај метод на ненулној температури и на коначној кубној решетки. Утврдили смо да су ефекти коначности решетке занемарљиви већ на решетки  $6 \times 6 \times 6$  (осим на најнижим температурама, дубоко у режиму Фермијеве течности). Затим смо се концентрисали на једну реализацију неуређености на решетки димензија  $6 \times 6 \times 6$  користећи квантни Монте Карло метод за решавање Андерсоновог модела и аналитичко продужење методом максималне ентропије у циљу добијања локалних величина на реалној фреквентној оси. Утврдили смо да је неуређеност снажно екранирана на металној страни Мотовог метал-изолатор прелаза и да је механизам нееластичног (електрон-електрон) расејања доминантан на коначним температурама. Дефинисали смо локалну отпорност и увели метод мреже отпорника за израчунавање отпора. Овај приступ је оправдан обзиром да су корелације електрона на суседним чворовима решетке веома слабе у режиму јаког нееластичног расејања. Уочили смо две врсте електрона: јако корелисане са локалном попуњеношћу близу вредности 1, и слабо корелисане са попуњеношћу која знатно одступа од вредности 1. Немонотона температурна зависност у отпорности потиче од температурне зависности расејања електрона на јако корелисаним чворовима решетке.

**Кључне речи:** јаке корелације, неуређеност, Мотов метал-изолатор прелаз, динамичка теорија средњег поља

**Научна област:** Физика

**Област истраживања:** Физика кондензованог стања материје

**УДК број:** 538.9(043.3)

# Contents

<b>Contents</b>	<b>viii</b>
<b>1 Introduction</b>	<b>1</b>
<b>2 Dynamical mean field theory for strongly interacting electrons</b>	<b>4</b>
2.1 Hubbard model . . . . .	5
2.2 Dynamical mean field theory . . . . .	7
2.2.1 General Formalism . . . . .	7
2.2.2 Mapping on the Anderson impurity model . . . . .	12
2.2.3 Impurity solvers . . . . .	13
2.3 Mott metal-insulator transition . . . . .	15
2.4 Optical and dc conductivity . . . . .	17
2.5 Phase diagram of the frustrated Hubbard model . . . . .	19
<b>3 Dynamical mean field theory for disordered strongly correlated systems</b>	<b>20</b>
3.1 Disordered Hubbard model (DHM) . . . . .	24
3.2 Coherent potential approximation for the correlated electrons . . . . .	25
3.2.1 Optical and dc conductivity within CPA . . . . .	26
3.3 Typical medium theory . . . . .	28
3.4 Statistical dynamical mean field theory . . . . .	30
<b>4 Influence of disorder on incoherent transport near the Mott transition</b>	<b>33</b>
4.1 Density of states and optical conductivity . . . . .	35
4.2 Increase of metallicity by disorder . . . . .	39
4.3 Conclusions . . . . .	42

<b>5</b>	<b>Scattering mechanism in diluted 2D electron gases: interaction vs. disorder</b>	<b>43</b>
5.1	Metal-insulator transition in two dimensions . . . . .	45
5.2	Scaling analysis of the resistivity maxima . . . . .	47
5.2.1	Phenomenological scaling hypothesis . . . . .	48
5.2.2	Critical behavior of the Wigner-Mott scaling . . . . .	50
5.2.3	Breakdown of the diffusion mode scaling . . . . .	52
5.3	Scaling in 3D materials . . . . .	54
5.4	Scaling in the microscopic model of the interaction driven MIT . . . .	56
5.5	Scaling in the model with disorder . . . . .	60
5.6	Conclusion and discussion . . . . .	61
<b>6</b>	<b>Resistivity in strongly disordered systems near the Mott transition</b>	<b>63</b>
6.1	Coherent potential approximation in strong disorder limit . . . . .	64
6.2	DMFT on the finite cubic lattice . . . . .	65
6.2.1	Finite size effects in three dimensions . . . . .	65
6.3	Statistical DMFT: elastic vs. inelastic scattering . . . . .	69
6.4	Inter-site correlations . . . . .	70
6.4.1	Local resistivity . . . . .	70
6.4.2	Correlation function . . . . .	72
6.5	Resistivity of the lattice . . . . .	73
6.5.1	Weak disorder . . . . .	74
6.5.2	Strong disorder . . . . .	74
6.5.3	Strongly and weakly correlated sites . . . . .	76
6.6	Summary and open questions . . . . .	81
<b>7</b>	<b>Conclusion</b>	<b>82</b>
	<b>References</b>	<b>85</b>

# 1. Introduction

Solid state physics is very large and fast growing area of research, driven by constant appetite of industry for new materials with specific, desired properties. It is also a quest to discover and understand fundamentally new phases of matter which may appear due to the specific band structure and topology, or electron-electron and electron-phonon interactions. Strong electron-electron interactions may lead to various ordered phases at low temperatures and various types of phase transitions separating magnetic, superconducting, metallic, or insulating phases. This is the subject of the physics of strongly correlated electronic systems.

Strongly correlated materials include various transition metal oxides [1], high-temperature superconductors [2], iron-based superconductors [3, 4], organic charge-transfer salts [5, 6], rare earth and actinide intermetallics [7] and also many low dimensional-structures, like the quantum Hall systems [8]. According to the band structure theory, the insulating state appears if the valence band is completely filled with the electrons. There are, however, many insulating materials with partially filled (typically half-filled) valence band. These insulators are called Mott insulators. Mott systems can be tuned between the metallic and the insulating state by doping, or changing external parameters like the magnetic field or pressure. The Mott metal-insulator transition (MIT) can be tuned by changing the interaction at half-filling (interaction-driven Mott MIT), or by doping (doping-driven Mott MIT). In this thesis we mostly focus on the interaction-driven MIT.

It is a very challenging task to construct a successful theoretical approach do deal with strongly correlated systems. The difficulty comes from the necessity for non-perturbative treatment of the Mott metal-insulator transition. The electrons on the metallic side of the Mott transition are halfway “between“ itinerant and localized. There are very few tenable theories that tackle this problem. The most successful one is certainly the Dynamical mean field theory (DMFT) and its extensions.

One of the key features of the DMFT is that it represents a nonperturbative

and well-controlled theory which becomes exact in the limit of infinite coordination numbers (or infinite dimensionality). The DMFT is truly a quantum many-body method which fully takes into account local correlations. The local quantum fluctuations are completely taken into account, while spatial fluctuations are, in the simplest implementation, frozen. The DMFT method treats low energy coherent and high energy incoherent excitations on the equal footing, which is essential for a study of the phase diagram in the whole range of parameters.

The biggest initial success of the DMFT was a description of the interaction-driven Mott transition in the half-filled Hubbard model [9]. The DMFT phase diagram is shown in Figure 1, upper panel [10]. For small interaction  $U$  the system is weakly correlated metal. As  $U$  increases, it becomes a strongly renormalized

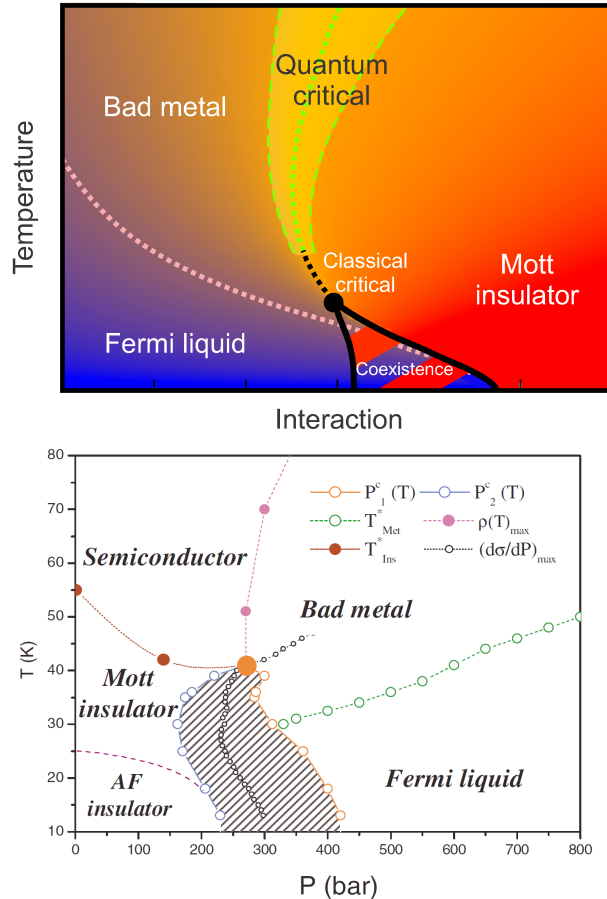


Figure 1.1: DMFT interaction-temperature phase diagram of Hubbard model obtained (upper panel) [10] and pressure-temperature phase diagram of organic material  $\kappa$ -(BEDT-TTF)<sub>2</sub>Cu[N(CN)<sub>2</sub>]Cl (lower panel) [5].

---

Fermi liquid. At higher temperatures the system behaves as "bad metal", where the transport is dominated by very strong electron-electron scattering. For large interaction  $U$  the Mott gap opens. Metallic and insulating solution are separated by the coexistence region where both solutions can be stabilized. This region ends with the  $(U_c, T_c)$  critical end-point. The same transport regimes are clearly seen in the experiments on correlated organic salts [5], lower panel in Figure 1.

All these materials, in "real life", contain some imperfections in structure or composition. The interplay between the interaction and disorder effects is particularly subtle in strongly correlated systems, where often is not clear whether the transport properties are dominated by the interaction or by the disorder [11, 12, 13, 14, 15, 16]. In this thesis we study the disordered Hubbard model within dynamical mean field theory. We particularly focus on the influence of disorder on the transport properties on the metallic side of the Mott transition.

The thesis is organized as follows. Chapters 2 and 3 contain an introduction to the dynamical mean field theory and its extension to the models with disorder. Chapter 4 presents a detailed study of the conductivity in weakly disordered Mott systems. Chapter 5 presents evidence that the transport in low density two-dimensional electron gases is dominated by the electron-electron scattering, while the disorder plays a sub-dominant role. Chapter 6 focuses on the study of temperature dependence of the conductivity in strongly disordered Mott systems. Chapter 7 contains the concluding remarks.

## 2. Dynamical mean field theory for strongly interacting electrons

The electron wave functions are well understood in two limits: localized and itinerant (forming extended Bloch waves due to the large overlap between the electron orbitals and leading to formation of the bands). The electrons in strongly correlated materials do not fit into any of these two cases: they cannot be treated just like the plane waves, or purely localized particles. The competition between strong Coulomb repulsion and kinetic energy may lead to the transition between localized and itinerant behavior, with subtle features in the spectral density near the MIT.

The simplest model for strongly correlated materials is the Hubbard model. Despite its simple form, it describes various phases of matter depending on the parameter values and lattice structure. It is rigorously solved only in the two cases: in one-dimension [17] and in the limit of infinite coordination number (or infinite dimension) using the dynamical mean field theory (DMFT) [18].

## 2.1 Hubbard model

Single orbital Hubbard model is the minimal lattice model for strongly correlated electronic systems, proposed by Hubbard in 1963. [19, 20]. The Hubbard model Hamiltonian consists of the hopping (kinetic energy) term and the on-site interaction term which originates from the Coulomb repulsion of two electrons (with spin up and spin down) on the same orbital,

$$H = - \sum_{ij,\sigma} t_{ij} c_{i\sigma}^\dagger c_{j\sigma} + U \sum_i n_{i\uparrow} n_{i\downarrow} - \mu \sum_{i\sigma} n_{i\sigma}. \quad (2.1)$$

Indexes  $i$  and  $j$  run through the lattice sites, and  $\sigma$  is the spin index. The operators  $c_{i\sigma}^\dagger$  and  $c_{i\sigma}$  create and annihilate the electron with the spin  $\sigma$  at the site  $i$  and  $n_{i\sigma} = c_{i\sigma}^\dagger c_{i\sigma}$  is the particle occupation number operator. The kinetic energy term is determined by the hopping parameters  $t_{ij}$ , where usually it is enough to consider just the nearest neighbor hopping. The strength of the Coulomb repulsion is given by the Hubbard parameter  $U$ . A model with the short-range interaction  $U$  is most realistic in the case of  $d$  or  $f$  electrons which have relatively small orbital radius, and its further justified by the effect of charge screening.

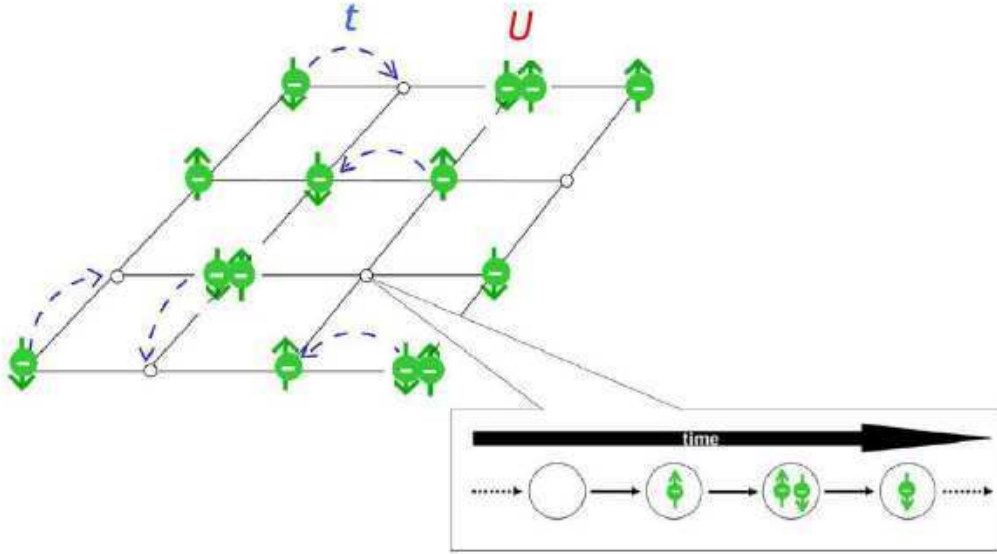


Figure 2.1: Schematic representation of the Hubbard model.

Despite its simplicity, this model exhibits a very rich phase diagram. Depending

on the parameters, the shape of the lattice and temperature, various phases of matter can be stabilized: metallic, Mott insulating, ferromagnetic or antiferromagnetic, and even  $d$ -wave superconducting phase. The most striking consequence of strong electronic correlations is the localization of the electronic wave functions due to the Coulomb repulsion - Mott insulating state which is the main focus of this thesis.

The Hubbard model is well explored in one dimension [17], where it is exactly solvable and where we have a variety of theoretical tools at disposal, necessary for systematic study. In two or three dimensions it is often impossible to distinguish whether the theoretical prediction reflects the true nature of the Hamiltonian, rather than an artifact of approximation used for its solution. The origin of these uncertainties is in the nonperturbative nature of the problem and in the existence of several competing phases for the ground state solution.

An important step forward in the study of the Hubbard model was a development of the dynamic mean field theory (DMFT) around twenty years ago [18]. This method treats only local correlations and thus the self-energy is only frequency-dependent,  $\Sigma(\mathbf{k}, \omega) \rightarrow \Sigma(\omega)$ . Therefore, the DMFT takes fully into account temporal (quantum) fluctuations, while spatial fluctuations are neglected. It becomes an exact theory in the limit of infinite coordination number or, equivalently, infinite dimensions. This approach allows treatment of the low energy (coherent) and the high energy (incoherent) excitations on the equal footing. This makes DMFT a unique method in a study of strongly correlated electronic systems.

The great success of the DMFT influenced development of several extensions suitable for a different types of problems. Cluster DMFT is developed in order to include non-local correlations and to reintroduce momentum-dependence into the self-energy [21, 22]. This has led to important advances in understanding the physics of the cuprates [23]. The multi orbital DMFT turns out to be particularly useful for the investigations of transition metal oxides, including the iron based superconductors [24]. For the investigation of the hetero-structures and layered materials the inhomogeneous DMFT is developed [25]. Further, the bosonic excitation of the bath can be taken into account using the extended DMFT (EDMFT). The DMFT method has been generalize also to the time-dependent [26] and bosonic Hubbard models. The extension to disordered systems has also lead to important physical insights [27, 15], and this line of work is the main focus of the following chapters in the thesis.

## 2.2 Dynamical mean field theory

Dynamical mean field theory method was first proposed in the pioneering work by Metzner and Vollhardt in 1989 [28], as the solution for the Hubbard model on infinite dimensional lattice ( $d \rightarrow \infty$ ). They showed that, with proper scaling of the hopping parameters, the Hubbard model remains meaningful and nontrivial in  $d \rightarrow \infty$ , and that the solution of the DMFT equations in this limit becomes exact. The DMFT approach has started to become widely recognized after the work of Georges, Kotliar and Rozenberg in 1992 [9] when they successfully described the Mott metal-insulator transition using the DMFT, which is a fully quantum mechanical treatment of the Mott transition.

In this chapter we will sketch a derivation of the DMFT equations and present the basic physical insights from their solution on the example of the single-band Hubbard model.

### 2.2.1 General Formalism

DMFT can be seen as an extension of Weiss mean field theory[18]. The main idea is to lower the number of degrees of freedom by approximating the full lattice problem by the on-site effective problem (Figure. 2.2). In this approach the single site is embedded in an effective medium originating from all other sites. Then the problem reduces to the famous Anderson impurity problem and the features of the lattice (dimensionality, hopping parameters) are included through the self-consistent calculation of the hybridization bath  $\Delta(\omega)$ . The impurity problem remains a quantum many-body problem, in contrast to the classical mean field theories. This approach freezes spatial fluctuations, but fully takes in account all local, temporal fluctuations (hence the name "dynamical"). By the construction, DMFT is exact in the limit of infinite lattice coordination number or, equivalently, in the case of infinite dimensions. It is important to have in mind that even for three dimensional cubic lattice with the coordination number  $z = 6$ , DMFT is a very good approximation (except at very low temperatures), and therefore a very useful method in a study of finite dimensional strongly correlated materials.

The partition function  $Z$  of the Hubbard model 2.1 can be represented as a

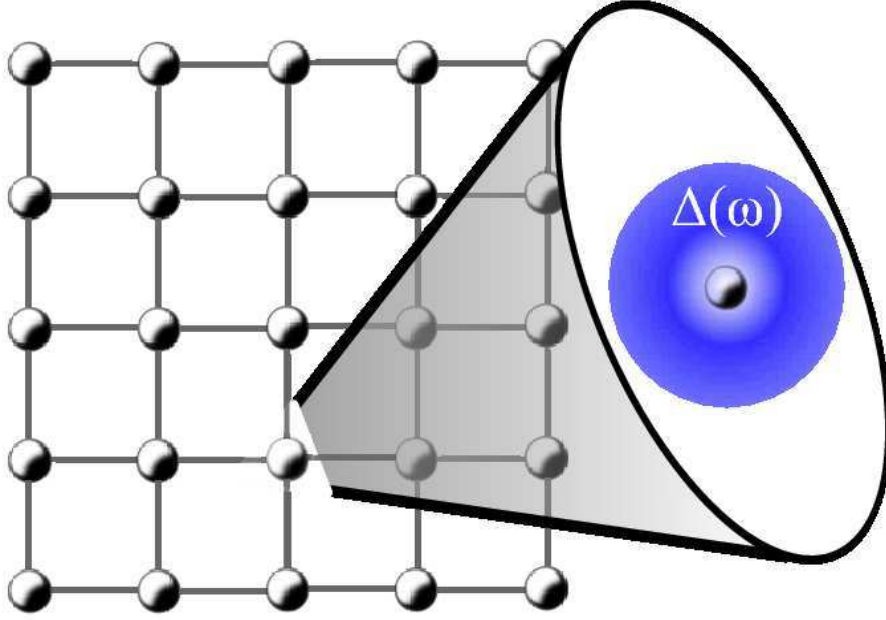


Figure 2.2: Lattice is replaced by a single site problem coupled to the external bath defined by all other sites.

functional integral over the Grassmann variables

$$Z = \int \prod_i Dc_{i\sigma}^\dagger Dc_{i\sigma} \exp(-S), \quad (2.2)$$

$$S = \int_0^\beta d\tau \left[ \sum_{i,\sigma} c_{i\sigma}^\dagger(\tau) \left( \frac{\partial}{\partial \tau} - \mu \right) c_{i\sigma}(\tau) - \sum_{ij,\sigma} t_{ij} c_{i\sigma}^\dagger(\tau) c_{j\sigma}(\tau) + \sum_i U n_{i\uparrow}(\tau) n_{i\downarrow}(\tau) \right], \quad (2.3)$$

where  $S$  is the action,  $c_{i\sigma}$  and  $c_{i\sigma}^\dagger$  are the Grassmann variables and  $\beta$  is inverse product of the temperature and the Boltzmann constant,  $\beta = 1/k_B T$ . In order to calculate partition function, we have to transform the action into more suitable

form. Following the spirit of DMFT, we separate the action into three parts,

$$S_0 = \int_0^\beta d\tau \left[ \sum_\sigma c_{0\sigma}^\dagger(\tau) \left( \frac{\partial}{\partial \tau} - \mu \right) c_{0\sigma}(\tau) + U n_{0\uparrow}(\tau) n_{0\downarrow}(\tau) \right], \quad (2.4)$$

$$S^{(0)} = \int_0^\beta d\tau \left[ \sum_{i \neq 0, \sigma} c_{i\sigma}^\dagger(\tau) \left( \frac{\partial}{\partial \tau} - \mu \right) c_{i\sigma}(\tau) - \sum_{i \neq 0, j \neq 0, \sigma} t_{ij} c_{i\sigma}^\dagger(\tau) c_{j\sigma}(\tau) \right. \\ \left. + \sum_{i \neq 0} U n_{i\uparrow}(\tau) n_{i\downarrow}(\tau) \right]. \quad (2.5)$$

$$S_c = - \int_0^\beta d\tau \left[ \sum_{i, \sigma} t_{i0} c_{i\sigma}^\dagger(\tau) c_{0\sigma}(\tau) + t_{0i} c_{0\sigma}^\dagger(\tau) c_{i\sigma}(\tau) \right]. \quad (2.6)$$

The first term,  $S_0$ , contains all local degrees of freedom of the chosen site, the second one,  $S^{(0)}$  (cavity term), includes all other degrees of freedom and third term,  $S_c$ , contains the coupling between the first two. After few steps of simple algebra and integrating out all degrees of freedom, except these on the one chosen site  $i = 0$  (impurity), we obtain the effective action

$$S_{\text{eff}} = S_0 + \sum_{n=1}^{\infty} \sum_{i_1, \dots, j_n, \sigma} \int t_{i_1 0} \dots t_{0 j_n} c_{0\sigma}^\dagger(\tau_{i_1}) \dots c_{0\sigma}^\dagger(\tau_{i_n}) c_{0\sigma}(\tau_{j_1}) \dots c_{0\sigma}(\tau_{j_n}) \\ \times G_{i_1 \dots j_n \sigma}^{(0)}(\tau_{i_1} \dots \tau_{i_n}, \tau_{j_1} \dots \tau_{j_n}) + \text{const.} \quad (2.7)$$

Here, the connected  $n$ -point Green's function of the bath degrees of freedom is introduced as

$$G_{i_1 \dots j_n \sigma}^{(0)}(\tau_{i_1} \dots \tau_{i_n}, \tau_{j_1} \dots \tau_{j_n}) = \langle T_\tau c_{i_1 \sigma}(\tau_{i_1}) \dots c_{i_n \sigma}(\tau_{i_n}) c_{j_1 \sigma}^\dagger(\tau_{j_1}) \dots c_{j_n \sigma}^\dagger(\tau_{j_n}) \rangle^{(0)}. \quad (2.8)$$

Averaging  $\langle \rangle^{(0)}$  is carried over the cavity action  $S^{(0)}$  and  $T_\tau$  is the imaginary time ordering operator. At this point, the derived effective action is very complicated and not very useful for applications, but how it evolves in the limit of infinite dimensions? In order to ensure a proper behavior of the kinetic and interaction energy terms, to remain of the same order of magnitude in  $d \rightarrow \infty$  limit, one can scale the hopping amplitude as  $t_{new} = t/\sqrt{2d}$ . The one particle Green's [29] function  $G_{ij}$ , which occurs in the Eq. 2.7, is proportional to  $t^{|i-j|} \sim 1/d^{|i-j|/2}$ . The two particle Green's function  $G_{ijkl}$  scales as  $1/(d^{|i-j|/2} d^{|i-k|/2} d^{|i-l|/2})$ . If we recall the effective action from Eq. 2.7, we can establish that the first term containing the one particle Green's function is of

the order of 1 (prefactor  $t^2$  times  $t^2$  from  $G_{ij}$  and summations over  $i$  and  $j$  provides a factor  $d^2$  which cancels the first two). To be more precise,  $G_{ij}$  is proportional to  $t^2$  when  $i$  and  $j$  are the nearest neighbors of the site 0. In all other cases Green's function is even smaller. Similar consideration shows that the next term in the summation in Eq. 2.7 is of the order of  $1/d$  and all others are even smaller in the limit of large dimensions.

Previous discussion allows us to keep just the first (one-particle) term of the effective action (2.7) in the large  $d$  limit

$$S_{\text{eff}} = - \int_0^\beta d\tau \int_0^\beta d\tau' \sum_\sigma c_{0\sigma}^+(\tau) \mathcal{G}_0^{-1}(\tau - \tau') c_{0\sigma}(\tau') + U \int_0^\beta d\tau n_\uparrow(\tau) n_\downarrow(\tau) . \quad (2.9)$$

$\mathcal{G}_0^{-1}(\tau - \tau')$  is a quantum generalization of the Weiss field and it is given by

$$\mathcal{G}_0^{-1}(\tau - \tau') = - \left( \frac{\partial}{\partial \tau} - \mu \right) \delta_{\tau\tau'} - \sum_{ij} t_{i0} t_{0j} G_{ij}^{(0)}(\tau - \tau') . \quad (2.10)$$

This quantity describes the local effective dynamics, or in the other words, quantum fluctuations between four available atomic states:  $|0\rangle, |\uparrow\rangle, |\downarrow\rangle, |\uparrow\downarrow\rangle$ . The main difference from the classical mean field case is that here the dynamical mean field is a function of time (frequency), instead of just a number. This dependence is crucial for full inclusion of local quantum fluctuations, which is the main advantage of the DMFT.  $\mathcal{G}_0$  plays the role of the noninteracting Green's function in the effective action  $S_{\text{eff}}$ , but it should not be confused with the noninteracting ( $U = 0$ ) local Green's function of the lattice.

We can express the cavity Green's function from Eq. 2.10 in terms of the local Green's functions in the following way [30]:

$$G_{ij}^{(0)} = G_{ij} - \frac{G_{i0} G_{0j}}{G_{00}} . \quad (2.11)$$

This means that in order to obtain the cavity Green's function, we need to subtract all contributions of the paths going through the site 0, from the full lattice Green's function. The denominator  $G_{00}$  is present due to the fact that all closed loops starting from the site 0 and ending in 0 are counted twice (once in  $G_{i0}$  and again in  $G_{0j}$ ).

It is more convenient to present Eq. 2.10 in the energy-momentum space,

$$\mathcal{G}_0^{-1}(i\omega) = i\omega + \mu - \sum_{ij} t_{i0}t_{0j}G_{ij}^{(0)}(i\omega) . \quad (2.12)$$

Since only the one-particle local interacting Green's function survives in the effective action (2.9), the Dyson equation,

$$G_{\mathbf{k}}(i\omega) = \frac{1}{i\omega + \mu - \varepsilon_{\mathbf{k}} - \Sigma(i\omega)} , \quad (2.13)$$

corresponds to

$$\begin{aligned} G_{00}(i\omega) &= \sum_{\mathbf{k}} G_{\mathbf{k}}(i\omega) = \sum_{\mathbf{k}} \frac{1}{i\omega + \mu - \varepsilon_{\mathbf{k}} - \Sigma(i\omega)} \\ &= \int d\varepsilon \frac{D(\varepsilon)}{\Delta(i\omega_n) + G(i\omega_n)^{-1} - \varepsilon} , \end{aligned} \quad (2.14)$$

where  $D(\varepsilon)$  is the noninteracting lattice density of states,

$$D(\varepsilon) \equiv \sum_{\mathbf{k}} \delta(\varepsilon - \varepsilon_{\mathbf{k}}) . \quad (2.15)$$

Here is important to emphasize that self-energy  $\Sigma$  is local ( $\mathbf{k}$  independent). Further, if we exploit the identity

$$\varepsilon_{\mathbf{k}} \equiv \sum_j t_{ij} e^{i\mathbf{k}(\mathbf{R}_i - \mathbf{R}_j)} , \quad (2.16)$$

and the relation (2.11), we can express the Weiss field in the following form,

$$\mathcal{G}_0^{-1}(i\omega) = i\omega + \mu - \left( \sum_{\mathbf{k}} \varepsilon_{\mathbf{k}}^2 G_{\mathbf{k}} - \frac{(\sum_{\mathbf{k}} \varepsilon_{\mathbf{k}} G_{\mathbf{k}})^2}{G_{00}} \right) . \quad (2.17)$$

After few steps of algebra, we obtain the central equation of the DMFT, connecting the Weiss field and the lattice Green's function

$$\mathcal{G}_0^{-1}(i\omega) = \Sigma(i\omega) + G_{00}^{-1}(i\omega) . \quad (2.18)$$

To complete the set of equations that makes DMFT self-consistency loop, we need

to calculate the impurity Green's function,

$$G_{00} = G_{impurity}(\mathcal{G}_0^{-1}) . \quad (2.19)$$

### 2.2.2 Mapping on the Anderson impurity model

The local effective action Eq. 2.9 corresponds to the action for the Anderson impurity immersed into the noninteracting conduction bath  $\mathcal{G}_0^{-1}(\tau - \tau')$ . This is a famous and very well studied model in condensed matter physics. There are several analytical and numerical methods for its solution. However, one has to be aware that this model is still rather complicated to solve. Before briefly mention the methods for its solution, it is instructive to also represent this model in the Hamiltonian form:

$$H_{AIM} = H_{atom} + H_{bath} + H_c , \quad (2.20)$$

where,

$$\begin{aligned} H_{atom} &= U n_{\uparrow}^{c_0} n_{\downarrow}^{c_0} + (\varepsilon_0 - \mu)(n_{\uparrow}^{c_0} + n_{\downarrow}^{c_0}) , \\ H_{bath} &= \sum_{i \neq 0, \sigma} \tilde{\varepsilon}_i c_{i\sigma}^{\dagger} c_{i\sigma} , \\ H_c &= \sum_{i \neq 0, \sigma} V_i (c_{i\sigma}^{\dagger} c_{0\sigma} + c_{0\sigma}^{\dagger} c_{i\sigma}) . \end{aligned} \quad (2.21)$$

$c_0^{\dagger}$  and  $c_0$  operators create and annihilate a particle at the interacting site (impurity), while  $c_i^{\dagger}$  and  $c_i$  create and annihilate particles in the noninteracting conducting bath.  $\tilde{\varepsilon}_i$  are effective parameters which, together with  $V_i$ , should be chosen in such a way that the impurity Green's function coincides with the local Green's function of the Hubbard model. The effective action of this model has the same functional form as derived effective action 2.9, with the difference,

$$\begin{aligned} \mathcal{G}_0^{-1}(\tau - \tau') &= -\left(\frac{\partial}{\partial \tau} - \mu\right) \delta_{\tau\tau'} - G_c(\tau - \tau') , \\ G_c(\tau - \tau') &= -\sum_{\mathbf{k}\sigma} |V_{\mathbf{k}}|^2 \frac{\delta_{\tau\tau'}}{\frac{\partial}{\partial \tau} + \tilde{\varepsilon}_{\mathbf{k}}} . \end{aligned} \quad (2.22)$$

We are now in position to complete the DMFT procedure. Equations 2.18 and 2.14, together with

$$G_{00} = G_{impurity}(\mathcal{G}_0^{-1}) , \quad (2.23)$$

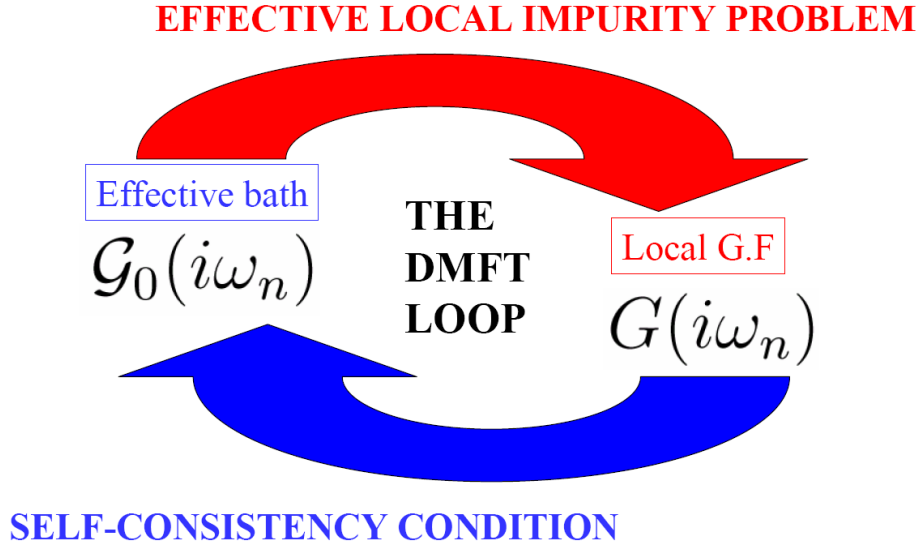


Figure 2.3: Schematic representation of the self-consistent DMFT loop.

form a closed set of DMFT equations for solving Hubbard model. The Weiss field has to be determined self-consistently in order to introduce the on-site interaction and the hopping in the bath. There are many available techniques for solving impurity model and obtaining impurity Green's function from a given Weiss field.

### 2.2.3 Impurity solvers

Technically the most difficult step in the DMFT self-consistency loop is solving the Anderson impurity model. This model and its various generalizations have been a subject of the intense study since the pioneering work of P.W. Anderson in 1961. [31]. Various analytical and numerical methods have been developed for its solution. All of these methods have their advantages but also drawbacks. Among the analytical methods, the most important are the slave boson methods (which introduce auxiliary particles - slave bosons) [32] and second order perturbation theory in  $U$  [9]. The numerical renormalization group (NRG) method allows the exact solution at  $T = 0$ , up to the error from the numerical discretization. The exact diagonalization method replaces the bath with a finite number (up to 10) orbitals.

For the solution of the AIM at finite temperatures the most useful are the non-crossing approximation (NCA) [33] (or one-crossing approximation - OCA) [34] and

quantum Monte Carlo (QMC) methods - Hirsch-Fye [35] and continuous time QMC (CTQMC) [36]. In this thesis we have used NCA (OCA) and CTQMC solver codes developed by K. Haule [34, 36], and the second order in  $U$  perturbative solver (Iterative Perturbative Theory - IPT) written in our group.

The IPT impurity solver is very fast and can be written both on the real and imaginary (Matsubara) frequency axis. In the context of the DMFT at half-filled lattice, it became very popular because it properly reproduces the limits of weak and strong interaction and reproduce all main features of the phase diagram of the single orbital half-filled Hubbard model.

Another popular impurity solvers, providing results directly on the real frequency axis are the non-crossing approximation (NCA)[33], the one-crossing approximation (OCA) [34], or even “symmetrized finite U” NCA (SUNCA) [34]. These solvers are based on the second order self-consistent perturbation theory in the hybridization function. The OCA has one more generating Feynman diagram for the self-energy than the NCA, which improves the solution, especially in the finite  $U$  case. One of the main drawbacks of these methods is failing to reproduce the Fermi-liquid behavior at lowest temperatures. An advantage is that they give results directly on the real frequency axis which is necessary for the calculation of the transport properties. They can also be relatively easily generalized to the multi orbital case and they are typically less time consuming than the QMC methods.

The most superior impurity solver is the continuous time quantum Monte Carlo (CTQMC) [36, 37] which is based on the sampling through the space of the Feynman diagrams in continuous time. In the strong coupling implementation, the perturbative expansion is done with respect to the hybridization (hopping  $t$ ), while the local (atomic) part is treated exactly. It is important to emphasize that this method is, in principle, exact since the Feynman diagrams are sampled to all orders. The only error comes from the statistical QMC noise. It is crucially that the method does not suffer from the minus sign-problem (at least for a single-orbital case) and that the method can be relatively easy generalized to the case of multiple orbitals. The resulting Green’s functions and the self-energies are given on the imaginary axis, which can be a drawback if one is interested on spectral functions and transport properties. Then the procedure for the analytical continuation has to be used - the maximum entropy method for the analytical continuation [38].

## 2.3 Mott metal-insulator transition

Mott metal-insulator transition (Mott MIT) was detected in numerous compounds of transition metal oxides, as well as rear earth and actinide intermetallics, where the valence orbitals form partially filled  $d$  or  $f$  shells. In these materials, the valence electrons sharing the same orbital experience strong Coulomb repulsion. The repulsion may localize the electrons in the case of half-filled orbital and open the gap (the Mott gap) at the Fermi level. First theoretical attempts to solve the Hubbard model were based on Hartree-Fock mean-field theory, which considers interaction between one electron and the averaged static field of all other electrons in the system, with approximate strong limit methods, like the Hubbard I approximation [30]. These attempts have roughly recovered the insulating phase, but failed to explain numerous pronounced features near the transition.

Most of the generic thermodynamic and transport properties near the Mott MIT can be successfully captured by the DMFT and its generalizations. Quite generally, there are two ways that the system can approach the Mott insulating state: by

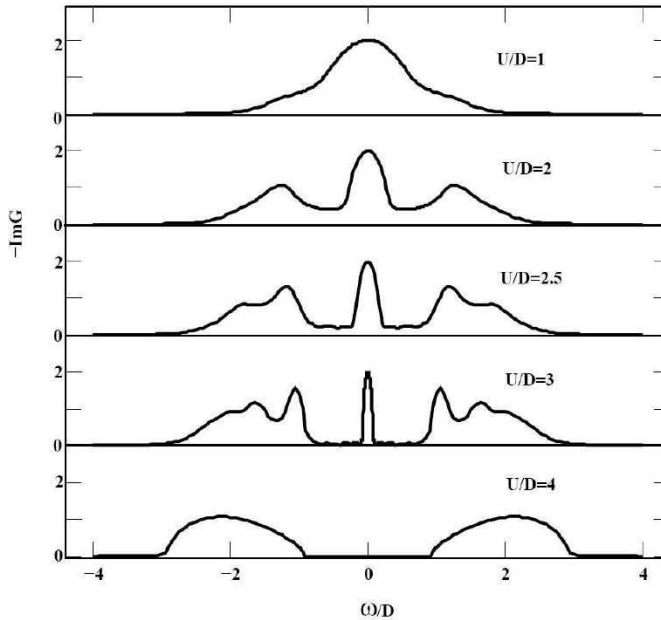


Figure 2.4: Local density of states for half-filled Hubbard model. At small  $U$  (upper panel) the system is weakly correlated metal. As  $U$  increases the quasiparticle peak narrows and, eventually, the Mott gap opens (lower panel).

increasing the interaction  $U$  - interaction-driven Mott MIT or, for large  $U$ , by doping - doping-driven Mott MIT. We will illustrate main features of the DMFT solution on the example of the half-filled Hubbard model.

Figure 2.4 shows the “prototype” of the density of states of the strongly correlated electrons. For the large value of the interaction  $U$  the Mott insulator occurs and the density of states consists of two Hubbard bands at the distance  $U$ . With decreasing interaction, the quasiparticle peak develops at the Fermi level and we enter into the metallic regime with strongly renormalized quasiparticle parameters. We have the famous three peak structure in the density of states. The quasiparticle peak appears due to the quantum fluctuations which are fully taken into account within the DMFT method. Precisely these strongly renormalized quasiparticles were the missing part in the puzzle of Mott MIT. When we further decrease the interaction, the Hubbard bands fully merge and the system becomes conventional, weakly correlated metal.

## 2.4 Optical and dc conductivity

Transport properties also relatively easily accessible in experiments due to variety of techniques that can probe them very accurately. They can be calculated from the correlation (two-particle Green's) functions. We will concentrate mostly on the on the optical and dc (direct current) conductivity, especially on direct-current (dc) conductivity and resistivity. Here, we will briefly sketch the derivation of the formula for the optical conductivity within the theory of linear response.

The optical conductivity  $\sigma(\omega)$  is defined by

$$\mathbf{j}(\omega) = \sigma(\omega)\mathbf{E}(\omega) , \quad (2.24)$$

where  $\mathbf{j}$  is the current and  $\mathbf{E}$  is the electric field. Our task is to calculate the current (and therefore the optical conductivity) in terms of the correlation function. First, we separate the current into the paramagnetic and the diamagnetic part, and after using the Coulomb gauge for the vector potential, we obtain the following relation

$$\mathbf{j}(\mathbf{x}, t) = \langle \mathbf{j}_P(\mathbf{x}, t) \rangle - \frac{ne^2}{m}\mathbf{A}(\mathbf{x}, t) , \quad (2.25)$$

where  $\mathbf{x}$  labels three Descartes coordinates and  $t$  is the time. The paramagnetic response to the applied field can be calculated within the theory of linear response:

$$\langle j_P^\alpha(\mathbf{x}, t) \rangle = \int d^3\mathbf{x}' \int_{t' < t} dt' i \langle [j_P^\alpha(\mathbf{x}, t), j_P^\beta(\mathbf{x}', t')] \rangle A^\beta(\mathbf{x}', t') . \quad (2.26)$$

Equivalently in the Fourier space,

$$\mathbf{j}(q) = \frac{1}{-i\nu} \left\{ \frac{ne^2}{m} \delta^{\alpha\beta} - i \langle [j^\alpha(q), j^\beta(-q)] \rangle \right\} \mathbf{E}(q) , \quad (2.27)$$

where  $q$  stands for  $q = (\mathbf{q}, \omega)$ .

In order to complete the derivation of the optical conductivity, we need to calculate current-current correlation function. In this thesis, we will briefly describe derivation presented in the section IV of Ref. [18]. The correlation function can be expressed as an infinite sum of two-particle vertex functions. It turns out that this infinite sum can be greatly simplified by making the following observations: Since a wave length of the incident light, used in experiments, is much shorter than the

wave length of the electronic wave vector,  $\omega/c \ll k_F$ , we consider the limit  $\mathbf{q} = 0$ , or in the other words  $q = (\omega, 0)$ . This observation, together with the limit of infinite dimensions (widely exploited within DMFT), allows us to drop all vertex corrections, keeping only the zeroth order vertex function. Calculating the only remaining vertex function and using the  $d \rightarrow \infty$  limit, we obtain the optical conductivity in the following form,

$$\sigma(i\omega) = \frac{1}{\omega} \int_{-\infty}^{+\infty} d\epsilon \int_{-\infty}^{+\infty} d\nu \int_{-\infty}^{+\infty} d\nu' D(\epsilon) \rho(\epsilon, \nu) \rho(\epsilon, \nu') \frac{f(\nu) - f(\nu')}{\nu - \nu' + i\omega}. \quad (2.28)$$

Here,  $D(\epsilon)$  is the noninteracting density of states,  $f(\nu)$  is the Fermi function, and  $\rho(\epsilon, \nu)$  represents the one particle spectral density

$$\rho(\epsilon, \nu) = -\frac{1}{\pi} \text{Im}G(\epsilon, \nu) = \frac{-1}{\pi} \frac{1}{\nu + \mu - \epsilon - \Sigma(\nu)}. \quad (2.29)$$

This equation is rigorously derived for the hypercubic (infinite dimensional cubic) lattice and it represents a reasonable approximation for the three-dimensional case, so we will use it in all calculations in the thesis.

One of the first and best known confirmations of DMFT was the comparison of calculated optical conductivity with the experimentally obtained, from photoemission spectrum of vanadium oxide  $V_2O_3$ . The theoretical calculations qualitatively recover the main aspects of the experiment [39].

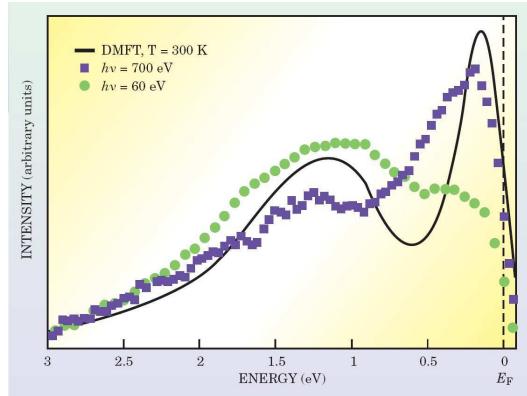


Figure 2.5: Photoemission spectrum of metallic vanadium oxide ( $V_2O_3$ ) near the metal-insulator transition (circles and squares) and optical conductivity calculated from DMFT (solid curve) [39].

## 2.5 Phase diagram of the frustrated Hubbard model

The DMFT phase diagram of half-filled Hubbard model displays metallic and Mott insulating phase and several crossover regions. Here we concentrate on the paramagnetic solution (which is relevant for geometrically frustrated lattices, e.g. triangular lattice).

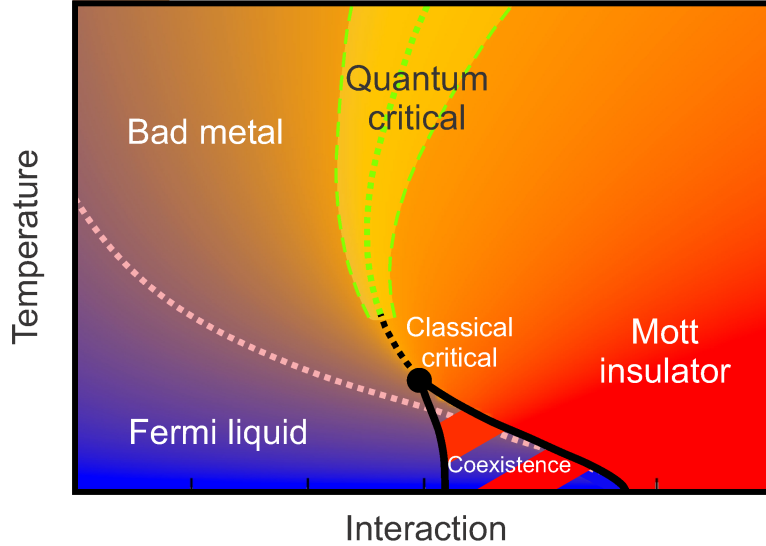


Figure 2.6: DMFT phase diagram of the half-filled Hubbard model.

At the low temperatures and weak interaction there is a Fermi liquid (conventional metallic) phase. When we increase the interaction  $U$ , we reach the region of coexistence of both metallic and insulating phase and for strong interaction we step into the Mott insulating phase. The coexistence region ends in the  $(U_c, T_c)$  critical point.  $T_c \approx 0.03E_F$  which is typically several tens of Kelvin in the experiments [6]. At high temperatures,  $T > T_c$ , we have bad metal phase characterized by very strong electron-electron scattering, followed by the "quantum critical" region [40, 10] and the insulating region characterized by the well developed gap and the activation temperature dependence of the resistivity.

### 3. Dynamical mean field theory for disordered strongly correlated systems

Every crystal structure has some level of disorder due to the presence of defects, impurities and or dopants. In the last twenty years, different classes of strongly correlated materials have appeared, many of them having a significant level of disorder. This is particularly the case with the complex materials obtained by doping, i.e. by replacing an atom of the starting compound with an atom of another element. The position of doped atoms in the lattice is usually random which introduces disorder into the system. Progress of the experimental techniques allowed systematic study of the effects of disorder in various materials of this kind. We will illustrate this in the next few examples.

A powerful experimental technique which allows local measurements at the nanoscale is the scanning tunneling microscopy (STM). Figure 3.1 represents the results of such measurements on high-temperature superconductor obtained by doping of

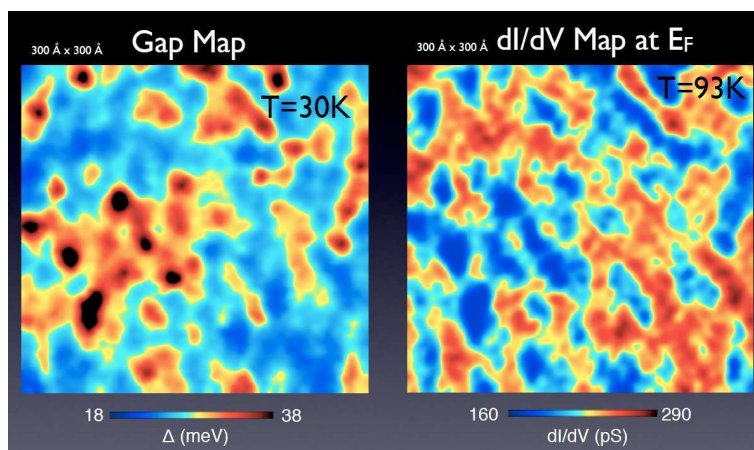


Figure 3.1: Spatial distribution of the superconducting gap in  $\text{Bi}_2\text{Sr}_2\text{CaCu}_2\text{O}_{8+\delta}$  at  $T = 30\text{ K}$  (left panel) and spatial distribution of the conductivity in the non-superconducting phase at  $T = 93\text{ K}$ . [41]

the Mott insulating material  $\text{Bi}_2\text{Sr}_2\text{CaCu}_2\text{O}_8$  by oxygen. The figure displays a spatial distribution of the superconducting gap at the temperature below critical temperature  $T_c$  and spatial distribution of the conductivity at temperature above  $T_c$ . The disorder and inhomogeneity in this system is most likely the consequence of doping.

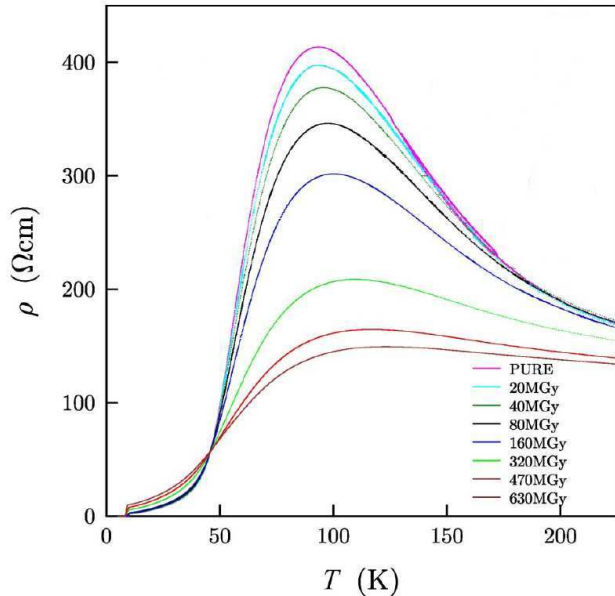


Figure 3.2: Resistance of the organic  $\kappa - (\text{BEDT} - \text{TTF})_2\text{Cu}(\text{SCN})_2$  as a function of temperature [42]. Level of disorder is proportional to the X-ray exposure time.

An appealing opportunity for a systematic study of the disorder effects is by introduction of structural defects by X-ray irradiation. Indeed, such a method is accessible in various organic charge-transfer salts. The temperature dependence of the resistance of the quasi two-dimensional organic material  $\kappa - (\text{BEDT} - \text{TTF})_2\text{Cu}(\text{SCN})_2$  for different irradiation exposure times is shown in Figure 3.2. The disorder strength is directly correlated with the X-ray exposure time (longer exposure time leads to more disordered system).

Another group of materials where both the interaction and disorder play an important role are diluted two-dimensional electron gasses in Si-MOSFETs and ultra-clean GaAs heterostructures. These systems display very sharp metal-insulator transition by tuning the concentration of charge carriers, see Figure 3.3. There is still controversy regarding the nature or even the driving force for this MIT transition and we will turn our attention toward this question Chapter 5.

The understanding of physical processes in the regime where both the electron-

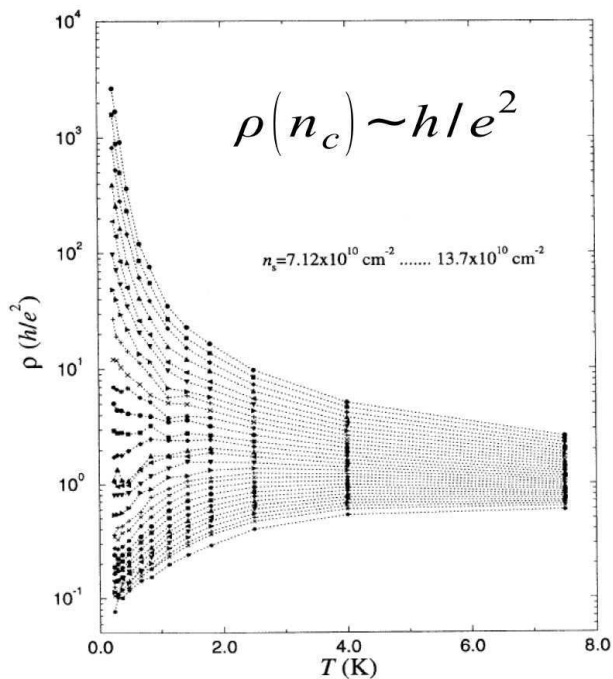


Figure 3.3: Resistivity of two-dimensional electron gas in Si-MOSFET as a function of temperature for different electron concentrations.

electron correlations and the disorder are strong is one of the most important open problems in the modern condensed matter physics. Explanation of the physical properties of strongly correlated disordered materials poses a major challenge, and also holds a promise for new technological applications.

There are few theoretical attempts to provide insight into the transport and thermodynamic properties of strongly disordered correlated systems [43]. In this thesis, we will follow the approach of the dynamical mean field theory, generalized in order to treat disordered systems. Most of the theoretical works on this subject have been restricted, so far, to binary disorder distribution [44], or low temperatures where the DMFT has been extended in order to incorporate the Anderson localization effects [27, 45, 46]. The generalized DMFT equations were usually solved with the approximate slave boson approach which is restricted to zero temperature, and can only indirectly address the finite temperature properties. The finite temperature transport properties in disordered systems, typically dominated by incoherent processes, is the main focus of the thesis.

In this chapter, we briefly review several generalizations of the DMFT method.

---

The first method of treating the disorder technically reduces to simple averaging of Green's functions over an ensemble of impurities in the DMFT self-consistency loop. This is the simplest approach which in the non-interacting limit reduces to the coherent potential approximation (CPA). The Anderson localization effects can be included through the approximate Typical medium theory. The spatial fluctuations in disordered finite dimensional systems are fully taken into account within the Statistical DMFT (StatDMFT), where the only approximation remains the assumption of the locality of the self-energy.

### 3.1 Disordered Hubbard model (DHM)

For the purpose of theoretical investigation of the disorder effects in strongly correlated materials, we consider the half-filled single-orbital Hubbard model with site-diagonal disorder and nearest neighbor hopping, given by the Hamiltonian

$$H = - \sum_{ij,\sigma} t_{i,j} c_{i\sigma}^\dagger c_{j\sigma} + U \sum_i n_{i\uparrow} n_{i\downarrow} + \sum_{i\sigma} v_i n_{i\sigma} - \mu \sum_{i\sigma} n_{i\sigma}. \quad (3.1)$$

Here  $t_{i,j}$  is the hopping amplitude,  $U$  the interaction strength,  $c_{i\sigma}^\dagger$  is the creation operator, and  $n_{i\sigma} = c_{i\sigma}^\dagger c_{i\sigma}$  the occupation number operator on site  $i$  for spin  $\sigma$ . The global occupation number is enforced by the chemical potential  $\mu$ . In this thesis we will concentrate on half-filled systems since we are primarily focuses on a study of interaction-driven Mott transition. The disorder is modeled by random energies  $v_i$  taken from uniform distribution in the interval  $(-W/2, W/2)$ . Most of the features of the disordered Hubbard model are expected to be insensitive to the particular form of the disorder distribution. Physically, the site disorder (random potential) can be due to the impurity atoms or dopants having different having different orbital energy levels.

Following the DMFT procedure, it is possible to reduce the disordered Hubbard model to the Anderson impurity model in a self-consistently determined conduction bath. Unlike to the clean case, in the presence of disorder, we need to consider an ensemble of impurities. There are several ways to set up the self-consistency equations for the calculation of the site-dependent conduction bath.

## 3.2 Coherent potential approximation for the correlated electrons

In the coherent potential approximation (CPA) of the DMFT model, we choose  $N$  values for site-disorder from the given distribution and solve a set of  $N$  Anderson impurity problems (one for each on-site energy). The conduction (hybridization) bath is obtained in the process of averaging over the disorder and it remains the same for each site within the CPA approach. In the non-interaction limit, the method reduces to the well studied CPA equations for non-interacting disordered electrons, which is formally exact in the limit of large coordination number [47].

The central quantity is the local Green's function,

$$G_{i\sigma}(\tau - \tau') = -\langle T c_{i\sigma}(\tau) c_{i\sigma}^\dagger(\tau') \rangle_{S_{\text{eff}}^i}, \quad (3.2)$$

which is a site-dependent quantity in the presence of disorder. The local effective action is given by

$$\begin{aligned} S_{\text{eff}}^i = & -\frac{1}{\beta} \sum_{i\omega_n, \sigma} c_{i\sigma}^\dagger(i\omega_n) [i\omega_n + \mu - v_i - \Delta(i\omega_n)] c_{i\sigma}(i\omega_n) \\ & + \frac{1}{\beta} U \sum_{i\omega_n} n_\uparrow(i\omega_n) n_\downarrow(i\omega_n), \end{aligned} \quad (3.3)$$

where  $\Delta$  is the conduction bath whose self-consistent value will be obtained in the iterative procedure. The quantity that we average over the disorder is the local Green's function,

$$G_{av}(i\omega_n) = \int dv P(v) G(i\omega_n, v). \quad (3.4)$$

Though we consider a continuous distribution of disorder  $P(v)$ , in practice it is sufficient to take a finite number of random energies, and the integral is replaced with a sum. In the case of uniform disorder

$$G_{av}(i\omega_n) = \frac{1}{N} \sum_{i=1}^N G_i(i\omega_n). \quad (3.5)$$

The averaged Green's function  $G_{av}$  and the conduction bath  $\Delta$  determine the

self-energy through the relation

$$G_{av}^{-1}(i\omega_n) = i\omega_n + \mu - \Delta(i\omega_n) - \Sigma(i\omega_n), \quad (3.6)$$

analogous to Eq. 2.18. The self-consistency condition follows from the assumption that the lattice self-energy coincides with the impurity self-energy. Then the disorder averaged local Green's function has to be equal to the local component of the lattice Green's function,

$$G_{av}(i\omega_n) = \int d\varepsilon \frac{D(\varepsilon)}{i\omega_n + \mu - \varepsilon - \Sigma(i\omega_n)}. \quad (3.7)$$

Here  $D(\varepsilon)$  is the density of states in the absence of disorder and interaction. Equation 3.6 determines new conduction bath which completes the self-consistency loop. The scheme of the CPA method is presented on the Figure 3.4.

This approach can be safely applied in the regime of weak or moderate disorder. However, it does not take into account spatial fluctuations of the conduction bath and Anderson localization in the limit of very strong disorder.

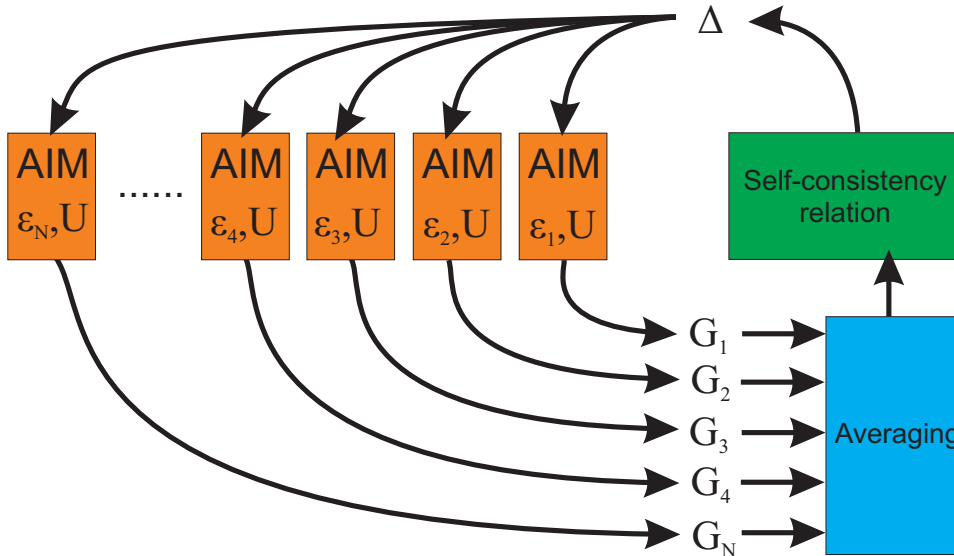


Figure 3.4: Schematic representation of the CPA algorithm.

### 3.2.1 Optical and dc conductivity within CPA

Taking into account the construction of the disorder treatment approach presented in section 3.2, we expect that optical conductivity assumes form analogous to that for

the clean Hubbard model 2.28. Since we are interested in the correlation functions on the real axis, we can perform an analytic continuation of Eq. 2.28 to the real axis,

$$\text{Re } \sigma(\omega + i0^+) = \frac{\pi e^2}{\hbar \text{ad}} \int_{-\infty}^{+\infty} d\epsilon \int_{-\infty}^{+\infty} d\nu D(\epsilon) \rho(\epsilon, \nu) \rho(\epsilon, \nu + \omega) \frac{f(\nu) - f(\nu + \omega)}{\omega}. \quad (3.8)$$

In this case the one particle spectral density depends of the self-energy obtained within CPA procedure,

$$\rho(\epsilon, \nu) = \frac{-1}{\pi} \text{Im} G(\epsilon, \nu) = \frac{-1}{\pi} \frac{1}{\nu + \mu - \epsilon - \Sigma_{CPA}(\nu)}, \quad (3.9)$$

where  $\Sigma_{CPA}$  is calculated from averaged Green's function (3.6).

The dc conductivity is defined as the conductivity at zero frequency and the dc resistivity is just inverse of that,

$$\sigma_{dc} = \text{Re } \sigma(\omega = 0) = \frac{\pi e^2}{\hbar \text{ad}} \int_{-\infty}^{+\infty} d\epsilon \int_{-\infty}^{+\infty} d\nu D(\epsilon) \rho^2(\epsilon, \nu) \frac{-df(\nu)}{d\nu}, \quad (3.10)$$

$$\rho_{dc} = \frac{1}{\sigma_{dc}}. \quad (3.11)$$

### 3.3 Typical medium theory

The interplay between Mott and Anderson localization has been studied on the disordered Hubbard model within an effective *typical medium theory* (TMT) [45]. A crucial step in the self-consistent calculation of the conduction bath, is geometrical averaging of the local density of states, in contrast to arithmetic averaging used in CPA. In this case, the effective DOS is calculated from,

$$\rho_{typ}(\omega) = \exp \left[ \int d\varepsilon P(\varepsilon) \ln \rho(\omega, \varepsilon) \right], \quad (3.12)$$

and the Green's function is obtained from the Hilbert transform,

$$G_{typ}(\omega) = \int_{-\infty}^{\infty} d\omega' \frac{\rho_{typ}(\omega')}{\omega - \omega'}. \quad (3.13)$$

This typical (geometrically averaged) DOS is the central quantity in the TMT. The criterion for the Anderson localization (disorder-driven MIT) is that the typical DOS goes to zero. While the average DOS at the Fermi level is finite both in a metal and Anderson insulator, typical DOS is finite (non-zero) in a metal, but vanishes in the Anderson insulator.

The zero temperature phase diagram for disordered half-filled Hubbard model is obtained using the numerical renormalization group (NGR) impurity solver 3.5. Correlated disordered metal is characterized by nonzero typical DOS at the Fermi level  $\rho_{typ}(0)$ . The boundary between this phase and the Anderson insulator is formed by the quantum critical line  $W_c(U)$  at which the system goes through a second order phase transition. The  $\rho_{typ}(0)$  is being reduced by disorder (for fixed interaction) and goes to zero precisely at  $W_c$ . On the other hand, the increase of the interaction for fixed finite  $W$ , restores the value of  $\rho_{typ}(0)$ , therefore improves the metallicity. System experience the Mott metal-insulator transition for weak to moderate disorder, together with the coexistence region. This transition qualitatively corresponds to the one in the clean case. Starting from the clean Mott insulator, for  $U \gtrsim U_c$ , the increase of disorder restores the metallic phase. The continuous transition between Mott and Anderson insulator has been detected for large values of interaction and disorder.

Despite the fact that this study is performed within effective theory it represents

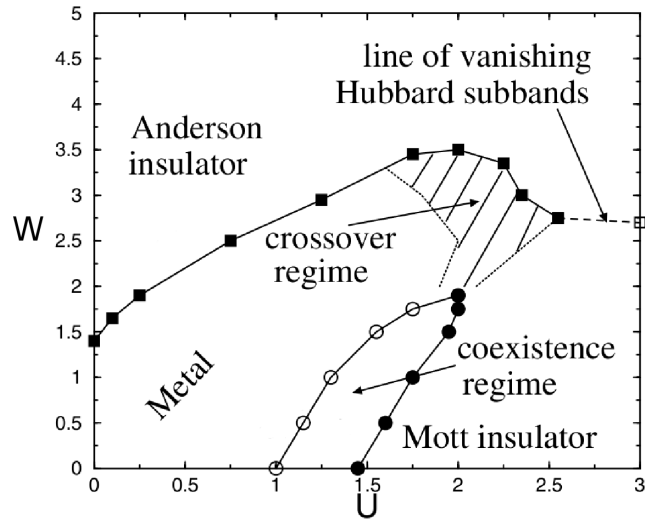


Figure 3.5: Phase diagram of the disordered Hubbard model at zero temperature within effective typical medium theory. Disorder strength and interaction are given in units of  $2/3 E_F$ .

a good starting ground for all other investigations in this direction. One of the important questions is how this picture evolves with the temperature and are there, and if there are, what are the artifacts of the used approximation.

### 3.4 Statistical dynamical mean field theory

We have argued in previous section that the simple approach like CPA can not give proper description of the strong disorder limit. Also many features of TMT solutions are questionable in this regime. In order to have a method capable to describe effects of disorder in a wide range of parameters, it is necessary to properly include spatial fluctuations. That can be accomplished by extending the ideas of dynamical mean field theory. A brief derivation of such extension of DMFT will be presented here.

We start from disordered Hubbard model Hamiltonian (3.1) with fixed realization of disorder. If we follow a standard DMFT procedure and we concentrate on a particular site of the lattice and integrate out all other sites, we obtain the local effective action for arbitrary site. The effective action has exactly the same form we have already seen in chapter 2 and the same conclusions and the procedures can be applied here. This will allow us to reduce solving of Hubbard model to the problem of solving an ensemble of Anderson impurity (AI) models. In this case our hybridization (bath) function will be different for each site in contrast to the clean case

$$\Delta_i(\omega_n) = \sum_{j,k=1}^z t_{ij}^2 G_{jk}^{(i)}(\omega_n). \quad (3.14)$$

Here,  $z$  is the coordination number and sums over  $j$  and  $k$  run over nearest neighbors of the site  $i$ .  $G_{jk}^{(i)}(\omega_n)$  are the cavity Green's functions, or the lattice Green's functions with site  $i$  removed,

$$G_{jk}^{(i)}(\omega_n) = \langle c_j^\dagger(\omega_n) c_k(\omega_n) \rangle^{(i)}. \quad (3.15)$$

Using the analogy with the derivation of the DMFT equations for the clean case, presented in the chapter 2, Eq. 2.11, the general result (regardless of the disorder) for the cavity Green's function can be obtained,

$$G_{jk}^{(i)} = G_{jk} - \frac{G_{ji} G_{ik}}{G_{ii}}. \quad (3.16)$$

The regular lattice Green's function from the previous equation is calculated from,

$$G^{latt}(\omega_g) = [\hat{I}(\omega_g + \mu) - \hat{\varepsilon} - \hat{\Sigma}(\omega_g) - \hat{H}^{clean}]^{-1}, \quad (3.17)$$

where,  $\hat{\varepsilon}$  and  $\hat{\Sigma}$  are diagonal matrices such that the elements of  $\hat{\varepsilon}$  are just on-site energies of each site,  $\hat{\varepsilon}_{ii} = \varepsilon_i$ , and self-energy contains the local self-energies  $\Sigma_j(\omega_g)$

(solutions of each AIM),

$$\langle i|\hat{\Sigma}(\omega_g)|j\rangle = \Sigma_j(\omega_g)\delta_{ij}. \quad (3.18)$$

$H^{\text{clean}}$  is the tight-binding Hamiltonian of the clean system ( $\varepsilon_i = 0$ ).

The cavity Green's function can be obtained in the same way as in the clean Hubbard model. Therefore, we can conclude that this procedure is exact in the limit of infinite coordination number in the presence of interaction, or for arbitrary coordination number for noninteracting particles. In the case of infinite coordination number, the bath function reduces to the simple average over sites, which leads to destruction of spatial correlations, which is essentially the CPA treatment of disorder described in previous section.

In order to allow for Anderson localization, we need to consider a finite lattice system. In this case hybridization function can be seen as a functional of the lattice Green's functions for fixed distribution of disorder. The finite number of sites allow us to keep track of hybridization functions on each site, which can fluctuate significantly from site to site, depending on the disorder strength. Precisely this feature is crucial for capturing the Anderson localization effects.

Again, we can establish direct correlation between our model and ensemble of Anderson impurity models, since the effective action has the same functional form. The solution of each AI model uniquely defines the corresponding local self-energy  $\Sigma_i$ ,

$$\Sigma_i(\omega_n) = i\omega_n + \mu - \varepsilon_i - \Delta_i(\omega_n) - (G_{ii}^{\text{loc}}(\omega_n))^{-1}, \quad (3.19)$$

where the local Green's function  $G_{ii}^{\text{loc}}$  is calculated in respect to the local effective action,

$$\langle i|\hat{G}(\omega_g)|i\rangle = G_{ii}^{\text{loc}}(\omega_n) = \langle c_i^\dagger(\omega_n)c_i(\omega_n)\rangle_{\text{loc}}. \quad (3.20)$$

Moreover, the full lattice self-energy assumes the local form,

In the last step, we are defining interacting lattice Green's function using non-interacting ("bare") Green's function for the same realization of disorder  $\varepsilon_i$ .

$$G_{ij} = G_{ij}^0[\varepsilon_i \rightarrow \varepsilon_i + \Sigma_i(\omega_n)] \quad (3.21)$$

Here we assumed that the self-energies describing the interaction renormalization have a strictly local character.

Now we have all necessary ingredients to write the iterative procedure of statistical DMFT:

1. make an initial guess for each hybridization function  $\Delta_i$ ,
2. solve the corresponding Anderson impurity model on every site of the lattice,
3. use the resulting self-energies  $\Sigma_i$  to calculate full Green's functions from Eq. 3.21,
4. calculate the new values of  $\Delta_i(\omega_n)$  from Eq. 3.19,
5. repeat the steps 2. to 4. until all  $\Delta_i$  converge.

To get the impression about the calculations involved in the statistical DMFT, we will briefly comment important features of the algorithm. Again, like in CPA case, the most demanding step is solving AI models (AIM) for every site in the lattice in every iteration. The statistical DMFT results we will present later are obtained mainly using the CTQMC solver, but the part concerning study of finite size effects (where we performed SDMFT calculation in absence of disorder) is obtained using the IPT solver, which is considerably faster. Its usage was necessary for studying large three dimensional lattices in reasonable time. Since the solution of the impurity problem for each site is the most demanding step, SDMFT code is parallelized over sites. The schematic description of the SDMFT is presented on the following figure.

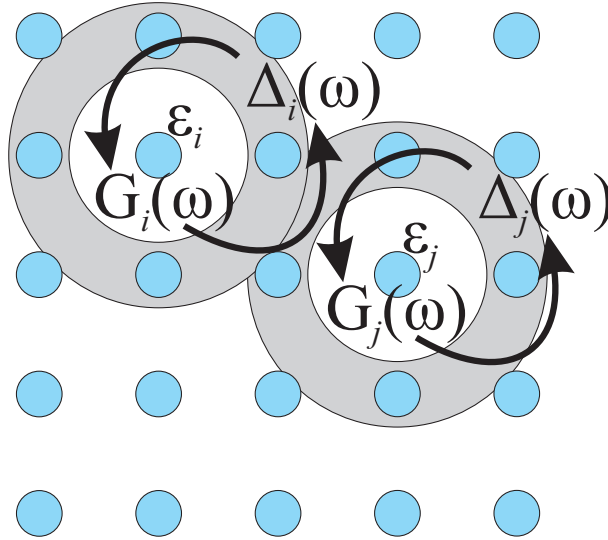


Figure 3.6: Schematic representation of the statistical DMFT algorithm.

## 4. Influence of disorder on incoherent transport near the Mott transition

Most of the theoretical work on the influence of disorder on physical properties near the Mott transition have been so far restricted to binary disorder distribution [44] or low temperatures, where the DMFT has been extended in order to incorporate the Anderson localization effects [27, 45, 46]. Different transport regimes in strongly correlated materials are, however, identified covering broad temperature range. These transport regimes are particularly clear in different compounds of  $\kappa$ -family organic charge-transfer salts, see Figure 1.1. These materials have half-filled conduction band with the effective Coulomb repulsion comparable to the bandwidth [48]. The proximity to the Mott metal-insulator transition can be tuned by applying the pressure.

On the metallic side of the Mott transition, the Fermi liquid transport at low temperatures is followed by an incoherent transport at higher temperatures dominated by the large scattering rate, and with resistivities an order of magnitude larger than the Mott-Ioffe-Regel (MIR) limit [49, 50, 51, 52], which is the maximal resistivity that can be reached in a metal according to the Boltzmann semiclassical theory. The resistivity of the MIR limit corresponds to the scattering length of one lattice spacing. From the theoretical point of view, the violation of the MIR condition and the appearance of the maximum in the resistivity temperature dependence is not easy to explain. However, at least for  $\kappa$ -organics, a significant progress has been recently achieved when the transport properties were successfully described even on the quantitative level within the dynamical mean field theory (DMFT) [6, 5, 53].

Very recently, the effects of disorder on the optical and dc conductivity of the organic charge-transfer salts have been systematically explored by introducing defects by X-ray irradiation [42, 54, 55]. The conductivity has proven to be very sensitive on the duration of the irradiation, and different physical mechanisms were advocated to explain such a behavior [42, 54, 55]. Since the disorder is gradually generated

---

by X-ray irradiation, the simplest approach of disorder averaging on the level of coherent-potential approximation (CPA), that we apply in this chapter, should be sufficient to explain the main modifications in the optical and dc conductivity caused by the disorder [11]. Motivated by the experiments on  $\kappa$ -organics, we calculate the resistivity in a wide temperature range for several levels of disorder. In this Chapter we present the results for the temperature dependence of the density of states, optical conductivity and dc resistivity near the Mott transition for the pure and disordered system. Our results are compared with the experiments on X-ray irradiated  $\kappa$ -organics. The high temperature results are obtained with OCA impurity solver and CTQMC is used for the lowest temperatures.

## 4.1 Density of states and optical conductivity

The phase diagram of fully frustrated half-filled Hubbard model in DMFT approximation is well known, see Figure 2.6. Here we focus on the crossover region from the Fermi liquid, across the incoherent metal to the high temperature insulating-like phase, for the values of interaction equal and slightly lower than  $U_c$  and for several levels of disorder. We consider the disordered half-filled Hubbard model (see section 3.1)

$$H = - \sum_{ij,\sigma} t_{i,j} c_{i\sigma}^\dagger c_{j\sigma} + U \sum_i n_{i\uparrow} n_{i\downarrow} + \sum_{i\sigma} v_i n_{i\sigma} - \mu \sum_{i\sigma} n_{i\sigma}. \quad (4.1)$$

where the disorder is modeled by random energies  $v_i$  taken from uniform distribution in the interval  $(-W/2, W/2)$ . Since the lattice structure enters the DMFT equations only through the density of states, the transport properties does not depend much on the details of the band structure, and we will consider the hypercubic lattice which has the density of states in the form of a Gaussian

$$D(\varepsilon) = \sqrt{\frac{2}{\pi}} e^{-2\varepsilon^2}, \quad (4.2)$$

where the energy is given in units of the half-bandwidth.

The central quantity that we calculate is the optical conductivity. The details of these calculations are presented in the chapter 3. Here we express the conductivity in units of the Mott-Ioffe-Regel limit for minimal metallic conductivity. The MIR limit,  $\sigma_{MIR}$ , is the conductivity which is reached when the electron mean free path becomes comparable to the lattice spacing,  $l \sim a$ . According to the semiclassical arguments, the electrons can scatter at most on every atom and the conductivity in a metal cannot be smaller than  $\sigma_{MIR}$ . For half-filled hypercubic lattice (which has Gaussian density of states), the MIR condition  $l = a$  is equivalent to  $E_F \tau = 1$ , where  $E_F$  is the bare Fermi energy, i.e. half-bandwidth of the noninteracting electrons, and  $\tau^{-1}$  is the scattering rate. Here  $\hbar$  is set to 1. Therefore, the MIR limit is set by a condition

$$\tau_{MIR}^{-1} = -2\text{Im}\Sigma(0^+) = 1, \quad (4.3)$$

where  $\Sigma$  is the self-energy measured in units of  $E_F$ .

The density of states and optical conductivity for a clean system and in a presence of moderate disorder,  $W = 1$ , are shown in Figure 4.1. The disorder effectively

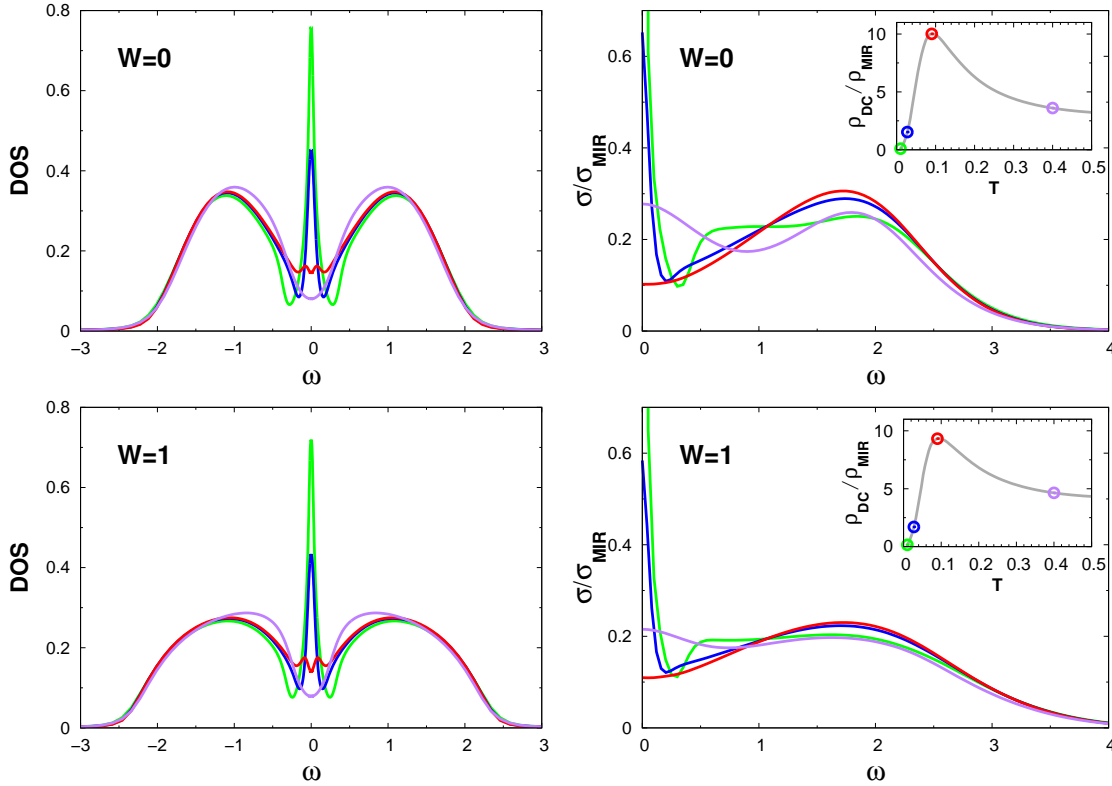


Figure 4.1: Density of states and optical conductivity as a function of frequency in the clean case for  $U = 0.94 U_c|_{W=0}$  (upper panel) and disordered case,  $U = 0.94 U_c|_{W=1}$  (lower panel). Different colors correspond to the four distinctive transport regimes (see the text). The insets show the temperature dependence of dc resistivity.  $T$ ,  $\omega$  and  $W$  are given in units of bare  $E_F$ .

increases the bandwidth and the critical interaction  $U_c$ . In our case, we find that  $U_c|_{W=0} = 2.2$  and  $U_c|_{W=1} = 2.45$ . The increase of  $U_c$  due to disorder is in agreement with earlier estimates obtained by iterated perturbation theory [56]. The critical temperature  $T_c$  weakly depends on the disorder strength,  $T_c|_{W=1} \approx T_c|_{W=0} = 0.04$ , where  $k_B$  is set to 1. On Figure 4.1 we compare the data at the same relative value  $U/U_c = 0.94$ , and for several characteristic temperatures. We see that the disorder does not lead to qualitative differences and if the interaction is the same when scaled with  $U_c$ , the density of states and the optical conductivity are even quantitatively very similar.

We can identify several regimes of the electron transport [11]. At low temperature (green dotted lines and crosses in the insets) the scattering rate,  $\tau^{-1} = -2\text{Im}\Sigma(0^+)$ ,

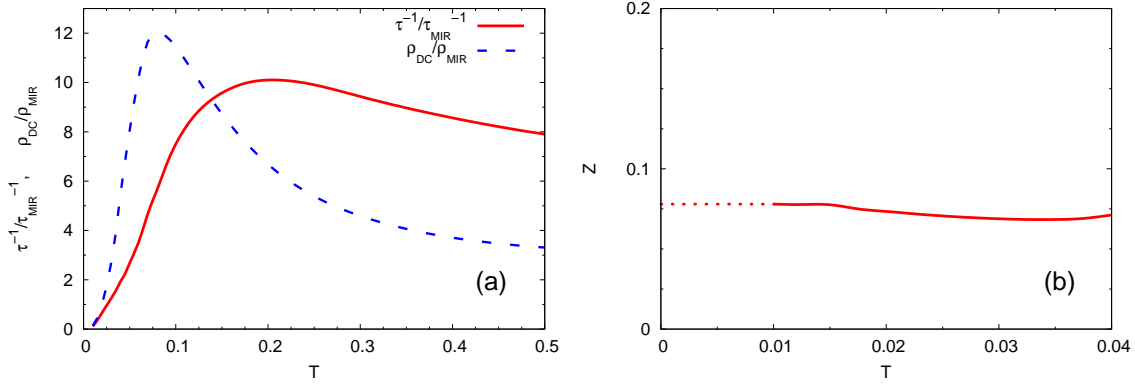


Figure 4.2: (a) Scattering rate (full line) and dc resistivity (dashed) as a function of temperature. (b) Quasiparticle weight as a function of temperature. The data are for the clean system at  $U = 0.95 U_c$ .

is small and the transport is dominated by long-lived coherently propagating quasiparticles. The blue dash-dotted lines (blue circles in the insets) correspond to the temperature when the resistivity is already larger than the MIR limit, the scattering rate  $\tau^{-1}$  is larger than  $E_F$ , and the Fermi liquid picture of well-defined quasiparticles ceases to be valid. However, a Drude-like peak in the optical conductivity, as well as a peak in the density of states, are still present. Our results show that this is the case also in the presence of moderate disorder. The resistivity maximum (red full line and square) is reached when the peak at the Fermi level is fully suppressed and when a dip at the Fermi level appears both in the density of states and in the optical conductivity. The resistivity maximum is more than an order of magnitude larger than  $\rho_{MIR} = \sigma_{MIR}^{-1}$ . At even higher temperatures (violet dashed line and triangle) low frequency optical conductivity increases due to the thermal excitations.

Figure 4.2 helps us to further distinguish the mechanism leading to the large resistivity and its strong temperature dependence. We see that the scattering rate gives the main contribution to the resistivity temperature dependence and causes the violation of the MIR limit, Figure 4.2(a), while the quasiparticle (Drude) weight  $Z = (1 + |\partial \text{Re} \Sigma(\omega)/\partial \omega|_{\omega=0})^{-1}$  is almost temperature independent, Figure 4.2(b). The dotted part of the line is an extrapolation of the OCA results to zero temperature. We have also checked that  $Z$  depends very weakly on the temperature using more reliable CTQMC impurity solver. Therefore, we can conclude that the driving mechanism for large resistivity is the large scattering rate and not the reduction

of the spectral weight near the Fermi level. This feature, already seen in the experiments on  $\text{VO}_2$  [57] and charge-transfer salts [53], seem to be common for the systems with half-filled conduction band near the Mott transition. This should be contrasted with the doped Mott insulators where the main reason for the violation of the MIR condition is a decimation of the Drude peak in the optical conductivity by the time MIR limit is reached, which can be interpreted as a reduction of the number of charge carriers [49, 52].

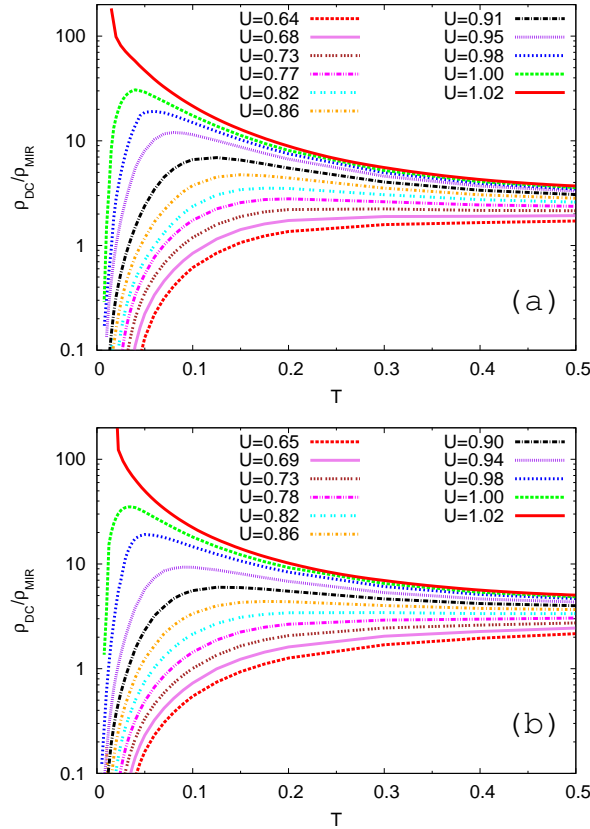


Figure 4.3: Temperature dependence of dc resistivity for different interaction  $U$  in the clean case,  $W = 0$  (a) and disordered case,  $W = 1$  (b).  $U$  is given in units of  $U_c(W)$ .

The results for temperature dependence of dc resistivity,  $\rho_{dc} = \sigma^{-1}(\omega \rightarrow 0)$ , for several values of interaction  $U$  are shown in Figure 4.3. The resistivity is given in units  $\rho_{MIR}$ . For clarity it is shown on a logarithmic scale. The resistivity in the clean and disordered case are even quantitatively very similar when the interaction is scaled with  $U_c(W)$ .

## 4.2 Increase of metallicity by disorder

Very recent experiments [42, 54, 55] on the charge-transfer organic salts provide a rather unique opportunity to study the effects of disorder on transport properties without changing external parameters or chemical composition. The level of defects (disorder) directly depends on the time of exposure to the X-rays. The optical and dc conductivity are proven to be very sensitive on irradiation time showing an increase in the conductivity with the time of irradiation. The experiments measured both interlayer and in-plane resistivity with similar conclusions. Different physical mechanisms were proposed to explain the increase of conductivity. Analytis *et al.* [42] proposed a defect-assisted interlayer conduction channel for the reduction of resistivity, and Sasaki *et al.* [54, 55] proposed that the irradiation leads to the effective doping of carriers into the half-filled Mott insulator.

The DMFT has successfully described the transport properties of organic salts even on the quantitative level [5, 53]. In order to make a comparison with the experiments with irradiation induced defects, we solve the DMFT equations for fixed interaction  $U$  and vary the level of disorder  $W$  [11]. The results for dc resistivity are shown in Figure 4.4(a). The data for  $T < 0.01$  are obtained using CTQMC impurity solver. The presence of even a weak disorder significantly decreases the resistivity by effectively moving the system away from the Mott insulator, as explained in the previous section. Our data are very similar to the measurements on charge-transfer salt  $\kappa$ -(BEDT-TTF)<sub>2</sub>Cu(SCN)<sub>2</sub> from Ref. [42], which are shown in Figure 4.4(b). We note that these data are for interlayer resistivity while our DMFT calculation corresponds to in-plane transport. However, the interlayer transport is due to incoherent tunneling which is proportional to in-plane conductivity [58]. Therefore the temperature dependence of out-of-plane resistivity should follow the temperature dependence of in-plane resistivity. Indeed, the in-plane optical conductivity measurements on the Mott insulator  $\kappa$ -(BEDT-TTF)<sub>2</sub>Cu[N(CN)<sub>2</sub>]Cl, also show that the Mott system becomes more metallic in a presence of disorder. These measurements show the transfer of the spectral weight to low frequency region as the irradiation time increases, followed by the collapse of the Mott gap [54, 55].

We emphasize that our model, as opposed to the physical mechanism proposed in Ref. [55], does not assume an introduction of new charge carriers since the total number of carriers per site remains equal to one. The local occupation number, however, depends on the random site potential, and we can say that the system is

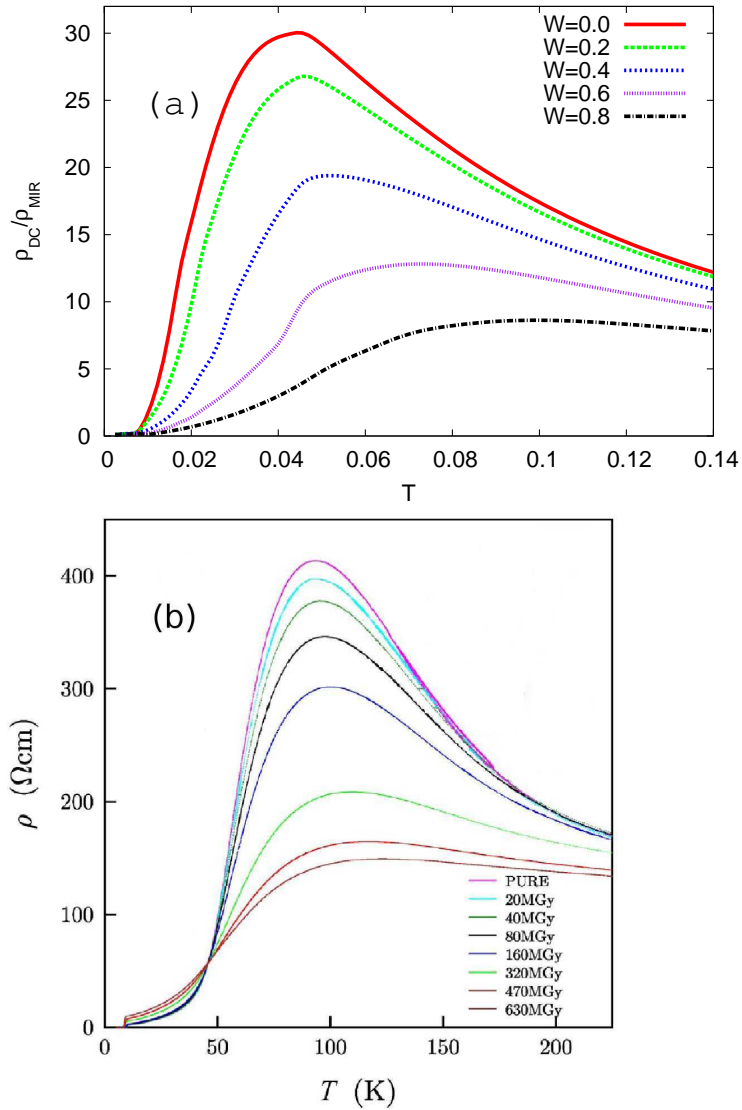


Figure 4.4: (a) Temperature dependence of dc resistivity for fixed  $U = 2.2 = U_c|_{W=0}$ , and various levels of disorder. (b) Experiments on  $\kappa$ -(BEDT-TTF) $_2$ Cu(SCN) $_2$ , taken from Ref. [42].

effectively locally doped [59]. The occupation number, for a given spin orientation, as a function of random site potential is shown in Figure 4.5. It is interesting to note that the local occupation number,  $n(v_i)$ , deviates much less from its average value than it would be the case in the absence of interaction. This is a consequence of very strong disorder screening of site-diagonal disorder on the metallic side of the Mott transition [60]. Therefore, the resistivity curves on Figure 4.4(a) cross

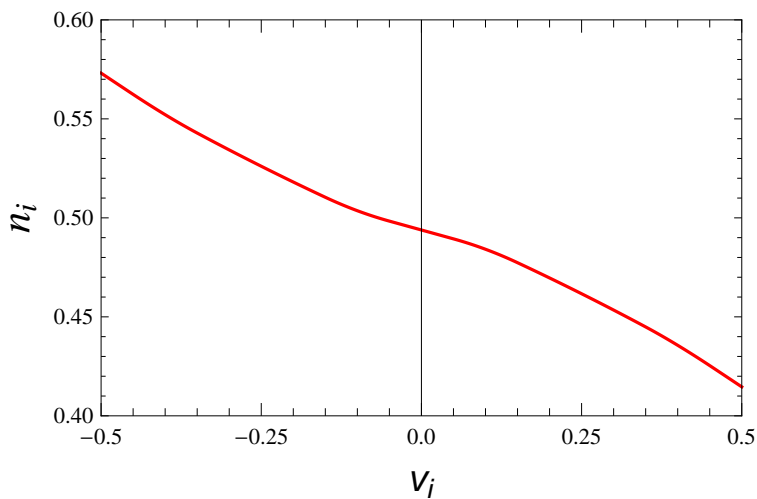


Figure 4.5: Local occupation number per spin as a function of site disorder  $v_i$  for  $T = 0.01$ ,  $U = 2.1$ , and  $W = 1$ .

at very low temperatures and our current model cannot explain the intersection of curves in Figure 4.4(b) which happens at much higher temperature. The dramatic reduction of the elastic scattering is also demonstrated in Ref. [61], which shows that the inelastic scattering dominates in the incoherent regime. We stress that we do not assume Matthiessen's rule. This is a salient feature of DMFT, which can operate in a regime where conventional approaches to the electron transport fail.

## 4.3 Conclusions

In summary, we have examined the influence of random potential on the optical and dc conductivity for half-filled Hubbard model in a vicinity of the Mott transition. Our results show, in agreement with the experiments on  $\kappa$ -organics, that the disorder can make the system effectively more metallic [11]. The disorder increases the bandwidth which increases  $U_c$  and weakens the correlation effects, moves the system away from the Mott transition and leads to a decrease in the scattering rate and resistivity. We emphasize that the randomness in our model does not change global doping, as the system remains on average half-filled, but the number of charge carriers locally deviates from the average value. Therefore, global carrier doping of a Mott insulator due to irradiation defects, proposed in Ref. [55], is not necessary to make the system more metallic. We also find that the maximal possible value of metallic resistivity remains more than an order of magnitude larger than the MIR limit even in a presence of moderate disorder. As in the clean case, the violation of the MIR limit is driven by a large scattering rate due to the electron-electron scattering, and Drude-like peak in the optical conductivity persists even at temperatures when the resistivity is well beyond the MIR limit.

## 5. Scattering mechanism in diluted 2D electron gases: interaction vs. disorder

The physical nature of scattering processes which control transport represents one of the most fundamental properties for any material. At the lowest temperatures the thermal excitations are few, and elastic impurity scattering dominates. Raising the temperature introduces two basic pathways to modify transport. First, elastic scattering can acquire a temperature dependence either through the modified screening of the impurity potential, or through dephasing processes [62, 63]. This general mechanism encapsulates the physical content of all “quantum corrections” – both in the diffusive and the ballistic regime – predicted within the Fermi liquid framework. Indeed, careful and precise experiments have confirmed the validity of this physical picture for many good metals with weak disorder [62]. Physically, it relies on the existence of long-lived quasiparticles within a degenerate electron gas.

The second route comes into play in instances where correlation effects due to electron-electron interactions are significant. Here, the Fermi liquid regime featuring degenerate quasiparticles is often restricted to a very limited temperature range  $T \ll T^* \ll T_F$ , well below the “coherence temperature”  $T^*$ , which itself is much smaller than the Fermi temperature  $T_F$ . In such materials, which include rare-earth intermetallics [64, 65], many transition metal oxides [57], and several classes of organic Mott systems [5, 66, 53], a broad intermediate temperature regime emerges  $T \sim T^* \ll T_F$  where *inelastic* electron-electron scattering dominates all transport properties. Such scattering directly reflects the thermal destruction of Landau quasiparticles – a situation describing the demise of a coherent Fermi liquid. In these materials, in the relevant temperature range, the electron-phonon scattering is much weaker than the electron-electron one.

When a material is tuned to the vicinity of any metal-insulator transition, both disorder and electron-electron interactions are of *a priori* importance. But which of these two scattering mechanisms – elastic or inelastic – dominates the experimen-

---

tally relevant temperature range? Answering this question should provide important clues as to which of the localization mechanisms dominate in any given material. Unfortunately, experimental systems permitting sufficiently precise tuning of control parameters are generally rather few. An attractive class of systems where a dramatic metal to insulator crossover is observed in a narrow parameter range is provided by 2D electron gases (2DEG), such as silicon MOSFETs or GaAs/AlGaAs heterostructures [67, 68, 69]. One of the most striking features observed in these systems is the pronounced resistivity drop on the metallic side of the transition. While conventional, relatively weak temperature dependence is found at high densities ( $n \gg n_c$ ), very strong temperature dependence is found near the critical density  $n_c$ , roughly in the same density range  $n_c \lesssim n \lesssim 2n_c$  where other strong correlation phenomena were observed, e.g. large  $m^*$  enhancement [70]. Here, pronounced resistivity maxima are observed at  $T \sim T_{max}(n)$ , followed by a dramatic resistivity drop at lower temperatures, whose physical origin remains a subject of much controversy and debate [67, 68, 69].

In this Chapter we argue that the electron-electron scattering dominates the transport in a broad concentration and temperature range on the metallic side of the metal-insulator transition [12] in Si MOSFETS and GaAs/AlGaAs heterostructures. This conclusion is reached by: (i) A detailed scaling analysis of the metallic resistivity curves; (ii) Establishing a similarity in the transport properties of the 2DEG and well-studied strongly correlated materials near the interaction-driven MIT; (iii) Making a comparison of the resistivity curves in 2DEG with those in a simple model of the Mott MIT. Our conclusions favor the interaction-driven (Wigner-Mott) scenario [71, 72, 73, 74, 75] of the MIT in 2DEG and give a guidance for the development of a microscopical theory of incoherent transport in diluted 2DEG.

## 5.1 Metal-insulator transition in two dimensions

The interest for the physics of the strongly-correlated, disordered systems has been renewed since the beginning of 1990's, due to many unexpected and puzzling transport properties of high mobility silicon metal-oxide semiconductor field-effect transistors (MOSFETs). Despite the extensive experimental and theoretical studies, many of the transport properties of these materials remained unclear.

In early 1980's there was a wide spread belief that there should be no metallic phase in (infinite) two dimensional disordered systems in zero magnetic field. In the case of noninteracting charge carriers such result was obtained within the scaling theory of localization [76]. This theory predicted that as the temperature approaches zero, the resistivity becomes infinite. The growth of resistivity is shown to be logarithmic in the case of "weak localization" and exponential for "strongly localized" charge carriers. Subsequent studies have shown that the localization effects increase even further in the presence of weak interaction [77]. In the opposite limit of the strongly interacting particles the Wigner crystallization occurs [78]. Even a small amount of disorder, in this case, leads to the pinning of the Wigner crystal that makes system insulating. Therefore, the two-dimensional electron systems were expected to be insulating in both limits: weak (or absent) and very strong interparticle interaction. That question was considered as resolved until the experiments on highly diluted 2D electron gases were performed.

Recent availability of high mobility MOSFET samples enabled the systematic research of 2D systems in the range of very low electron densities, typically below  $10^{11} \text{ cm}^{-2}$  [79]. An important result of these studies is the strong temperature dependence of the resistivity well below Fermi temperature. In addition, the existence of the critical density  $n_c$  is obtained for which the resistivity is almost temperature independent and it is of the order of the quantum unit of resistance,  $h/e^2 \approx 25.6 \text{ k}\Omega$ . Above  $n_c$  the resistivity decreases with the temperature down to the lowest accessible temperatures of  $\sim 4 \text{ mK}$ . All this strongly suggests that there is a metal-insulator transition at  $T = 0$ .

The first experiments indicating the existence of MIT in 2D electron systems were performed on highly diluted silicon MOSFETs [80, 81]. Significant property of these materials was an order of magnitude larger mobility than in previous investigations, reaching more than  $4 \times 10^4 \text{ cm}^2/\text{Vs}$  at  $T = 4.2 \text{ K}$ . At these very low electron concentrations the electron-electron interaction  $E_{e-e}$  becomes dominant and much

larger than the Fermi energy. Estimates of these energies for Si MOSFETs at  $n_s = 10^{11} \text{ cm}^{-2}$  yield

$$E_{e-e} \sim \frac{e^2}{\epsilon} (\pi n_s)^{1/2} \approx 10 \text{ meV}, \quad (5.1)$$

while

$$E_F = \frac{\pi \hbar^2 n_s}{2m^*} \approx 0.58 \text{ meV}, \quad (5.2)$$

where  $e$  is the electron charge,  $\epsilon$  is the dielectric constant,  $E_F$  is the Fermi energy, and  $m^*$  is the effective electron mass. Typical values of dimensionless parameter  $r_s \equiv E_{e-e}/E_F$  in these samples is above 10. In the very dilute 2D electron systems the formation of the Wigner crystal is expected, and according to the numerical simulation [78] this should occur at  $r_s \approx 37 \pm 5$ , and at even higher density in the presence of disorder [82]. Hence, these 2D systems can be considered as strongly correlated electron liquids at  $r_s \sim 10$ .

These findings were supported by subsequent experiments in diluted 2D electron systems like silicon MOSFETs with different geometry and oxide thicknesses [83] and other 2D systems (p-GaAs, n-GaAs, p-SiGe, etc.). Typical experimental results [80, 81] of the resistivity dependence on the electron density and temperature are presented in Figure 3.3. Aforementioned critical electron density  $n_c$  is clearly distinguished together with the metallic family of the curves having  $n_s > n_c$  and insulating curves with negative slope for  $n_s < n_c$ . The most striking property is change in resistivity by several orders of magnitude, caused by change of the concentration of only a few percent. The temperature dependence of the resistivity becomes weak above  $T^* \approx 2 \text{ K}$ . At higher densities, of the order of those used in the experiments in the 1980s, a weak insulating temperature dependence is observed, reminiscent of Anderson localization.

## 5.2 Scaling analysis of the resistivity maxima

The experimental data reveal well defined trends in the density dependence of the resistivity maxima, suggesting a scaling analysis. While many different scenarios for the metal-insulator transition predict some form of scaling, its precise features may provide clues to what mechanism dominates the transport.

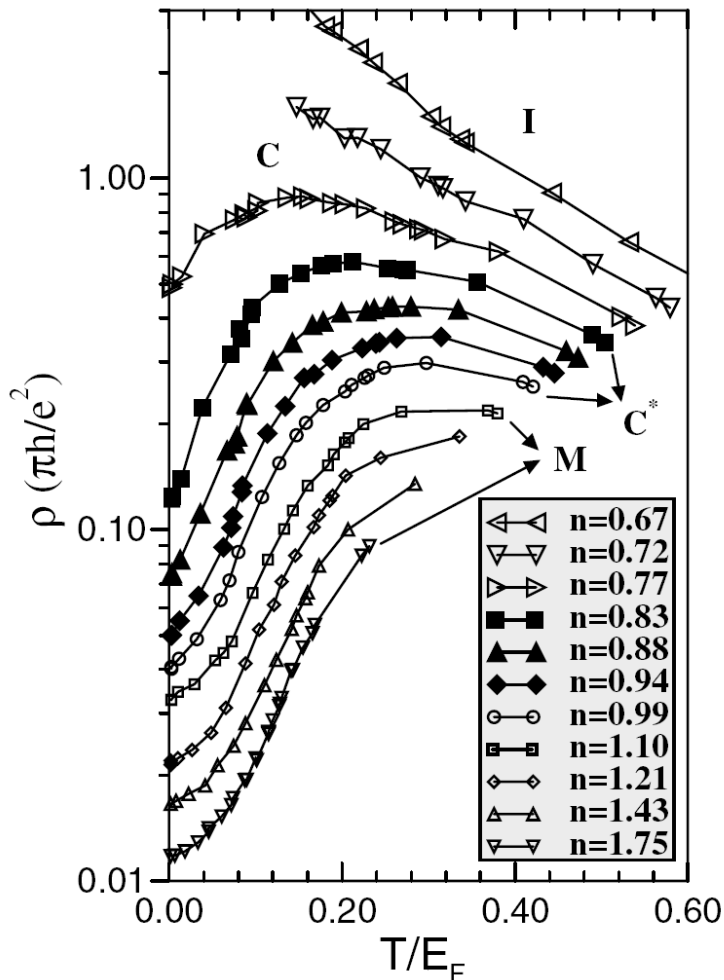


Figure 5.1: Resistivity as a function of temperature from the experiments on Si MOSFET by Pudalov *et al.* [84].

All the curves displaying a resistivity maximum have an almost identical shape Figure 5.1, strongly suggesting that unique physical processes are responsible for a strong temperature dependence of the resistivity [12] in a large range of concentrations. The resistivity maxima are typically observed at temperatures comparable to the Fermi temperature, where a physical picture of long-lived quasiparticles is

no more valid. Complementary experiments [70, 68] on the same material have revealed that large effective mass  $m^*$  enhancements are observed in the same density range. This behavior is a clear signature of strong correlation effects which, in all known examples, produce very strong inelastic electron-electron scattering in the appropriate temperature range. The electron-phonon scattering is negligibly small for  $T < T_F \lesssim 10$  K [85]. Since a strongly correlated system is typically characterized by a single characteristic energy scale  $T^* \sim (m/m^*) T_F$ , we expect the scaling function  $f(x)$  to assume a universal form, while the scaling parameters  $T_{max} \equiv T^*$  and  $\rho_{max}$  to assume a simple, power-law dependence on the effective mass  $m^*$ . Guided by these observations, in this Section we introduce a scaling ansatz and perform a scaling analysis of the resistivity curves in Si MOSFETs and GaAs heterostructures.

### 5.2.1 Phenomenological scaling hypothesis

In accordance to what is typically found in other examples of strongly correlated metals with weak to moderate disorder [5], we expect the resistivity to assume an additive form,  $\rho(T) = \rho_o + \delta\rho(T)$ . Here,  $\rho_o$  is the residual resistivity due to impurity scattering, and the temperature-dependent contribution  $\delta\rho(T)$  is expected to be dominated by inelastic electron-electron scattering. Based on these general considerations, we propose that the temperature-dependent term assumes a scaling form

$$\delta\rho(T) = \delta\rho_{max} f(T/T_{max}), \quad (5.3)$$

where  $\delta\rho_{max} = \rho_{max} - \rho_o$ .

To test this phenomenological scaling hypothesis, we perform a corresponding analysis of experimental data in several systems displaying 2D-MIT [12]. We start with the Si MOSFET data [84] analyzed in Ref. [86]. We concentrate on metallic curves below the separatrix C. In the range of concentrations  $0.83 < n < 1.10$ , the resistivity curves have a clear maximum, and nicely collapse with the proposed scaling ansatz, Figure 5.2(a). In fact, we can use the scaling ansatz to collapse also the data for  $1.21 < n < 1.75$ , where  $T_{max}$  and  $\rho_{max}$  are determined from the least square fit to the scaling curve. Clearly all eight resistivity curves belong to the same family (have the same functional form), and thus must be explained by a *single dominant transport mechanism*. This conclusion is even more convincing if we apply the same analysis to several different materials, including ultra high mobility GaAs sample, Figure 5.2(b). While the diffusive physics cannot possible apply in

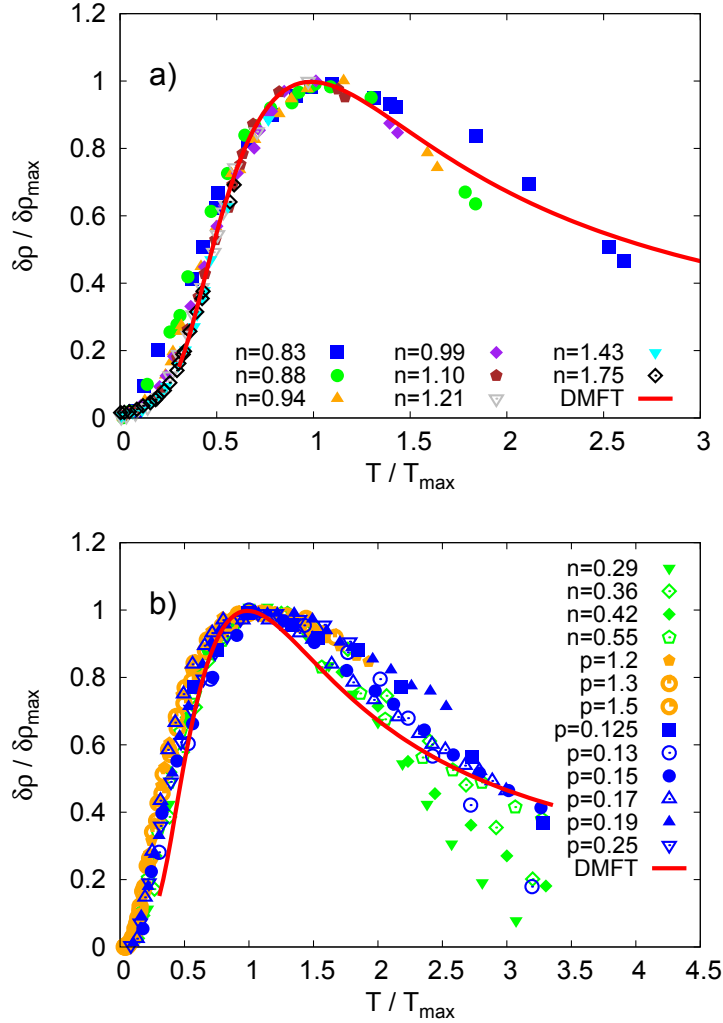


Figure 5.2: Scaled resistivity as a function of scaled temperature for different electron (hole) concentrations, for Si MOSFET (a) and GaAs heterostructures (b). The experimental data are taken from Ref. [86] (MOSFETs), Ref. [87] (p-GaAs/AlGaAs, blue symbols), Ref. [88] (n-GaAs/AlGaAs, green symbols), and Ref. [89] (p-GaAs, orange symbols). The solid line is the scaling function obtained for a simple model of the MIT (see section 5.4).

such a broad parameter range, we see that the scaling form we propose proves to be an extremely robust feature of all available 2D-MIT systems. This result is very significant, because disorder effects must be significantly weaker in these ultra-clean materials, while the interaction effects are expected to be even stronger.

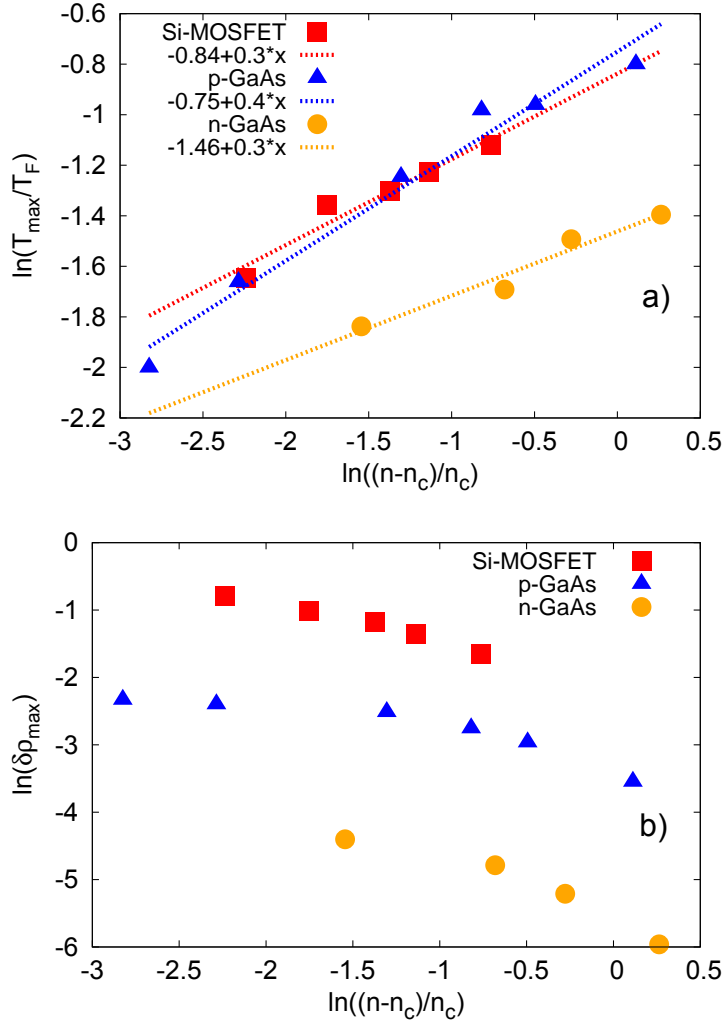


Figure 5.3:  $T_{max}$  normalized to Fermi temperature (a), and maximal resistivity  $\delta\rho_{max} = \rho_{max} - \rho_o$  in units  $\pi h/e^2$  (b), as a function of a reduced density. The data are taken from Refs. [86, 87, 88].

### 5.2.2 Critical behavior of the Wigner-Mott scaling

Having demonstrated data collapse, we are now in a position to examine the critical behavior of the relevant crossover scale. We thus examine the behavior of  $T_{max}$  and  $\rho_{max}$  as a function of reduced concentration  $(n - n_c)/n_c$  and effective mass  $m^*$  (as determined by complementary experiments).

For different realizations of 2DEG,  $T_{max}$  shows approximately power law dependence on the reduced concentration, Figure 5.3(a), and even the exponents are similar.  $T_{max}$  in our physical picture has a clear physical interpretation as a coher-

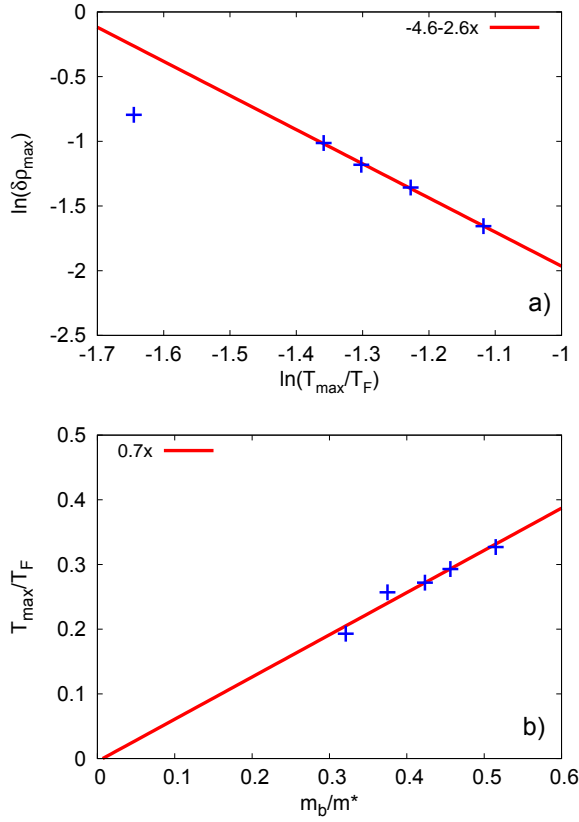


Figure 5.4: (a) Maximum resistivity  $\delta\rho_{max} = \rho_{max} - \rho_o$  as a function of  $T_{max}$ . (b)  $T_{max}$  as a function of inverse effective mass  $m^*$ .  $m_b$  is the band mass in Si MOSFETs. The data are taken from Refs. [86], [90].

ence temperature - the temperature when the inelastic electron-electron scattering time becomes comparable to  $\hbar/E_F$ , leading to incoherent transport. The resistivity maximum, however, shows less universal form. It varies a lot in different physical systems. This does not come as a surprise since the resistivity shows nonuniversal features also in three dimensional strongly correlated materials near the Mott transition. We discuss in detail the analogy with the Mott systems in sections. 5.3 and 5.4.

In a Si MOSFET the resistivity maximum  $\delta\rho_{max} = \rho_{max} - \rho_o$  shows power law dependence on  $T_{max}$  in a fairly broad concentration range, Figure 5.4(a). We further analyze the critical behavior for Si MOSFET using the data for the effective mass as determined by Shashkin *et al.* [70] from magnetoresistance measurements in a parallel magnetic field. We find that  $T_{max}$  is inversely proportional to the effective mass  $m^*$ . This behavior is typical to all systems near the Mott MIT, where the

coherence temperature is inversely proportional to the effective mass, as a landmark of strong correlations.

### 5.2.3 Breakdown of the diffusion mode scaling

We have successfully collapsed resistivity curves in a broad temperature and concentration range and for several physical realizations of 2DEG. The physical picture behind the proposed scaling is that the 2D MIT is an interaction-driven (Wigner-Mott) MIT [71, 72, 73, 74, 75], and that the dominant temperature dependence in the resistivity originates from strong electron-electron scattering. Another proposed

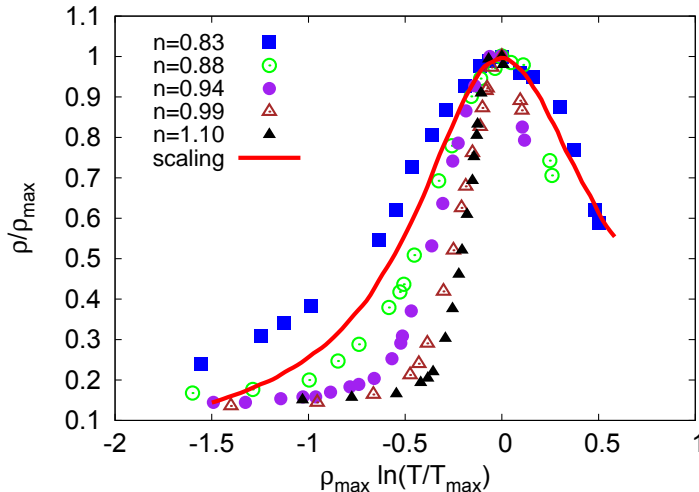


Figure 5.5: Resistivity as a function of temperature scaled as in Ref. [86]. Red solid line is the calculated scaling curve.

scenario envisions disorder as the principal driving force for localization [86, 91], while the interactions are most important above the critical density and at low temperatures, where they suppress the tendency to localization. An appropriate theory, based on Fermi liquid framework [86], has predicted that a resistivity maximum should be observed on the metallic side, with the resistivity assuming the scaling form

$$\rho(T)/\rho_{max} = f[\rho_{max} \ln(T/T_{max})]. \quad (5.4)$$

Here  $f(x)$  is a universal scaling function predicted by theory. The authors point out, though, that this prediction is expected to be valid only within the diffusive regime, where the thermal energy  $k_B T$  is smaller than the elastic scattering rate

$\hbar/\tau$ . According to this picture, a different (ballistic) mechanism for transport is expected outside the diffusive regime, presumably leading to a different temperature dependence, so the proposed scaling no longer holds. This analysis was applied to the experimental data of Ref. [84], but was accordingly restricted to only three densities closest to the transition. Indeed, if the scaling formula is applied in a broader range of concentrations, the resistivity curves clearly do not collapse [Figure 5.5. While the Fermi liquid renormalization group calculations are very important in order to answer a fundamental question of necessary conditions for a true MIT at zero temperature, our analysis emphasizes that the understanding of various diluted 2DEG in a broad range of parameters requires the physics beyond the conventional Fermi liquid framework.

### 5.3 Scaling in 3D materials

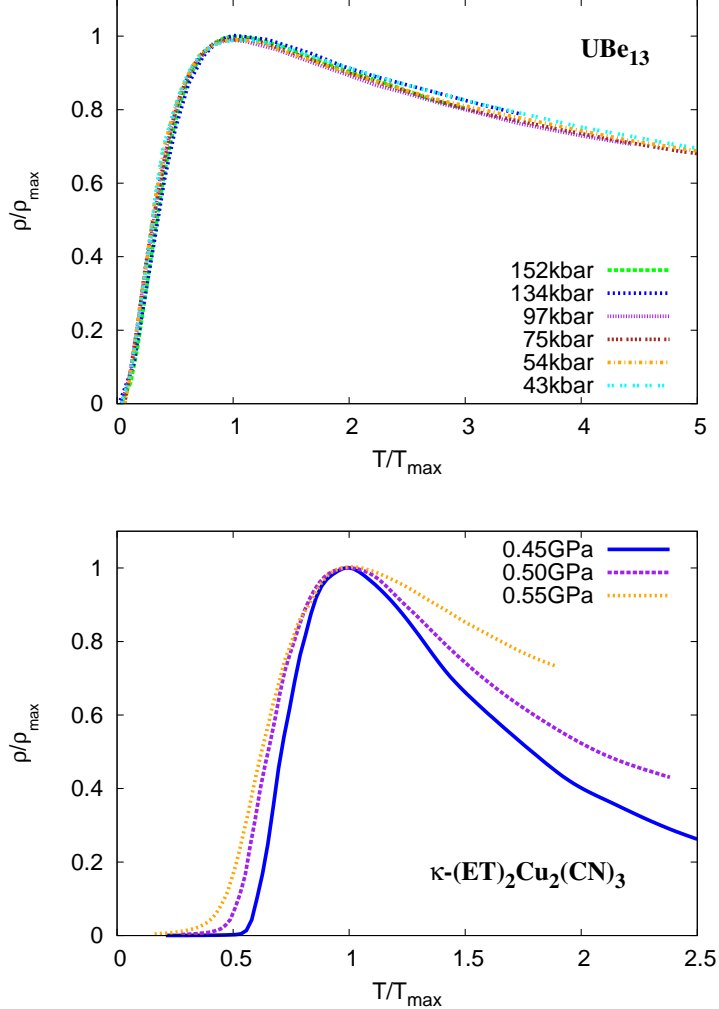


Figure 5.6: Scaled resistivity curves for  $\text{UBe}_{13}$  (upper panel) and  $\kappa\text{-(ET)}_2\text{Cu}_2(\text{CN})_3$  (lower panel), for different external pressure. The data are taken from Refs. [65, 66].

Strong temperature dependence of resistivity is well known feature of many strongly correlated materials. A pronounced resistivity maximum is observed in heavy fermions [64, 65], and charge transfer organic salts [5, 66, 53], where the correlation strength is tuned by applying an external pressure. The essential mechanism of transport in these materials relies on strong inelastic electron-electron scattering, and the Fermi liquid behavior is restricted to the lowest temperatures. As the temperature increases, the electron mean free path becomes comparable, or smaller than

the lattice spacing, and the transport becomes incoherent. The electron-phonon scattering is here much weaker than the electron-electron one. The temperature of resistivity maximum can be taken as a definition of the coherence temperature  $T^*$  [12]. It is inversely proportional to the effective mass, and much smaller than the bare Fermi temperature,  $T^* \sim (m_b/m^*)T_F$ . The same scaling ansatz as given by Eq. 5.3 was used to collapse the resistivity curves for CeCu<sub>6</sub> already in an early paper by Thompson and Fisk [64].

Here we illustrate the similarity in transport properties of these systems and 2DEG by scaling the resistivity data for heavy fermion UBe<sub>13</sub> from Ref. [65], Figure 5.6 (upper panel), and for a charge-transfer conductor  $\kappa$ -(ET)<sub>2</sub>Cu<sub>2</sub>(CN)<sub>3</sub> Figure 5.6 (lower panel). The collapse of the resistivity curves is excellent for UBe<sub>13</sub>, and well-defined trends are seen in  $\kappa$ -(ET)<sub>2</sub>Cu<sub>2</sub>(CN)<sub>3</sub>. Remarkable similarity in resistivity curves in so diverse physical systems like Si MOSFETs, GaAS heterostructures, heavy fermions and charge-transfer organic conductors, is in our view, a manifestation of the same physical processes in the vicinity of the interaction-driven MIT.

## 5.4 Scaling in the microscopic model of the interaction driven MIT

Having phenomenologically established precise and well defined scaling behavior of the experimental curves on the metallic side of the 2D MIT for temperatures near  $T^*$ , we now address its microscopic origin. More precisely, we would like to understand just how robust this result is. Does it depend on subtle details describing the interplay of disorder and interactions of 2DEG materials, as suggested in Ref. [92], or is it a generic feature of strong correlation near interaction-driven MIT. To answer this important question we deliberately focus on the simplest microscopic model for interaction-driven MIT: The clean single-band Hubbard model at half-filling. Accurate and quantitatively precise results can be obtained for temperature-dependent transport for this model within the DMFT approximation [18]. While the DMFT reproduces Fermi liquid behavior at the lowest temperatures, it is particularly useful in the studies of “high temperature” incoherent transport. Results of such calculation, obtained by the Continuous Time Quantum Monte Carlo (CTQMC) impurity solver [37, 36] followed by the analytical continuation by the Maximum Entropy Method[38], can be analyzed using precisely the same scaling procedure we proposed for experimental data. We concentrate on the metallic phase of the Hubbard model with the interaction parameter  $U$  smaller than the value at the critical end-point  $U_c$ . The resistivity curves in Figure 5.7(a) have qualitatively the same form as in 2DEG. The resistivity sharply increases with temperature, reaches a maximum and then decreases. The temperature of resistivity maximum decreases as the system approaches the MIT.

Most remarkably, precisely the same scaling form as in 2DEG is found to describe all resistivity curves close to the Mott transition [12] Figure 5.7(b). In addition, we find that the scaling parameters  $T_{max}$  and  $\rho_{max}$  again display a power law dependence on the effective mass, Figure 5.8, and even the exponents are similar. Finally, we contrast the DMFT scaling function with that obtained from 2DEG experiments. We find surprisingly accurate agreement between the DMFT prediction for the scaling function  $f(x)$  and experimental data on all available materials Figure 5.2. We emphasize, however, that our scaling hypothesis is valid only in the metallic phase for  $U < U_c$  and for temperatures comparable to  $T^* \sim 1/m^*$ . It should be contrasted with the scaling near the critical end-point  $(U_c, T_c)$  [93, 94], or the proposed quantum critical scaling in the high-temperature regime above the critical end-point [40].

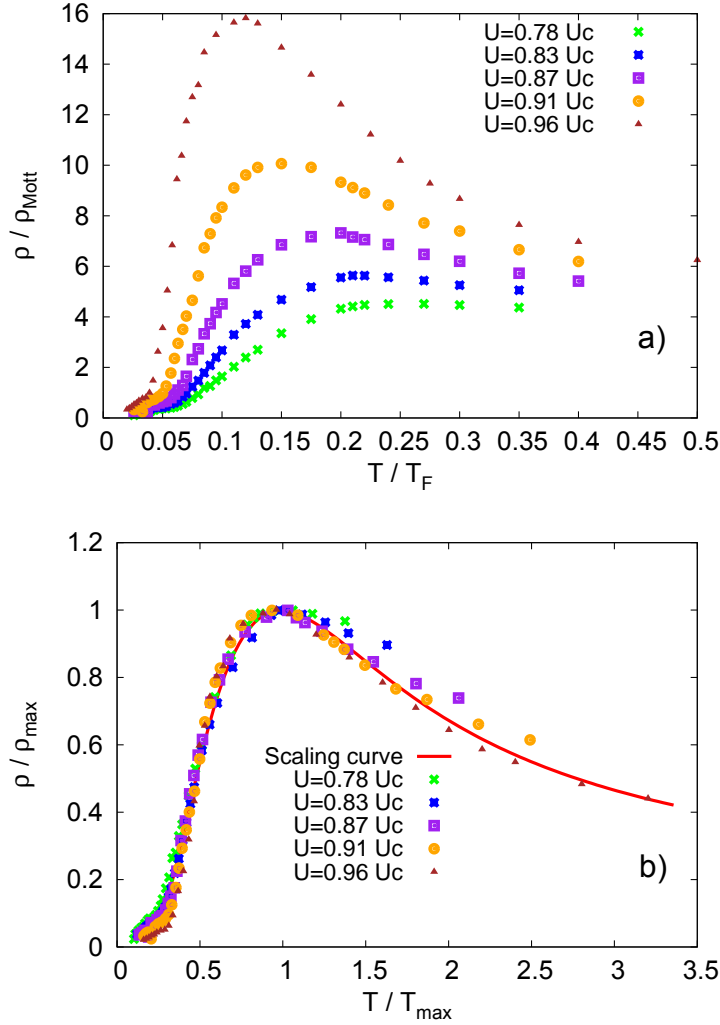


Figure 5.7: (a) Resistivity as a function of temperature for several interaction strengths in the half-filled Hubbard model solved within the DMFT. The resistivity is normalized to the Mott limit value, which corresponds to the scattering length of one lattice spacing. (b) Scaled resistivity curves.

We should point out that for this model, the proposed resistivity scaling is not valid at the lowest temperatures  $T \ll T_{\text{max}}$ , deep within the Fermi liquid region: According to the Kadowaki-Woods relation, here  $\rho \approx AT^2$  where  $A \sim 1/m^{*2} \sim 1/T_{\text{max}}^2$ , and the scaling is violated if the resistivity is scaled by  $\rho_{\text{max}}$ . For  $T \gtrsim 0.3T_{\text{max}}$  the collapse of the resistivity curves is excellent, see the Figure 5.7(b), and we define the DMFT scaling curve for this temperature range. This is also the reason of the deviations in the scaling in Figure 5.6(b) for  $\kappa$ -organics, the materials

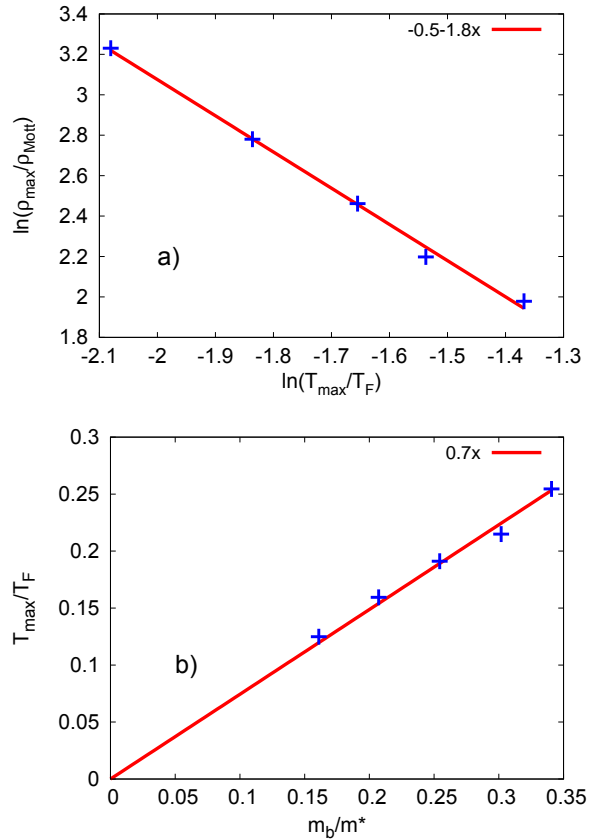


Figure 5.8: (a) Maximum resistivity as a function of the corresponding temperature from the DMFT solution of the Hubbard model. (b)  $T_{\max}$  as a function of the inverse effective mass.

whose properties are described remarkably well within the Hubbard model [5, 53]. In the Anderson lattice model, on the other hand, the resistivity maximum does not change much near the MIT and it saturates approximately to the value which corresponds to the scattering length of one lattice spacing (Mott limit). In this case our scaling ansatz is valid in the whole temperature range up  $T = 0$  [95], and the collapse of the resistivity curves seen in the experiments is excellent Figure 5.6(a).

Microscopic theory of the 2DEG should also include nonlocal correlations which are neglected in a simple DMFT approach. A more realistic extended Hubbard model displays a two-stage Wigner-Mott localization [74, 75]. The metal-insulator transition in this model is found in the region with already developed nonlocal charge correlations. In the immediate critical regime, the critical behavior can be represented by an effective Hubbard model, partially justifying the success of the present modeling. The existence of a coherence scale  $T^*$  which vanishes at the

onset of charge order is also found in the 2D extended Hubbard model solved by finite- $T$  Lanczos diagonalization [96]. This result is relevant for quarter-filled layered organic materials, which further supports the importance and generality of the ideas presented here.

## 5.5 Scaling in the model with disorder

We have already tested our phenomenological scaling on various strongly correlated systems dominated by the strong electron-electron scattering. The phenomenological scaling we have proposed is obviously the common feature of strongly correlated systems. If this is true it should hold for systems with weak or moderate disorder. We have tested our scaling procedure on the resistivity results in the presence of disorder. We have concentrate on the regime of strong disorder  $W = 2.5$ , but the physical picture is qualitatively the same as for weak or moderate disorder (see section 6.1). The same scaling hypothesis holds in this case. The main effect of

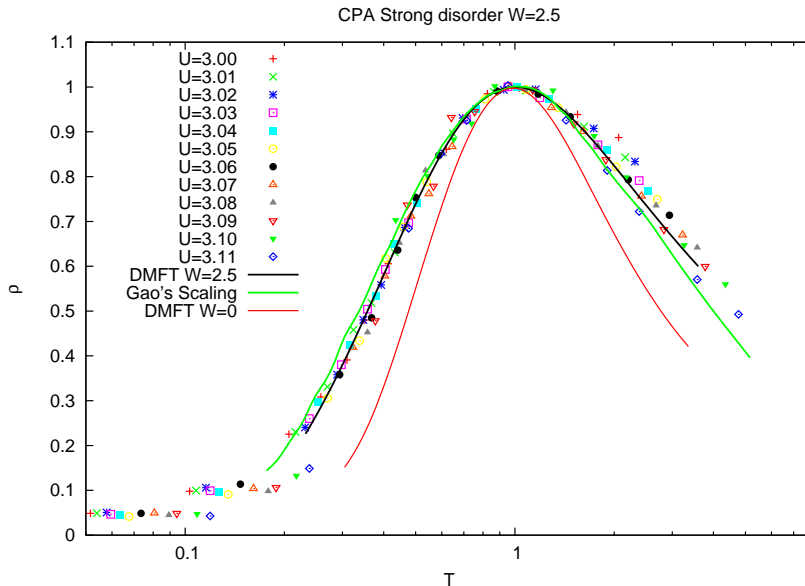


Figure 5.9: Scaled resistivity curves for several interaction strengths in the presence of disorder (dots), DMFT disordered scaling curve (black), scaling curve of experiments on disordered GaAs heterostructures [97] (green), DMFT scaling curve in the clean case (red).

disorder is the broadening of the scaling curve. Even more, our CPA-DMFT scaling curve surprisingly well coincides with the scaling curve obtained from experiments on disordered GaAs heterostructures [97].

## 5.6 Conclusion and discussion

In this Chapter we argued that the emergence of resistivity maxima upon thermal destruction of heavy Fermi liquids should be regarded as a generic phenomenon in strongly correlated systems [12]. We demonstrated that the resulting family of resistivity curves typically obeys a simple phenomenology displaying scaling behavior. Our detailed model calculations show that all the qualitative and even quantitative features of this scaling phenomenology are obtained from a microscopic model of heavy electrons close to the Mott metal-insulator transition. We should stress, however, that the proposed scaling behavior obtains - both in our theory and in experiments - only within the metallic regime not too close to the transition and the temperature regime around the resistivity maxima. In contrast, earlier experiments focused on the immediate vicinity of the metal-insulator transition, where different “quantum critical” scaling was found [81, 67, 83, 98]. Remarkably, precisely such behavior is also found in very recent studies of quantum critical transport near interaction-driven transitions [40], but this was identified in a different parameter regime than the one studied in the present chapter.

Our results provide compelling evidence that several puzzling aspects of transport in low density two-dimensional electron gases in zero magnetic fields can be understood and explained within the Wigner-Mott scenario of strong correlation [71, 72, 73, 74, 75]. This physical picture views the strong correlation effects in the low density 2DEG as the primary driving force behind the transition, and additional disorder effects as less significant, secondary processes. In the Wigner-Mott picture the insulator essentially consists of interaction-localized magnetic moments. Remarkably, magneto-capacitance measurements of Prus *et al.* [90] show that the behavior characteristic of localized magnetic moments,  $\chi(T)/n \approx g\mu_B^2/T$ , is seen near the critical density, while only weak Pauli-like temperature dependence was observed at higher density. Very recent experiments on Si MOSFETs find that the thermopower diverges near the MIT [99]. The authors argue that divergence of the thermopower is not related to the degree of disorder and reflects the divergence of the effective mass at a disorder-independent density, behavior that is typical in the vicinity of an interaction-induced phase transition. Additional hints supporting this physical picture of 2D MIT are provided by existing first principle Quantum (diffusion) Monte Carlo results for the low density 2DEG of Ceperley [100] and others [82, 101, 92]. These calculations find that the correlated metallic state has an “almost crystalline”

structure, thus having very strong short range charge-order (i.e, as seen, for example, in the density correlation function).

Within the physical picture that we propose, the inelastic electron-electron scattering takes central stage [12, 61, 102], in contrast to disorder-dominated scenarios, where the interaction effects mainly introduce temperature dependence of *elastic* electron-impurity scattering [63]. The two physical pictures describe two completely different scattering processes, which are expected to be of relevance in complementary but in essentially non-overlapping parameter regimes. Indeed, inelastic scattering dominates only outside the coherent Fermi-liquid regime, which in good metals happens only at fairly high temperatures. In strongly correlated regimes that we consider, the situation is different. Here the Fermi liquid coherence is found only at very low temperatures  $T < T^* \ll T_F$ , behavior which is generally observed in all system with appreciable effective mass enhancement. The results presented in this chapter provide precise and detailed characterization of this incoherent regime, revealing remarkable coincidence of trends observed in the experiment to those found from the Wigner-Mott picture of the interaction-driven metal-insulator transition. Our scaling ansatz is proposed based on the physical arguments and the experimental data. While consistent with simple model calculations for strongly correlated electronic systems, our work does not directly address specific microscopic mechanism responsible current dissipation, a process that in 2DEG systems should be facilitated by impurities and imperfections [102]. Still, it provides very strong motivation to develop a more realistic microscopic theory of incoherent transport in the strongly correlated regime of diluted 2DEG. This important task remains a challenge for future work.

## 6. Resistivity in strongly disordered systems near the Mott transition

The understanding of the physical processes in the regime where both the electron-electron correlations and the disorder are strong is one of the most important open problems in the modern condensed matter physics. For the case of noninteracting electrons, strong enough disorder localizes the wave functions even in three dimensions and the system becomes Anderson insulator. In the clean strongly interacting systems the electrons localize forming local moments through the interaction- or doping-driven Mott metal-insulator transition. How these processes, Anderson and Mott localization, influence each other is a very difficult physical question. It is also a very important question, specially having in mind that many strongly correlated compounds are non-stoichiometric and, therefore, intrinsically disordered systems.

In this chapter we study the disordered half-filled Hubbard model within the statistical DMFT which is a unique theoretical method that is reliable and controllable in a wide temperature, disorder and interaction range. As a reference value for disorder strength, we focus here mostly on  $W = 2.5$  in units of the half bandwidth  $D = 6t = 1$  for the noninteracting cubic lattice (site disorder  $\varepsilon_i$  is uniformly distributed in the interval  $(-W/2, W/2)$ ). This level of disorder correspond to the critical value for the Anderson localization in 3 dimensions for  $U = 0$ . The interaction, however, screens the disorder and the system is metallic for  $W = 2.5$  at small  $U$ . At large  $U$  the system faces the Mott metal-insulator transition modified by the disorder. Transport properties on the metallic side of such a metal-insulator transition are the main focus of this Chapter.

## 6.1 Coherent potential approximation in strong disorder limit

The CPA approximation displays same trends in strong disorder case ( $W = 2.5$ ), as for weak disorder, with an important difference that the coexistence region of metallic and insulating solutions is much narrower. The resistivity maximum exists very near the metal-insulator transition, and greatly exceeds the Mott-Ioffe-Regel limit  $\rho_{MIR}$  (Figure 6.1).  $\rho_{MIR}$  is again used as the unite of resistivity. For sufficiently strong interaction (larger than  $U_c = 3.16$ ) the system becomes Mott insulator. The region of interactions where the resistivity curves display maxima narrows with increasing of disorder. Similar as in the case of weak disorder, the bandwidth increases due to the disorder. The density of states, obtained using the maximum entropy analytic continuation from the imaginary axis is shown in Figure 6.2. The renormalized energy level of each site remains in the band.

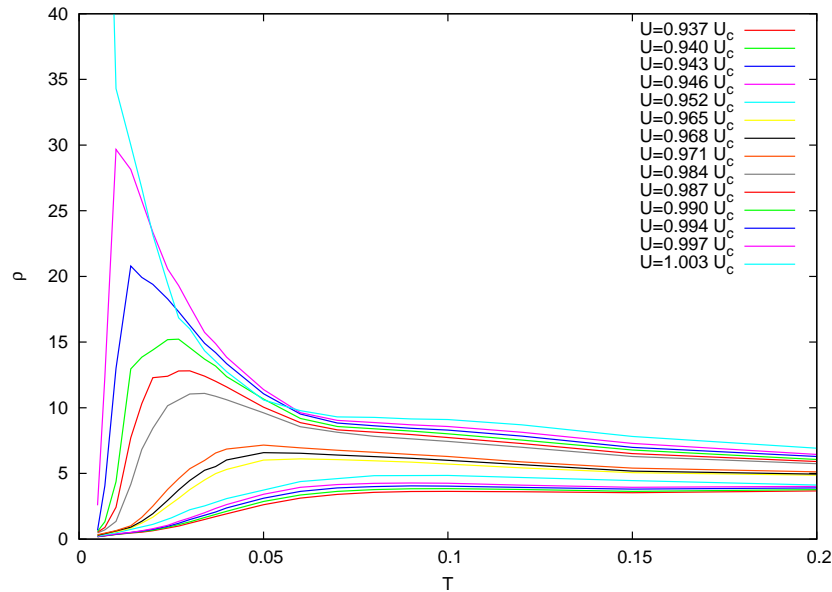


Figure 6.1: Temperature dependence of the resistivity for several interactions near the Mott transition for  $W = 2.5$ .

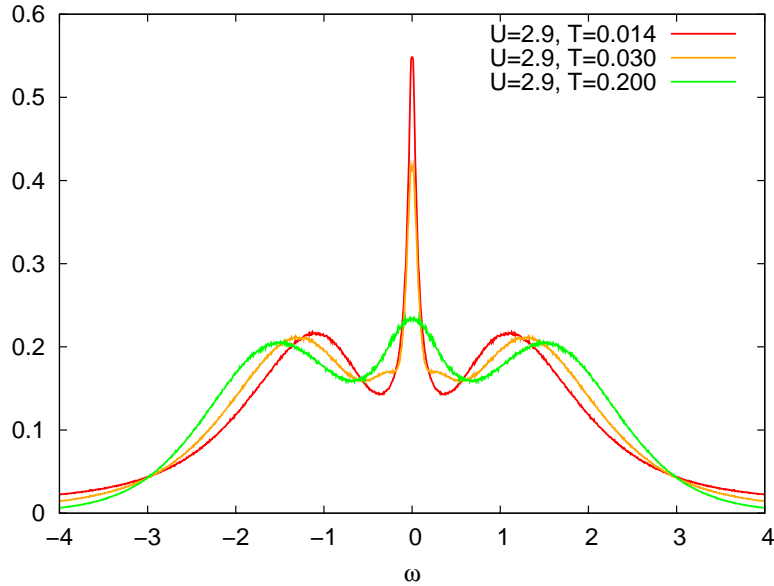


Figure 6.2: Density of states for  $W = 2.5$ ,  $U = 2.9$  and few temperatures.

## 6.2 DMFT on the finite cubic lattice

Study of the correlated electrons in strong disorder regime, requires a method capable to describe spatial fluctuations in the conduction bath, which in the limit of very strong disorder may lead even to the localization of the electron wave functions. For this purpose we use statistical DMFT (StatDMFT) which considers finite dimensional lattice. The self-energy is still local (momentum-independent) quantity, but now varies from site to site.

### 6.2.1 Finite size effects in three dimensions

To explore the finite size effects, we are solving the statistical DMFT equations for several sizes of the cubic lattice in the absence of disorder and with periodic boundary conditions. In this way we obtain the Green's functions and the self-energies on every site of the lattice which are all here equal (due to the absence of disorder). The obtained results for the lattice of the sufficient size should coincide with the DMFT solution of the infinite cubic lattice. Therefore, for a comparison, we consider also the DMFT solution using the noninteracting density of states of the three-dimensional cubic lattice. This is the only part of the StatDMFT study where we used the real axis IPT impurity solver. In the remaining part of the Chapter,

the impurity problem in StatDMFT equations are solved using the CTQMC.

Figure 6.3 (6.4) displays the imaginary part of the Green's function (self-energy) for the  $10 \times 10 \times 10$  cubic lattice compared with the same quantity for the infinite cubic lattice at low temperature  $T = 0.02$  (Fermi liquid regime). The finite size

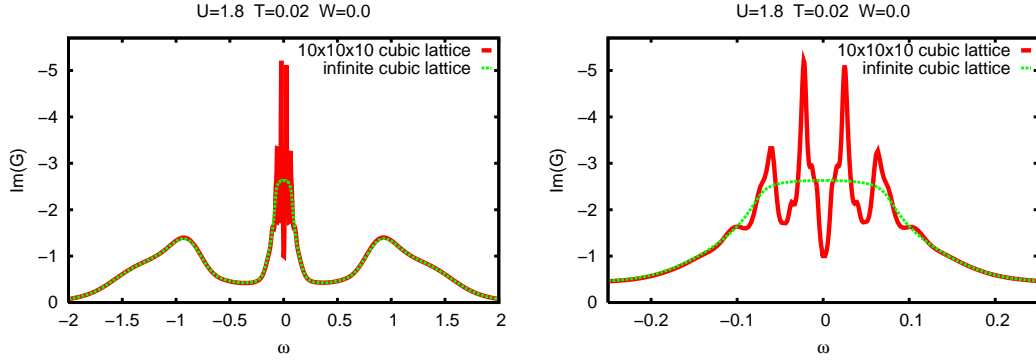


Figure 6.3: Imaginary part of Green's function for clean system ( $W = 0$ ) calculated within statistical DMFT on the cubic lattice of the size  $10 \times 10 \times 10$  (red line), and within DMFT for infinite cubic lattice (green line). Plots on the right display the quasi-particle peak, for better view.

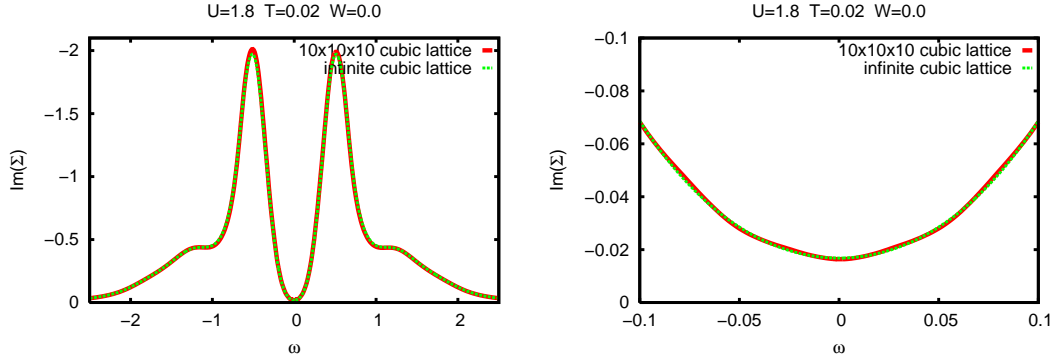


Figure 6.4: Imaginary part of self-energy for the clean system ( $W = 0$ ) calculated with the statistical DMFT on the cubic lattice of the size  $10 \times 10 \times 10$  (red line), and within DMFT for infinite cubic lattice (green line). Plots on the right display narrow region around Fermi level, for better view.

effects are clearly visible in the density of states due to the finite lattice size, which leads to the poles in the Green's function at  $T = 0$ . The finite size effects for

the self-energy are present as small oscillations, around the solution for the infinite system.

If we increase the temperature, the finite size effects decrease and become negligible for the lattices of the size  $6 \times 6 \times 6$  and larger [16]. This is due to the electron-electron scattering, which increases the imaginary part of the self-energy and broadens the peaks in the density of states, Figures 6.5 and 6.6. The tem-

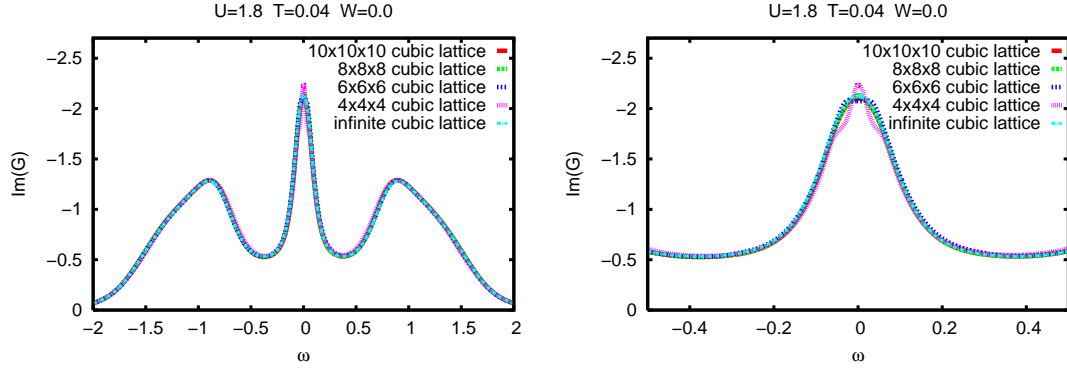


Figure 6.5: Comparison of the imaginary parts of Green's functions for clean system ( $W = 0$ ) calculated within statistical DMFT for different sizes of cubic lattices, and within DMFT for the infinite cubic lattice.

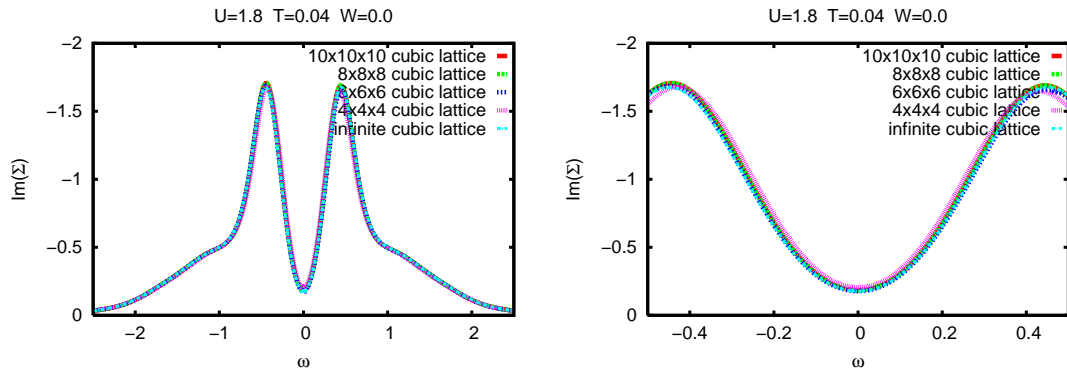


Figure 6.6: Comparison of the imaginary parts of self-energies for clean system ( $W = 0$ ) calculated within statistical DMFT for different sizes of cubic lattices, and within DMFT for the infinite cubic lattice.

perature  $T = 0.04$  used in these figures corresponds to the boundary of the Fermi liquid region for  $U = 1.8$ . Further increase of temperature drives the system into

bad metallic regime. The StatDMFT is a unique theoretical method for the study of disordered strongly correlated systems in a broad temperature range, including the incoherent regime, which is the main interest of this work.

In conclusion, we have established that the finite size effects are negligible at finite temperature, in the range of strong incoherent scattering. Concerning the finite size effects when disorder is included, they are expected to be even weaker. Intersite correlations due to disorder are explored in section 6.4.2.

## 6.3 Statistical DMFT: elastic vs. inelastic scattering

There are two types of scattering in disordered interacting electronic systems: Elastic (impurity) scattering and inelastic (electron-electron) scattering [16]. The inelastic scattering exists only at finite temperatures. Establishing the dominant scattering mechanism is crucial for the understanding of the transport properties. Quite generally, the incoherent scattering is more important near the Mott transition, except at the lowest temperatures (in the Fermi liquid regime).

The scattering rate in the CPA for  $W = 2.5$  and  $U = 2.9$  is shown in Figure 6.7. This scattering rate takes into the account both the elastic and the inelastic component. The importance of the elastic scattering can be estimated in the following way. In the non-interacting case ( $U = 0$ ) the scattering rate  $\tau_0^{-1} = -2\text{Im}\Sigma(0)$  increases quadratically with the disorder strength  $W$  [60] for small  $W$  and roughly linearly for large  $W$  (Figure 6.8). For  $W = 2.5$  this gives  $\tau_0^{-1} = 1.47$ . However, the interaction strongly renormalizes (screens) random potential [60], and the renormalized site disorder can be defined as

$$\tilde{\varepsilon}_i = \varepsilon_i + \text{Re}[\Sigma_i(0)] - \mu. \quad (6.1)$$

For  $U = 2.9$  the renormalized scattering rate is only  $\tilde{\tau}_0^{-1} = 0.07$ , which is much smaller than the total scattering in the CPA. Therefore, the role of the elastic scattering can be neglected in the remaining part of this chapter.

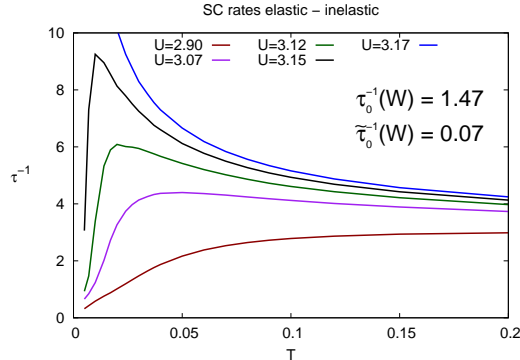


Figure 6.7: Temperature dependence of the CPA scattering rate for several interactions and for  $W = 2.5$ .  $\tau_0^{-1}$  is the elastic scattering rate for  $U = 0$  and  $\tilde{\tau}_0^{-1}$  is obtained using renormalized  $\tilde{\varepsilon}_i$  for  $U = 2.9$ .

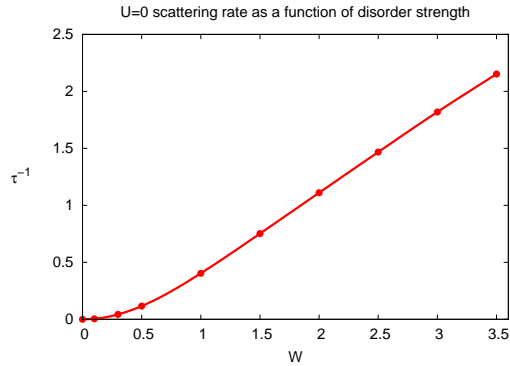


Figure 6.8: Scattering rate as a function of the disorder strength for  $U = 0$ .

## 6.4 Inter-site correlations

Exact treatment of spatial fluctuations within the StatDMFT opens possibility of developing inter-site correlations. These correlations can lead to the clustering of the sites with the strong (weak) resistivity, formation of clusters with finite magnetization or, at low temperatures to the localization of the electron wave functions (Anderson localization). Here we explore the inter-site correlations in the local resistivity.

### 6.4.1 Local resistivity

Within the statistical DMFT, there is no well established procedure for calculating the resistivity. The most rigorous approach implies the usage of the Meir-Wingreen formula in the zero bias regime and the usage of the formalism of non-equilibrium Green's functions. However, the proper application of this approach requires access to the non-equilibrium impurity solver, which development is complicated task and story for itself. To the best of our knowledge, the Meir-Wingreen formula for the interacting system at finite temperature cannot be reduced to the much simpler Landauer-like formula (which uses only the equilibrium quantities), so we need a different approach to calculate the resistivity of the lattice.

Here we will use an effective approach to calculate the lattice resistivity [16]. In order to do that, we concentrate on the local resistivity that we calculate from the standard Kubo formula in the DMFT form, using the Eq. (2.28). Figure 6.9 presents the local resistivity distribution in the lattice for the parameters  $W = 2.5$ ,  $U = 3.12$ ,

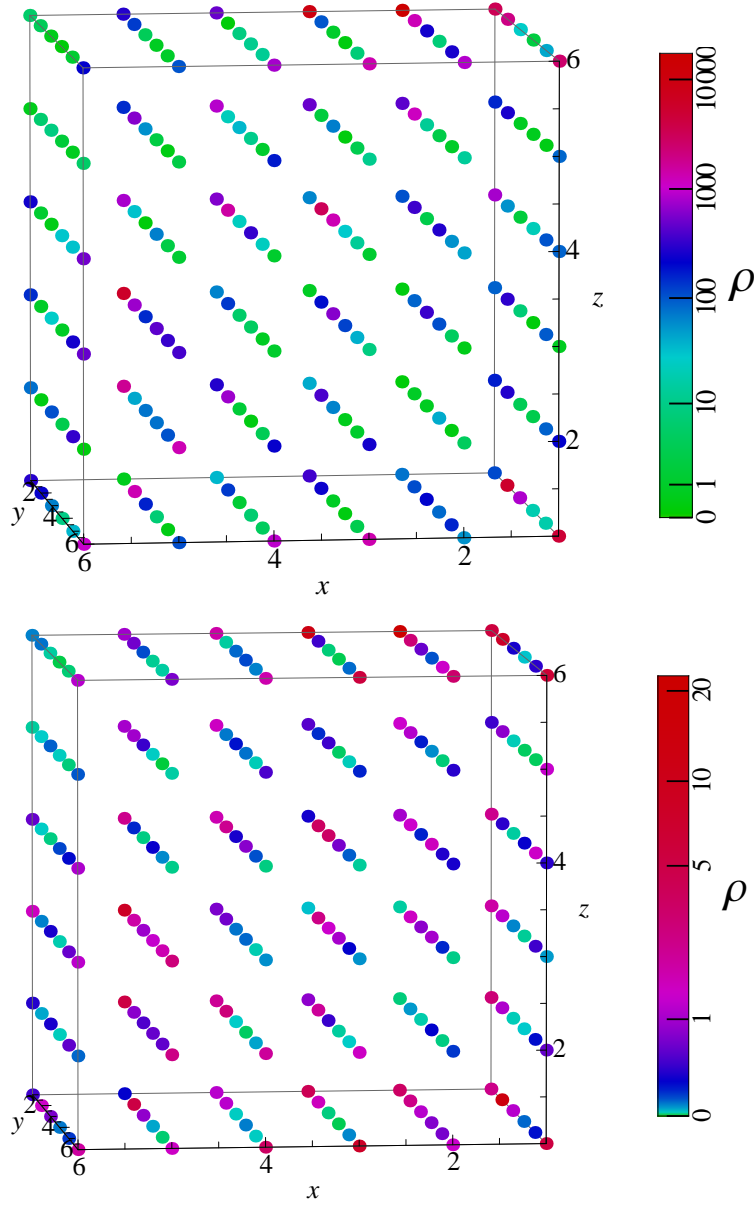


Figure 6.9: Local resistivity of the lattice for one realization of disorder and parameters  $W = 2.5$ ,  $U = 3.12$ ,  $T = 0.04$  (upper panel) and  $W = 2.5$ ,  $U = 2.90$ ,  $T = 0.007$  (lower panel).

$T = 0.04$  (upper panel) and  $W = 2.5$ ,  $U = 2.90$ ,  $T = 0.007$  (lower panel). We can see that there is no distinguished clustering of the sites with strong or weak local resistivity. This can be determined more rigorously from the correlation function.

### 6.4.2 Correlation function

Statistical dynamical mean field theory, by construction, fully includes the spatial fluctuations and allows the inter-site correlations. In order to study these correlations, we define the local resistivity correlation function in the following way

$$\chi_\rho(r_{ij}) = \langle (\rho_i - \rho_{av})(\rho_j - \rho_{av}) \rangle, \quad (6.2)$$

where  $\rho_i$  is the resistivity at the site  $i$ ,  $r_{ij}$  is the distance between sites  $i$  and  $j$  and  $\rho_{av}$  is the average local resistivity of the lattice. The correlation function assumes the exponential form

$$\chi_\rho(r_{ij}) = c \exp(-r_{ij}/\xi), \quad (6.3)$$

where  $\xi$  plays a role of the correlation length and the inequality  $\xi \lesssim 1$  holds in wide range of parameters that we explored. This result proves that the inter-site correlations are negligible [16].

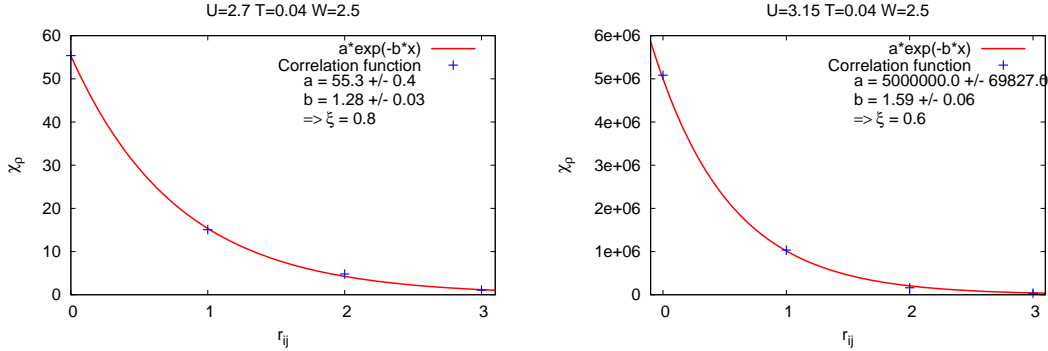


Figure 6.10: Local resistivity correlation functions for two values of the interaction  $U$ .

## 6.5 Resistivity of the lattice

There is no exact formula for calculating the lattice resistivity within the Statistical DMFT. Here we use an effective approach to this problem. We consider the lattice as a resistor network constructed from local resistivities that we have defined in the previous Section. On every link between neighboring sites  $i$  and  $j$  we place a resistor with the value of average resistance of the linked sites

$$r_{ij} = \frac{\rho_i + \rho_j}{2}. \quad (6.4)$$

Here the prefactor which includes the length of the link and its cross section is taken to be equal to 1. This construction is already used in a slightly different context [? ]. We define the resistivity of the lattice, up to the prefactor, as the equivalent resistance between the two groups of sites, where the incoming and outgoing leads are attached. The prefactor is determined to ensure the proper limit of the resistivity in the case where all the resistors have the same resistance. It corresponds to the equivalent resistance of the lattice in the case when all the resistors have the resistance equal to 1.

Following the Kirchhoff rules, the equivalent resistance can be calculated from the matrix defined by

$$A_{ij} = \begin{cases} \sum_{k \neq i} C_{ik}, & i = j \\ -C_{ij}, & i \neq j \end{cases}, \quad (6.5)$$

where  $C_{ij}$  is the conductance matrix  $C_{ij} = 1/r_{ij}$ . The equivalent resistance between two sites  $i$  and  $j$  is equal to the ratio between two minors of the determinant  $\det A$ ,

$$R_{ij} = \frac{\det A^{(ij)}}{\det A^{(j)}}, \quad (6.6)$$

where we obtain  $A^{(i)}$  by removing  $i$ -th row and column, and  $A^{(ij)}$  by removing  $i$ -th and  $j$ -th rows and columns. In order to calculate the resistivity of the lattice, we take for the contacts the short-circuited sites, where the incoming and outgoing leads are attached. This corresponds to the way that resistivity is measured in most of experiments.

### 6.5.1 Weak disorder

The CPA approximation gives a good understanding of the processes in the regime of weak disorder, when we expect that the CPA and the StatDMFT coincide. The agreement can be understood in the following way: For weak disorder, the spatial fluctuations in the local conduction bath  $\Delta_i(\omega)$  are rather small, and it is approximately equal to  $\Delta_{CPA}(\omega)$  in the CPA approximation. Therefore, the main disorder effect originates from the effective local doping which is (in the case of weak disorder) well captured by the CPA. Roughly speaking, the local doping causes a shift of the Hubbard bands in the local density of states (LDOS), while the quasiparticle peak remains at the Fermi level. Another consequence of doping is the decrease of the inelastic scattering rate due to changes in the local occupation number (electron-electron scattering is the strongest at half-filling and goes to zero for unoccupied and doubly occupied sites).

Concerning weakly doped sites, we should keep in mind that the system is in the vicinity of the Mott transition, thus the inelastic scattering rate is significantly enhanced on these sites and the quasiparticle peak (if exists) is very narrow. This causes larger local resistivity than for strongly doped (weakly correlated) sites. One has to keep in mind that we concentrate on the temperature region  $T \gtrsim T_{FL}$ , where transport is dominated by the electron-electron scattering.

### 6.5.2 Strong disorder

Increase of the disorder leads to the qualitative difference between the CPA and statistical DMFT. The reason for such behavior is in the spatial fluctuations in  $\Delta_i(\omega)$  which become much more pronounced in this case. The fluctuations in the local bath are larger due to the wider on-site energy distribution. This leads to the deviation of the local resistivity (obtained within StatDMFT) from the CPA curves, Figure 6.11. Very close to the Mott transition, Figure 6.11 (lower panel), these fluctuations can even switch some site from being metallic to insulating, or in other words, to open a gap in the local density of states at the Fermi level. This influences the abrupt changes in the local resistivity.

The temperature dependence of the resistivity of the lattice calculated using the resistor network method is shown in Figure 6.12. We have chosen two maximally distant plains of 36 sites each as the spots where we attach the leads [16]. Because

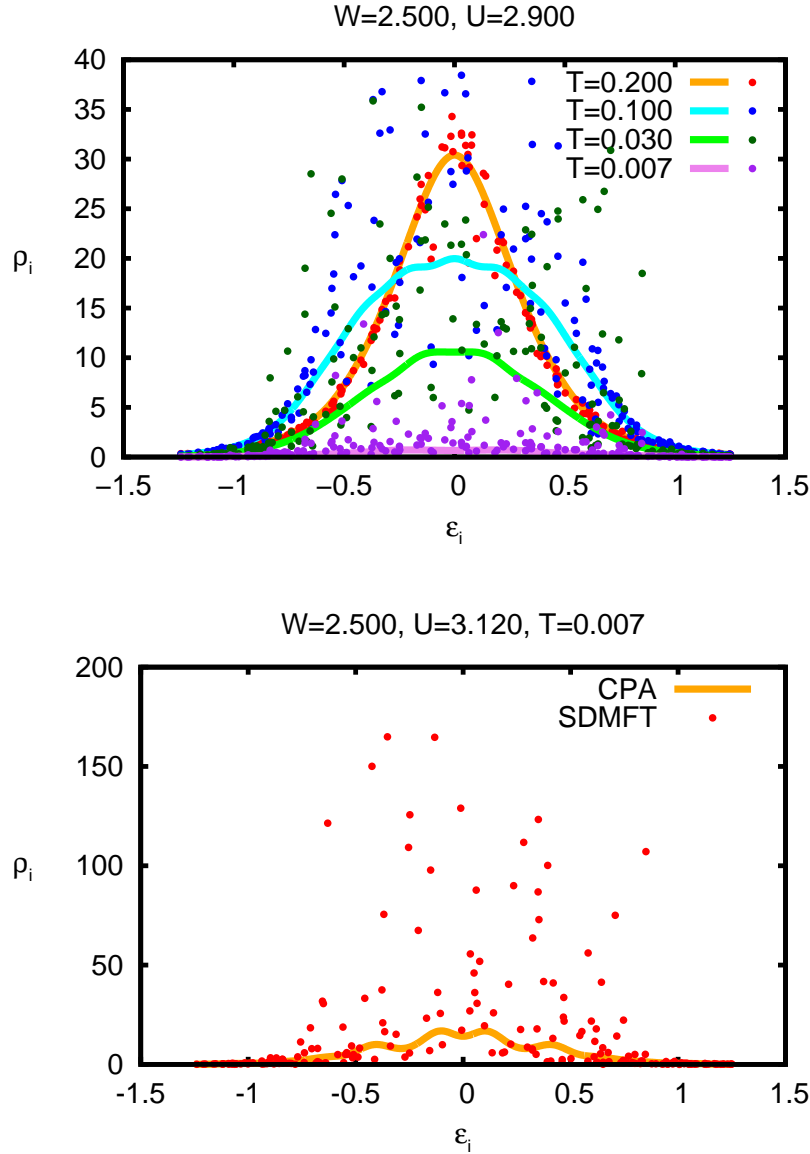


Figure 6.11: Comparison of CPA and StatDMFT local resistivity at several temperatures for strong disorder ( $W = 2.5$ ) and interaction  $U = 0.918 U_c$  (upper panel) and the same comparison at low temperature  $T = 0.007$  for interaction very close to critical  $U = 0.987 U_c$  (lower panel).

of the periodic boundary conditions that distance is three lattice spacing. We have checked that the result is not sensitive to the particular positioning of the leads. The resistivity maxima are few times lower than in the CPA (for the same parameters) and arises at higher temperatures. Also the maxima are wider and the metallic phase

persists for stronger interactions as compared to the CPA. It remains to be precisely determined what is the critical interaction  $U_c$  for the metal-insulator transition. Also it appears that the lattice resistivity saturates to a larger value at  $T = 0$  very near the Mott transition than in the CPA case.

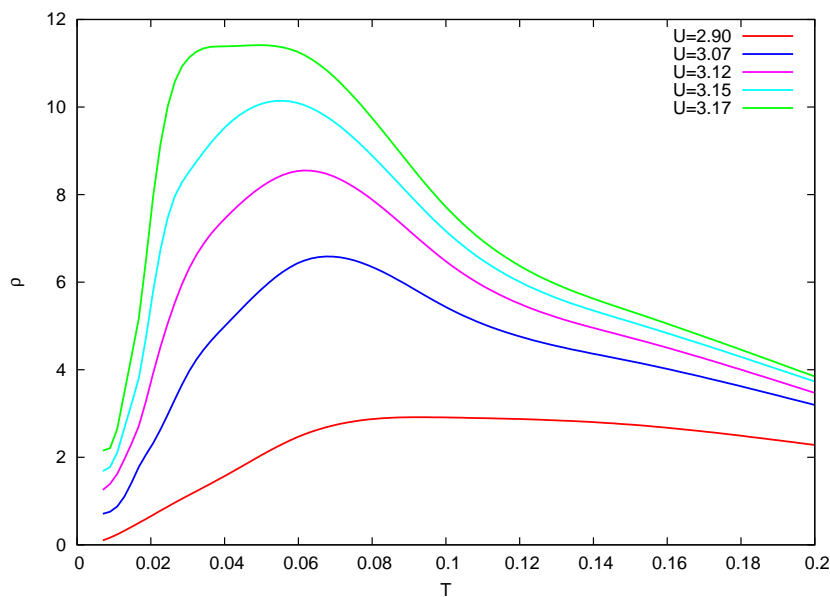


Figure 6.12: Temperature dependence of the resistivity for  $W = 2.5$ , for several interaction strengths.

### 6.5.3 Strongly and weakly correlated sites

It is interesting to explore the local resistivity  $\rho_i$  and the local occupation number  $n_i$  as a function of the on-site energy  $\varepsilon_i$ . Figure 6.13 displays  $\rho_i$  vs.  $\varepsilon_i$  and  $n_i$  vs.  $\varepsilon_i$  for  $U = 2.90$  (upper panel) and  $U = 3.15$  (lower panel). The curve  $n(\varepsilon_i)$  is a smoothed spline through actual data (which do not fluctuate much). This plot suggests that we can distinguish two groups of sites: Strongly correlated (sc), close to half-filling, and weakly correlated (wc). The local quasiparticle weight

$$Z_i = \frac{1}{1 - \frac{\partial}{\partial \omega} \text{Im} \Sigma_i(i\omega)} \Big|_{\omega \rightarrow 0} \quad (6.7)$$

is much smaller at the weakly correlated sites, Figure 6.14.

We also notice that the range of the on-site energies, where the bath spatial fluctuations are dominant, is expanding with increase of temperature until it becomes comparable to the Kondo temperature [16] and this is the most clearly seen very close to the transition (Figure 6.13, lower panel). The local resistivity calculated within StatDMFT deviates from the CPA for the largest local doping at Kondo temperature. This is the same temperature where the resistivity curves (Figure 6.12) reach their maximum. Further increase of the temperature opens pseudo gap in LDOS on every site and smears the spatial fluctuations in the bath. The on-site energy region of dominant spatial fluctuations is then narrowing and finally the StatDMFT data approaches to the CPA.

Figure 6.16 illustrates the temperature dependence of the local resistivity for these two groups of sites. We have geometrically averaged the resistivity of *sc* and *wc* sites, and compared with the geometrical average of all sites and with the lattice resistivity calculated using the resistor network approach. Striking feature is that the resistivity of weakly correlated sites is almost temperature independent, except at the lowest temperatures, where the disorder screening due to the interaction is strong [60], while the strongly correlated sites display very strong temperature dependence. The typical average of the local resistivity including all sites qualitatively follows the calculated lattice resistivity.

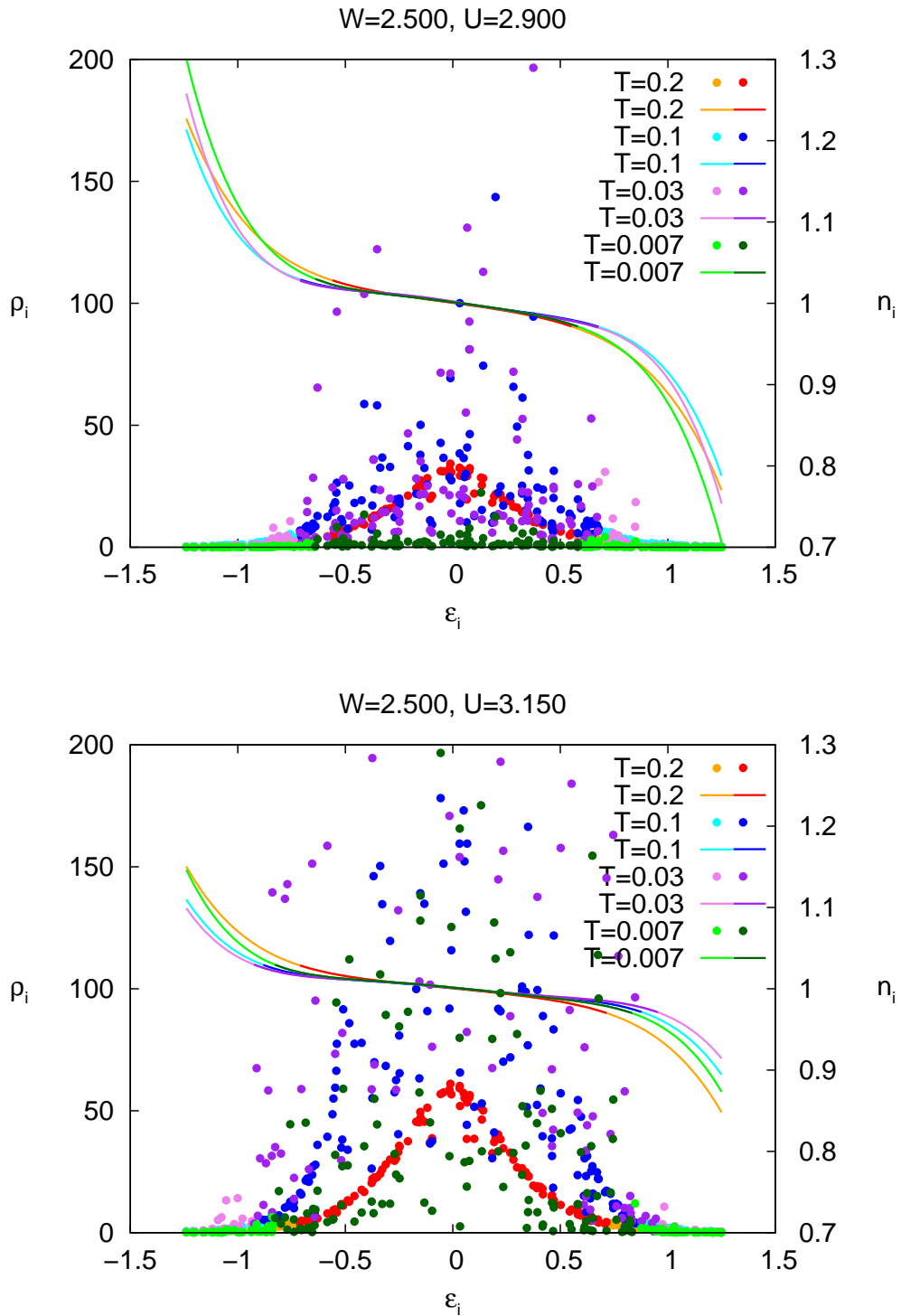


Figure 6.13: Local resistivity and occupation number distributions of on-site energy at few temperatures.

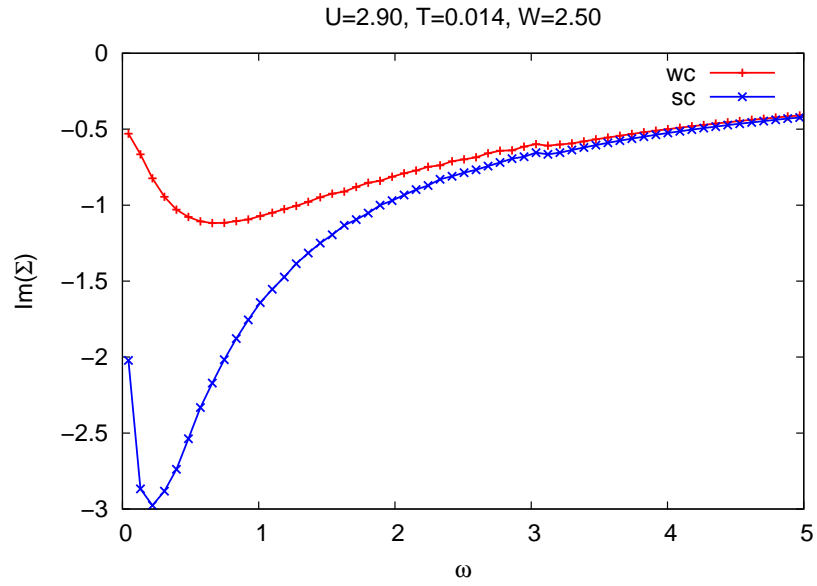


Figure 6.14: Imaginary parts of self-energies of a typical weakly (wc) and strongly correlated (sc) site.

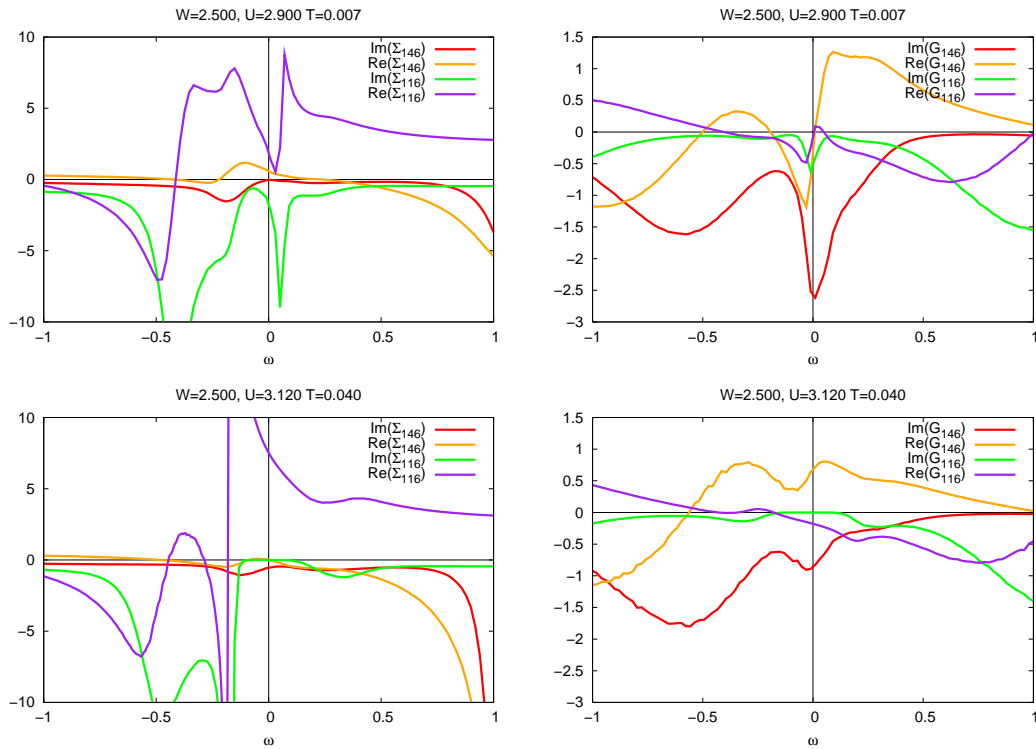


Figure 6.15: Green's functions and self-energies for an insulating and a conducting site.

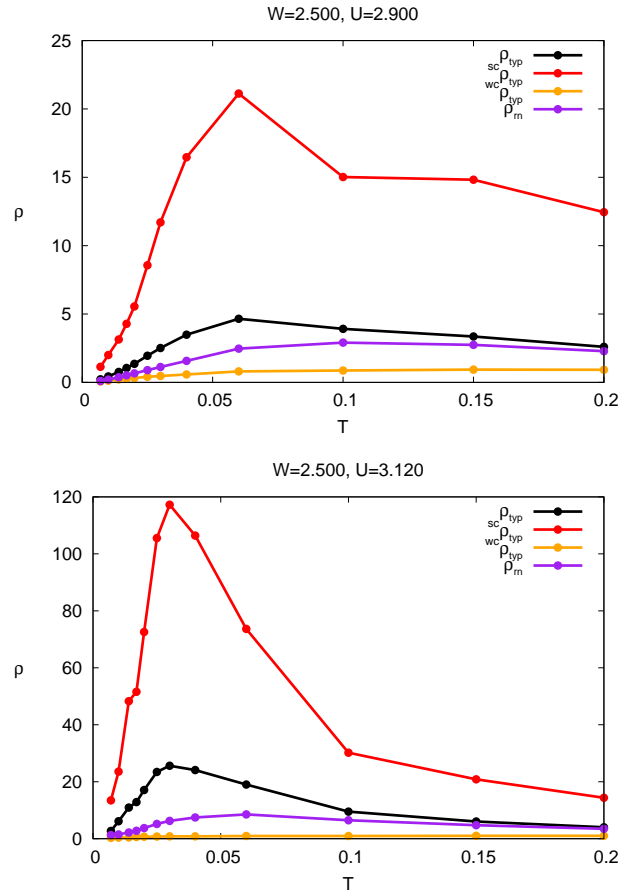


Figure 6.16: Geometrically averaged (typical) local resistivity for strongly correlated (sc), weakly correlated (wc) and all sites together, and the resistivity  $\rho_{rn}$  of the lattice calculated using the resistor network method.

## 6.6 Summary and open questions

We have successfully applied for the first time the Statistical DMFT method on the finite size cubic lattice. We used the real axis IPT impurity solver to determine the importance of the finite size effects, by concentrating on the clean lattice of the size up to  $10 \times 10 \times 10$ . We determined that the finite size effects are negligible already on the lattice  $6 \times 6 \times 6$  (except at the lowest temperatures, deep in the Fermi liquid regime).

Then we concentrated on a single realization of disorder on the lattice  $6 \times 6 \times 6$  using the CTQMC as the impurity solver, and the analytical continuation by the maximum entropy method in order to obtain local quantities on the real frequency axis. We confirmed that the disorder is strongly screened on the metallic side of the Mott MIT and that the inelastic scattering is dominant at temperatures  $T > T_{FL}$ . We defined a local resistivity and proposed a resistor network method for calculating the dc resistivity. This approach is justified by the observation that the inter-site correlations are very weak and that the incoherent scattering is dominant. We identified two types of sites: strongly correlated with the local occupation close to 1, and weakly correlated away from local half-filling. Non-monotonic temperature dependence in the resistivity originates from strong temperature dependence of the local resistivity on strongly correlated sites.

It remains to explore the critical region very near the MIT transition more closely. There are indications that some sites Mott localize in this regime, while the system is still overall metallic. Also, it is important to investigate the solution of the model in the presence of even stronger disorder, where one might expect a two-fluid behavior where a fraction of sites becomes Anderson localized. The solution of the model in two dimensions, where the spatial fluctuations are stronger, may reveal new interesting features as well.

## 7. Conclusion

In this thesis we have examined the influence of disorder on the strongly correlated systems in a wide range of parameters, in the vicinity of the Mott transition. The disorder is modeled by the random potential (uniform distribution of the on-site energies) introduced into half-filled Hubbard model. The solutions are obtained within dynamical mean field theory and its extensions.

In the weakly disordered case we used the coherent potential approximation, which assumes the averaging of the local Green's functions over the on-site energy distribution. Our focus was to understand the consequences of the presence of inhomogeneities onto the optical conductivity and the dc resistivity. The main effects captured within the CPA are the increasing of metallicity of the system with disorder while the interaction is kept constant. The disorder increases the bandwidth, which leads to the increase of the critical interaction  $U_c$ , where the Mott transition occurs. For fixed interaction  $U$  this effectively weakens the electron-electron correlations and causes the decrease of the scattering rate, and dc resistivity. The same effect of restoring metallicity with disorder was observed in the experiments on organic charge-transfer salts. Disorder in this experiments was tuned by the X-ray irradiation. We emphasize that the randomness in our model does not change the global doping, as the system remains on average half-filled. However, locally half-filling is not preserved. This provides another view to the explanation of the observations seen in these experiments. We also find that the maximal possible value of the resistivity greatly exceeds (more than an order of magnitude) the quasi-classical Mott-Ioffe-Regel limit for maximal metallic resistivity even in the presence of moderate disorder. As in the clean case, the violation of the MIR limit is driven by a large scattering rate due to the electron-electron scattering. Interestingly, the Drude-like peak in the optical conductivity persists even at temperatures when the resistivity is well beyond the MIR limit.

The same trends in the resistivity curves are present in a totally different group

---

of materials - diluted two dimensional electron gases in Si MOSFETs and GaAs heterostructures. The Coulomb interaction in these materials can easily be tuned by changing concentration of carriers. There were a number of theoretical proposals that suggested the decisive influence of disorder to the transport properties of these materials. However, all these theoretical attempts failed to describe observed effects in a wide range of concentrations, while their application in the high temperature regime is questionable. We have proposed a phenomenological scaling of the metallic curves based on the insight obtained from the study of various strongly correlated systems. By testing the scaling ansatz on several classes of strongly correlated materials and the half-filled Hubbard model (in disordered and clean case), we have established that the emergence of resistivity maxima upon thermal destruction of heavy Fermi liquids should be regarded as a generic phenomenon in strongly correlated systems. From the fact that the same scaling works very well for different two-dimensional electron gases in a wide range of concentrations (practically for all metallic curves near the transition), we conclude that the strong electron correlations in the incoherent regime are the primary driving force behind the metal-insulator transition and that additional disorder effects are less significant. Moreover, we have documented that practically all main signatures of the strongly correlated systems are present in these experiments, and that the critical behavior of the crossover (coherence) scale  $T^*$  in both two dimensional diluted electron gases and strongly correlated systems (experimental and theoretical) is basically the same. Despite that we have not included all microscopic aspects of the 2DEG, our analysis presents compelling evidences that the strong inelastic electron-electron scattering and not disorder is the driving force behind the unusual transport properties, advocating a Wigner-Mott scenario for the metal-insulator transition in these systems.

In order to investigate the systems in strong disorder regime, the spatial fluctuations must be treated properly. For this purpose, we employ the statistical dynamical mean field theory to solve the disordered half-filled Hubbard model for the first time at finite temperatures. This method treats the spatial fluctuations on the finite dimensional lattice while keeping only the local part of correlations. The CPA and StatDMFT approaches approximately coincide in the regime of weak disorder. The elastic (impurity) scattering is strongly screened near the Mott transition and the inelastic (electron-electron) scattering is dominant in the regime of our interest ( $T \gtrsim T_{FL}$ ). We have also documented that the finite size effects, are negligible in this case. The inter-site correlations in the system are weak due to the relatively

---

large coordination number ( $z = 6$ ) in three dimensional cubic lattice. Spatial fluctuations in the local bath greatly influence electron properties in the very vicinity of the Mott transition in the strong disorder regime. The local resistivity analysis showed that two groups of sites emerge. One group consists of strongly correlated sites which are close to half-filling and with the strong temperature dependence of the local resistivity, and the other group of weakly correlated sites which are shifted from half-filling and display weak temperature dependence of the resistivity. Finally, since there is no established exact way of calculating the lattice resistivity within the StatDMFT, we proposed an effective approach. We constructed the resistor network from the local resistivities and calculated the equivalent resistance between the sites where the leads are attached. The maxima in the resistivity calculated in this way are few times lower than in the CPA and the peak in the resistivity vs. temperature curve is not as pronounced as in the clean case, or in the CPA approximation. There are signatures of two fluid behavior near the Mott transition, where a fraction of the sites are localized, while the system is overall still metallic. This remains to be more carefully explored in the future work and particularly for the case of even stronger disorder. Also, an important direction for future work is to explore the two dimensional systems where the spatial fluctuations can have more dramatic consequences.

# References

- [1] Masatoshi Imada, Atsushi Fujimori, and Yoshinori Tokura, *Metal-insulator transitions*, Rev. Mod. Phys. **70**, 1039–1263 (1998). 1
- [2] D. N. Basov and T. Timusk, *Electrodynamics of high- $T_c$  superconductors*, Rev. Mod. Phys. **77**, 721–779 (2005). 1
- [3] Elbio Dagotto, *Colloquium: The unexpected properties of alkali metal iron selenide superconductors*, Rev. Mod. Phys. **85**, 849–867 (2013). 1
- [4] G. R. Stewart, *Superconductivity in iron compounds*, Rev. Mod. Phys. **83**, 1589–1652 (2011). 1
- [5] P. Limelette, P. Wzietek, S. Florens, A. Georges, T. A. Costi, C. Pasquier, D. Jérôme, C. Mézière, and P. Batail, *Mott Transition and Transport Crossovers in the Organic Compound  $\kappa$ -(BEDT-TTF) $_2$ Cu[N(CN) $_2$ ]Cl*, Phys. Rev. Lett. **91**, 016401 (2003). 1, 2, 3, 33, 39, 43, 48, 54, 58
- [6] Jaime Merino and Ross H. McKenzie, *Transport properties of strongly correlated metals: A dynamical mean-field approach*, Phys. Rev. B **61**, 7996 (2000). 1, 19, 33
- [7] G. R. Stewart, *Non-Fermi-liquid behavior in  $d$ - and  $f$ -electron metals*, Rev. Mod. Phys. **73**, 797–855 (2001). 1
- [8] Chetan Nayak, Steven H. Simon, Ady Stern, Michael Freedman, and Sankar Das Sarma, *Non-Abelian anyons and topological quantum computation*, Rev. Mod. Phys. **80**, 1083–1159 (2008). 1
- [9] X. Y. Zhang, M. J. Rozenberg, and G. Kotliar, *Mott transition in the  $d = \infty$  Hubbard model at zero temperature*, Phys. Rev. Lett. **70**, 1666–1669 (1993). 2, 7, 13

- 
- [10] J. Vučićević, H. Terletska, D. Tanasković, and V. Dobrosavljević, *Finite-temperature crossover and the quantum Widom line near the Mott transition*, Phys. Rev. B **88**, 075143 (2013). 2, 19
- [11] Miloš M. Radonjić, D. Tanasković, V. Dobrosavljević, and K. Haule, *Influence of disorder on incoherent transport near the Mott transition*, Phys. Rev. B **81**, 075118 (2010). 3, 34, 36, 39, 42
- [12] M. M. Radonjić, D. Tanasković, V. Dobrosavljević, K. Haule, and G. Kotliar, *Wigner-Mott scaling of transport near the two-dimensional metal-insulator transition*, Phys. Rev. B **85**, 085133 (2012). 3, 44, 47, 48, 55, 56, 61, 62
- [13] V. Dobrosavljević, *Introduction to Metal-Insulator Transitions*, pre-print (2011). 3
- [14] E. Miranda and V. Dobrosavljević, *Dynamical mean-field theories of correlation and disorder*, pre-print (2011). 3
- [15] V. Dobrosavljević, N. Trivedi, and J. M. Valles, Jr., *Conductor-Insulator Quantum Phase Transitions*, Oxford University Press (2012). 3, 6
- [16] M. M. Radonjić, J. Vučićević, D. Tanasković, V. Dobrosavljević, K. Haule, and G. Kotliar, *Transport in strongly disordered Mott systems - Statistical DMFT study*, pre-print (2014). 3, 67, 69, 70, 72, 74, 77
- [17] Elliott H. Lieb and F.Y. Wu, *The one-dimensional Hubbard model: a reminiscence*, Physica A: Statistical Mechanics and its Applications **321**(1–2), 1 – 27 (2003), Statphys-Taiwan-2002: Lattice Models and Complex Systems. 4, 6
- [18] Antoine Georges and Gabriel Kotliar, *Dynamical mean-field theory of strongly correlated fermion systems and the limit of infinite dimensions*, Rev. Mod. Phys. **68**, 13 (1996). 4, 6, 7, 17, 56
- [19] Martin C. Gutzwiller, *Effect of Correlation on the Ferromagnetism of Transition Metals*, Phys. Rev. Lett. **10**, 159–162 (1963). 5
- [20] J. Hubbard, *Electron Correlations in Narrow Energy Bands*, Proceedings of the Royal Society of London. Series A. Mathematical and Physical Sciences **276**(1365), 238–257 (1963). 5

- 
- [21] Gabriel Kotliar, Sergej Y. Savrasov, Gunnar Pálsson, and Giulio Biroli, *Cellular Dynamical Mean Field Approach to Strongly Correlated Systems*, Phys. Rev. Lett. **87**, 186401 (2001). 6
- [22] Thomas Maier, Mark Jarrell, Thomas Pruschke, and Matthias H. Hettler, *Quantum cluster theories*, Rev. Mod. Phys. **77**, 1027–1080 (2005). 6
- [23] G. Sordi, P. Sémon, and A.-M.S. Tremblay, *Pseudogap temperature as a Widom line in doped Mott insulators*, Scientific Reports **2**, 547 (2012). 6
- [24] K. Haule, J. H. Shim, and G. Kotliar, *Correlated Electronic Structure of  $LaO_{1-x}F_xFeAs$* , Phys. Rev. Lett. **100**, 226402 (2008). 6
- [25] M. J. Han, Xin Wang, C. A. Marianetti, and A. J. Millis, *Dynamical Mean-Field Theory of Nickelate Superlattices*, Phys. Rev. Lett. **107**, 206804 (2011). 6
- [26] Martin Eckstein Marcus Kollar Takashi Oka Philipp Werner Hideo Aoki, Naoto Tsuji, *Nonequilibrium dynamical mean-field theory and its applications*, arXiv:1310.5329 (2013). 6
- [27] V. Dobrosavljević and G. Kotliar, *Mean field theory of the Mott-Anderson transition*, Phys. Rev. Lett. **78**, 3943 (1997). 6, 22, 33
- [28] Walter Metzner and Dieter Vollhardt, *Correlated Lattice Fermions in  $d = \infty$  Dimensions*, Phys. Rev. Lett. **62**, 324–327 (1989). 7
- [29] Piers Coleman, *Introduction to Many Body Physics*, Cambridge University Press (2012). 9
- [30] J. Hubbard, *Electron Correlations in Narrow Energy Bands. III. An Improved Solution*, Proceedings of the Royal Society of London. Series A. Mathematical and Physical Sciences **281**(1386), 401–419 (1964). 10, 15
- [31] P. W. Anderson, *Localized Magnetic States in Metals*, Phys. Rev. **124**, 41–53 (1961). 13
- [32] Gabriel Kotliar and Andrei E. Ruckenstein, *New Functional Integral Approach to Strongly Correlated Fermi Systems: The Gutzwiller Approximation as a Saddle Point*, Phys. Rev. Lett. **57**, 1362–1365 (1986). 13

- 
- [33] N. Grewe and H. Keiter, *Diagrammatic approach to the intermediate-valence compounds*, Phys. Rev. B **24**, 4420–4444 (1981). 13, 14
- [34] K. Haule, S. Kirchner, J. Kroha, and P. Wölfle, *Anderson impurity model at finite Coulomb interaction  $U$ : Generalized noncrossing approximation*, Phys. Rev. B **64**, 155111 (2001). 13, 14
- [35] J. E. Hirsch and R. M. Fye, *Monte Carlo Method for Magnetic Impurities in Metals*, Phys. Rev. Lett. **56**, 2521–2524 (1986). 14
- [36] Kristjan Haule, *Quantum Monte Carlo impurity solver for cluster dynamical mean-field theory and electronic structure calculations with adjustable cluster base*, Phys. Rev. B **75**, 155113 (2007). 14, 56
- [37] Philipp Werner, Armin Comanac, Luca de’ Medici, Matthias Troyer, and Andrew J. Millis, *Continuous-Time Solver for Quantum Impurity Models*, Phys. Rev. Lett. **97**, 076405 (2006). 14, 56
- [38] M. Jarrell and J. E. Gubernatis, *Bayesian inference and the analytic continuation of imaginary-time quantum Monte Carlo data*, Physics Reports **269**, 133 (1996). 14, 56
- [39] Gabriel Kotliar and Dieter Vollhardt, *Strongly correlated materials: Insights from dynamical mean-field theory*, Print edition **57**(3) (2004). 18
- [40] H. Terletska, J. Vučičević, D. Tanasković, and V. Dobrosavljević, *Quantum Critical Transport near the Mott Transition*, Phys. Rev. Lett. **107**, 026401 (2011). 19, 56, 61
- [41] Abhay N. Pasupathy, Aakash Pushp, Kenjiro K. Gomes, Colin V. Parker, Jinsheng Wen, Zhijun Xu, Genda Gu, Shimpei Ono, Yoichi Ando, and Ali Yazdani, *Electronic Origin of the Inhomogeneous Pairing Interaction in the High- $T_c$  Superconductor  $Bi_2Sr_2CaCu_2O_{8+\delta}$* , Science **320**, 196 (2008). 20
- [42] James G. Analytis, Arzhang Ardavan, Stephen J. Blundell, Robin L. Owen, Elspeth F. Garman, Chris Jeynes, and Ben J. Powell, *Effect of Irradiation-Induced Disorder on the Conductivity and Critical Temperature of the Organic Superconductor  $\kappa$ -(BEDT-TTF) $_2$ Cu(SCN) $_2$* , Phys. Rev. Lett. **96**, 177002 (2006). 21, 33, 39, 40

- 
- [43] E. Miranda and V. Dobrosavljević, *Disorder-Driven Non-Fermi Liquid Behavior of Correlated Electrons*, Rep. Prog. Phys. **68**, 2337 (2005). 22
- [44] M. S. Laad, L. Craco, and E. Müller-Hartmann, *Effect of strong correlations and static diagonal disorder in the  $d=\infty$  Hubbard model*, Phys. Rev. B **64**, 195114 (2001). 22, 33
- [45] V. Dobrosavljević, A. A. Pastor, and Branislav K. Nikolić, *Typical medium theory of Anderson localization: A local order parameter approach to strong disorder effects*, Europhys. Lett. **62**, 76 (2003). 22, 28, 33
- [46] Krzysztof Byczuk, Walter Hofstetter, and Dieter Vollhardt, *Mott-Hubbard Transition versus Anderson Localization in Correlated Electron Systems with Disorder*, Phys. Rev. Lett. **94**, 056404 (2005). 22, 33
- [47] R. Vlaming and D. Vollhardt, *Controlled mean-field theory for disordered electronic systems: Single-particle properties*, Phys. Rev. B **45**, 4637–4649 (1992). 25
- [48] B. J. Powell and Ross H. McKenzie, *Strong electronic correlations in superconducting organic charge transfer salts*, J. Phys.: Condens. Matter **18**, R827 (2006). 33
- [49] O. Gunnarsson, M. Calandra, and J. E. Han, *Colloquium: Saturation of electrical resistivity*, Rev. Mod. Phys. **75**, 1085 (2003). 33, 38
- [50] M. Calandra and O. Gunnarsson, *Saturation of Electrical Resistivity in Metals at Large Temperatures*, Phys. Rev. Lett. **87**, 266601 (2001). 33
- [51] M. B. Allen, *Metals with small electron mean-free path: saturation versus escalation of resistivity*, Physica B **318**, 24 (2002). 33
- [52] N. E. Hussey, K. Takenaka, and H. Takagi, *Universality of the Mott-Ioffe-Regel limit in metals*, Philos. Mag. **84**, 2847 (2004). 33, 38
- [53] J. Merino, M. Dumm, N. Drichko, M. Dressel, and Ross H. McKenzie, *Quasiparticles at the Verge of Localization near the Mott Metal-Insulator Transition in a Two-Dimensional Material*, Phys. Rev. Lett. **100**, 086404 (2008). 33, 38, 39, 43, 54, 58

- 
- [54] T. Sasaki, H. Oizumi, N. Yoneyama, N. Kobayashi, and N. Toyota, *X-ray Irradiation-Induced Carrier Doping Effects in Organic Dimer-Mott Insulators*, J. Phys. Soc. Jpn. **76**, 123701 (2007). 33, 39
- [55] T. Sasaki, N. Yoneyama, Y. Nakamura, N. Kobayashi, Y. Ikemoto, T. Moriwaki, and H. Kimura, *Optical Probe of Carrier Doping by X-Ray Irradiation in the Organic Dimer Mott Insulator  $\kappa$ -(BEDT-TTF)<sub>2</sub>Cu[N(CN)<sub>2</sub>]Cl*, Phys. Rev. Lett. **101**, 206403 (2008). 33, 39, 42
- [56] M. C. Aguiar, V. Dobrosavljević, E. Abrahams, and G. Kotliar, *Effects of disorder on the non-zero temperature Mott transition*, Phys. Rev. B **71**, 205115 (2005). 36
- [57] M. M. Qazilbash, K. S. Burch, D. Whisler, D. Shrekenhamer, B. G. Chae, H. T. Kim, and D. N. Basov, *Correlated metallic state of vanadium dioxide*, Phys. Rev. B **74**, 205118 (2006). 38, 43
- [58] Ross H. McKenzie and Perez Moses, *Incoherent Interlayer Transport and Angular-Dependent Magnetoresistance Oscillations in Layered Metals*, Phys. Rev. Lett. **81**, 4492 (1998). 39
- [59] D. Heidarian and N. Trivedi, *Inhomogeneous Metallic Phase in a Disordered Mott Insulator in Two Dimensions*, Phys. Rev. Lett. **93**, 126401 (2004). 40
- [60] D. Tanasković, V. Dobrosavljević, E. Abrahams, and G. Kotliar, *Disorder Screening in Strongly Correlated Systems*, Phys. Rev. Lett. **91**, 066603 (2003). 40, 69, 77
- [61] M. C. Aguiar, E. Miranda, V. Dobrosavljević, E. Abrahams, and G. Kotliar, *Effects of disorder on the non-zero temperature Mott transition*, Europhys. Lett. **67**, 226 (2004). 41, 62
- [62] Patrick A. Lee and T. V. Ramakrishnan, *Disordered electronic systems*, Rev. Mod. Phys. **57**, 287–337 (1985). 43
- [63] Gábor Zala, B. N. Narozhny, and I. L. Aleiner, *Interaction corrections at intermediate temperatures: Longitudinal conductivity and kinetic equation*, Phys. Rev. B **64**, 214204 (2001). 43, 62

- 
- [64] J. D. Thompson and Z. Fisk, *Kondo-lattice-mixed-valence resistance scaling in heavy-fermion  $CeCu_6$  under pressure*, Phys. Rev. B **31**, 389–391 (1985). 43, 54, 55
- [65] M. W. McElfresh, M. B. Maple, J. O. Willis, Z. Fisk, J. L. Smith, and J. D. Thompson, *Effect of high pressure on the electrical resistivity of the heavy-fermion compound  $UBe_{13}$* , Phys. Rev. B **42**, 6062–6067 (1990). 43, 54, 55
- [66] Y. Kurosaki, Y. Shimizu, K. Miyagawa, K. Kanoda, and G. Saito, *Mott Transition from a Spin Liquid to a Fermi Liquid in the Spin-Frustrated Organic Conductor  $\kappa$ -( $ET$ ) $_2$  $Cu_2(CN)_3$* , Phys. Rev. Lett. **95**, 177001 (2005). 43, 54
- [67] Elihu Abrahams, Sergey V. Kravchenko, and Myriam P. Sarachik, *Metallic behavior and related phenomena in two dimensions*, Rev. Mod. Phys. **73**, 251–266 (2001). 44, 61
- [68] S V Kravchenko and M P Sarachik, *Metal-insulator transition in two-dimensional electron systems*, Reports on Progress in Physics **67**(1), 1 (2004). 44, 48
- [69] B. Spivak, S. V. Kravchenko, S. A. Kivelson, and X. P. A. Gao, *Colloquium : Transport in strongly correlated two dimensional electron fluids*, Rev. Mod. Phys. **82**, 1743–1766 (2010). 44
- [70] A. A. Shashkin, S. V. Kravchenko, V. T. Dolgoplov, and T. M. Klapwijk, *Sharp increase of the effective mass near the critical density in a metallic two-dimensional electron system*, Phys. Rev. B **66**, 073303 (2002). 44, 48, 51
- [71] J. S. Thakur and D. Neilson, *Phase diagram of the metal-insulator transition in two-dimensional electronic systems*, Phys. Rev. B **59**, R5280–R5283 (1999). 44, 52, 61
- [72] B. Spivak, *Properties of the strongly correlated two-dimensional electron gas in Si MOSFET's*, Phys. Rev. B **64**, 085317 (2001). 44, 52, 61
- [73] S. Pankov and V. Dobrosavljević, *Self-doping instability of the Wigner-Mott insulator*, Phys. Rev. B **77**, 085104 (2008). 44, 52, 61

- 
- [74] A. Camjayi, V. Haule, K. and Dobrosavljević, and G. Kotliar, *Coulomb correlations and the Wigner-Mott transition*, Nat. Phys **4**, 932–935 (2008). 44, 52, 58, 61
- [75] A. Amaricci, A. Camjayi, K. Haule, G. Kotliar, D. Tanasković, and V. Dobrosavljević, *Extended Hubbard model: Charge ordering and Wigner-Mott transition*, Phys. Rev. B **82**, 155102 (2010). 44, 52, 58, 61
- [76] E. Abrahams, P. W. Anderson, D. C. Licciardello, and T. V. Ramakrishnan, *Scaling theory of localization: Absence of quantum diffusion in two dimensions*, Phys. Rev. Lett. **42**, 673–676 (1979). 45
- [77] B. L. Altshuler, A. G. Aronov, and P. A. Lee, *Interaction Effects in Disordered Fermi Systems in Two Dimensions*, Phys. Rev. Lett. **44**, 1288–1291 (1980). 45
- [78] B. Tanatar and D. M. Ceperley, *Ground state of the two-dimensional electron gas*, Phys. Rev. B **39**, 5005–5016 (1989). 45, 46
- [79] E. Abrahams, S. V. Kravchenko, and M. P. Sarachik, *Colloquium: Metallic behavior and related phenomena in two dimensions*, Rev. Mod. Phys. **73**, 251 (2001). 45
- [80] S. V. Kravchenko, G. V. Kravchenko, J. E. Furneaux, V. M. Pudalov, and M. D’Iorio, *Possible metal-insulator transition at  $B = 0$  in two dimensions*, Phys. Rev. B **50**, 8039 (1994). 45, 46
- [81] S. V. Kravchenko, W. E. Mason, G. E. Bowker, J. E. Furneaux, V. M. Pudalov, and M. D’Iorio, *Scaling of an anomalous metal-insulator transition in a two-dimensional system in silicon at  $B = 0$* , Phys. Rev. B **51**, 7038 (1995). 45, 46, 61
- [82] S. T. Chui and B. Tanatar, *Impurity Effect on the Two-Dimensional-Electron Fluid-Solid Transition in Zero Field*, Phys. Rev. Lett. **74**, 458 (1995). 46, 61
- [83] D. Popović, A. B. Fowler, and S. Washburn, *Metal-insulator transition in two dimensions: effects of disorder and magnetic field*, Phys. Rev. Lett. **79**, 1543 (1997). 46, 61

- 
- [84] V. M. Pudalov, G. Brunthaler, A. Prinz, and G. Bauer, *Metal-insulator transition in two dimensions*, *Physica E* **3**(1), 79–88 (1998). 47, 48, 53
- [85] Tsuneya Ando, Alan B. Fowler, and Frank Stern, *Electronic properties of two-dimensional systems*, *Rev. Mod. Phys.* **54**, 437–672 (1982). 48
- [86] Alexander Punnoose and Alexander M. Finkel’stein, *Dilute Electron Gas near the Metal-Insulator Transition: Role of Valleys in Silicon Inversion Layers*, *Phys. Rev. Lett.* **88**, 016802 (2001). 48, 49, 50, 51, 52
- [87] U. Meirav Y. Hanein and D. Shahar, *The metalliclike conductivity of a two-dimensional hole system*, *Phys. Rev. Lett.* **80**, 1288 (1998). 49, 50
- [88] M. P. Lilly, J. L. Reno, J. A. Simmons, I. B. Spielman, J. P. Eisenstein, L. N. Pfeiffer, K. W. West, E. H. Hwang, , and S. Das Sarma, *Resistivity of Dilute 2D Electrons in an Undoped GaAs Heterostructure*, *Phys. Rev. Lett.* **90**(5), 056806 (2003). 49, 50
- [89] X. P. A. Gao, G. S. Boebinger, A. P. Mills, Jr., A. P. Ramirez, L. N. Pfeiffer, and K.W. West, *Strongly Enhanced Hole-Phonon Coupling in the Metallic State of the Dilute Two-Dimensional Hole Gas*, *Phys. Rev. Lett.* **94**(8), 086402 (2005). 49
- [90] O. Prus, Y. Yaish, M. Reznikov, U. Sivan, and V. Pudalov, *Thermodynamic spin magnetization of strongly correlated two-dimensional electrons in a silicon inversion layer*, *Phys. Rev. B* **67**, 205407(6) (2003). 51, 61
- [91] A. R. Hamilton, M. Y. Simmons, M. Pepper, E. H. Linfield, and D. A. Ritchie, *Metallic Behavior in Dilute Two-Dimensional Hole Systems*, *Phys. Rev. Lett.* **87**, 126802 (2001). 52
- [92] Geneviève Fleury and Xavier Waintal, *Energy scale behind the metallic behaviors in low-density Si MOSFETs*, *Phys. Rev. B* **81**(16), 165117 (2010). 56, 61
- [93] G. Kotliar, E. Lange, and M. J. Rozenberg, *Landau Theory of the Finite Temperature Mott Transition*, *Phys. Rev. Lett.* **84**, 5180–5183 (2000). 56

- 
- [94] P. Limelette, A. Georges, D. Jérôme, P. Wzietek, P. Metcalf, and J. M. Honig, *Universality and Critical Behavior at the Mott Transition*, *Science* **302**, 89 (2003). 56
- [95] D. Tanasković, K. Haule, G. Kotliar, and V. Dobrosavljević, *Phase diagram, energy scales, and nonlocal correlations in the Anderson lattice model*, *Phys. Rev. B* **84**, 115105 (2011). 58
- [96] L. Cano-Cortés, J. Merino, and S. Fratini, *Quantum Critical Behavior of Electrons at the Edge of Charge Order*, *Phys. Rev. Lett.* **105**, 036405 (2010). 59
- [97] Goble Nicholas, J., Watson John, D., Manfra Michael, J., and A. Gao Xuan, P., *Impact of Interface Roughness on the Metallic Transport of Strongly Correlated 2D Holes in GaAs Quantum Wells*, pre-print (2013). 60
- [98] V. Dobrosavljević, Elihu Abrahams, E. Miranda, and Sudip Chakravarty, *Scaling Theory of Two-Dimensional Metal-Insulator Transitions*, *Phys. Rev. Lett.* **79**, 455–458 (1997). 61
- [99] E. Miranda and V. Dobrosavljević, *Dynamical mean-field theories of correlation and disorder*, pre-print (2011). 61
- [100] D. M. Ceperley and B. J. Alder, *Ground State of the Electron Gas by a Stochastic Method*, *Phys. Rev. Lett.* **45**, 566–569 (1980). 61
- [101] X. Waintal, *On the quantum melting of the two-dimensional Wigner crystal*, *Phys. Rev. B* **73**, 075417 (2006). 61
- [102] A. V. Andreev, Steven A. Kivelson, and B. Spivak, *Hydrodynamic Description of Transport in Strongly Correlated Electron Systems*, *Phys. Rev. Lett.* **106**, 256804 (2011). 62

# CURRICULUM VITAE

## Miloš Radonjić

*Scientific Computing Laboratory, Institute of Physics Belgrade*

*University of Belgrade*

*Pregrevica 118, 11080 Belgrade, Serbia*

*phone: (+381) 11 3713152*

*email: milos.radonjic@ipb.ac.rs*

### Personal Data

Date of birth: 19<sup>th</sup> October 1984.

### Education

2014 (expected) Ph.D., Faculty of Physics, University of Belgrade, Serbia

2008 M.Sc., Faculty of Physics, University of Belgrade, Serbia

### Employment and Research Experience

**2008 - present**     **Research Assistant**, Scientific Computing Laboratory,  
Institute of Physics Belgrade, Serbia

**2012**     Two months research visit to National High Magnetic Field Laboratory,  
Florida State University, USA

### Research Topics

- Influence of Disorder on Incoherent Transport Near the Mott Transition  
The optical and dc conductivity for half-filled disordered Hubbard model near the Mott metal-insulator transition are calculated within the coherent particle approximation (CPA) and DMFT using the OCA impurity solver. Numerical findings are in the agreement with the experiments on x-ray irradiated charge-transfer salts.

- Wigner-Mott Scaling of Transport Near the Two-dimensional Metal-insulator Transition

Entire family of resistivity curves of strongly correlated systems in the incoherent regime, displays a characteristic scaling behavior, while the characteristic resistivity and temperature scales assume a power-law dependence on the quasiparticle effective mass. Precisely such trends are found from an appropriate scaling analysis of experimental data obtained from diluted two-dimensional electron gases in zero magnetic fields. Our analysis provides strong evidence that inelastic electron-electron scattering - and not disorder effects - dominates finite-temperature transport in these systems, validating the Wigner-Mott picture of the two-dimensional metal-insulator transition.

- Electron transport in strongly-correlated disordered systems within Statistical (Real Space) Dynamical Mean Field Theory

In order to explore more closely the effects of disorder in strongly-correlated systems, we have applied Statistical DMFT to solve the disordered Hubbard model on the cubic lattice. The questions we want to address are the range of validity of CPA approximation, influence of the inter-site correlations and the behavior of the dc resistivity in the regime of very strong disorder. Stat DMFT presents a self-consistent calculation on a finite lattice. With our computational resources, we can treat lattices of up to 1000 sites. For the Anderson impurity solver we are using parallelized IPT code on the real axis that we have developed and CTQMC developed by Kristjan Haule. This procedure can be easily adopted for studying heterostructures of correlated materials.

- Density functional study of the lattice dynamics of various pnictide and chalcogenide systems

This work is done in close collaboration with the Raman spectroscopy group from the Institute of Physics in Belgrade. The numerical investigation includes band structure calculations within DFT and lattice dynamics calculations within density functional perturbation theory (DFPT) for several systems. For all calculations the QUANTUM ESPRESSO package was used.

- Non-equilibrium Green's Function

We discussed this formalism and its possible applications to strongly correlated

systems, following several internal seminars that I presented for the group members of Prof. Vladimir Dobrosavljević, during my stay in Tallahassee.

### Computer Skills

- Programming C, C++, Fortran, Python, Bash, Mathematica, MatLab
- Operating systems Linux, Microsoft Windows

### PhD Training Programs

- Autumn School on Correlated Electrons, Julich, Germany 2013 *Emergent Phenomena in Correlated Matter*
- Les Houches Doctoral training, Les Houches, France 2012, *Doctoral training: Statistical physics*
- Theory Winter School, NHMFL, FSU, Talahassee, USA 2012 *Computational Approaches for Electronic/Magnetic Materials*
- Autumn-School Hands-on LDA+DMFT, Julich, Germany, 2011, *Practical introduction to modeling strongly correlated matter*
- Advanced School in High Performance and GRID Computing, ICTP, Trieste, Italy, 2009
- European School on Magnetism 2009, Timisoara, Romania, 2009 *Models in magnetism, from basic aspects to practical uses*

### Conference Presentations

1. *Wigner-Mott scaling of transport near the two-dimensional metal-insulator transition*, APS Meeting, Boston, March 2012.
2. *Wigner-Mott scaling of transport near the two-dimensional metal-insulator transition*, NGSCES 2012, Portoroz, Slovenia

---

**Publications directly included in this thesis**

1. M. M. Radonjić, J. Vučičević, D. Tanasković, V. Dobrosavljević: *Transport in strongly disordered Mott systems - Statistical DMFT study*, in preparation.
2. M. M. Radonjić, D. Tanasković, V. Dobrosavljević, G. Kotliar and K. Haule: *Wigner-Mott Scaling of Transport Near the Two-dimensional Metal-insulator Transition*, Phys. Rev. B **85** (2012) 085133.
3. M. M. Radonjić, D. Tanasković, V. Dobrosavljević and K. Haule: *Influence of Disorder on Incoherent Transport Near the Mott Transition*, Phys. Rev. B **81** (2010) 075118

**Other publications**

1. Z. V. Popović, M. Šćepanović, N. Lazarević, M. M. Radonjić, D. Tanasković, and C. Petrovic: *Phonon and magnetic dimer excitations in new Fe-based  $S=2$  spin ladder compound  $BaFe_2Se_2O$* , Phys. Rev. B **89** (2014) 014301.
2. J. J. Lazarević, S. Uskoković-Marković, M. Jelikić-Stankov, M. Radonjić, D. Tanasković, N. Lazarević, and Z.V. Popović: *Intermolecular and low-frequency intramolecular Raman scattering study of racemic ibuprofen*, Spectroc. Acta Pt. A-Molec. Biomolec. Spectr., **126**, 301 (2014).
3. N. Lazarević, M. Radonjić, M. Šćepanović, H. Lei, D. Tanasković, C. Petrovic, and Z. V. Popović: *Lattice dynamics of  $KNi_2Se_2$  single crystal*, Phys. Rev. B **87** (2013) 144305.
4. N. Lazarević, M. M. Radonjić, D. Tanasković, R. Hu, C. Petrovic and Z. V. Popović: *Lattice Dynamics of  $FeSb_2$* , J. Phys. Cond. Matt. **24** (2012) 255402.
5. N. Lazarević, M. M. Radonjić, R. Hu, D. Tanasković, C. Petrovic and Z. V. Popović: *Phonon Properties of  $CoSb_2$  Single Crystals*, J. Phys. Cond. Matt. **24** (2012) 135402.

Прилог 1.

## Изјава о ауторству

Потписани-а Милош Радоњић

број индекса D18/2008

### Изјављујем

да је докторска дисертација под насловом

### **Influence of disorder on charge transport in strongly correlated materials near the metal-insulator transition**

- резултат сопственог истраживачког рада,
- да предложена дисертација у целини ни у деловима није била предложена за добијање било које дипломе према студијским програмима других високошколских установа,
- да су резултати коректно наведени и
- да нисам кршио/ла ауторска права и користио интелектуалну својину других лица.

Потпис докторанда

У Београду, \_\_24.03.2014.\_\_\_\_

Милош Радоњић

Прилог 2.

## Изјава о истоветности штампане и електронске верзије докторског рада

Име и презиме аутора \_\_\_\_\_ Милош Радоњић \_\_\_\_\_

Број индекса \_\_\_\_\_ D18/2008 \_\_\_\_\_

Студијски програм \_\_\_\_\_ Физика кондензованог стања материје \_\_\_\_\_

Наслов рада \_\_\_\_\_ Influence of disorder on charge transport in strongly correlated  
materials near the metal-insulator transition \_\_\_\_\_

Ментор \_\_\_\_\_ др Дарко Танасковић \_\_\_\_\_

Потписани/а \_\_\_\_\_ Милош Радоњић \_\_\_\_\_

Изјављујем да је штампана верзија мог докторског рада истоветна електронској верзији коју сам предао/ла за објављивање на порталу **Дигиталног репозиторијума Универзитета у Београду**.

Дозвољавам да се објаве моји лични подаци везани за добијање академског звања доктора наука, као што су име и презиме, година и место рођења и датум одбране рада.

Ови лични подаци могу се објавити на мрежним страницама дигиталне библиотеке, у електронском каталогу и у публикацијама Универзитета у Београду.

Потпис докторанда

У Београду, \_\_\_24.03.2014.\_\_\_\_

Милош Радоњић

Прилог 3.

## Изјава о коришћењу

Овлашћујем Универзитетску библиотеку „Светозар Марковић“ да у Дигитални репозиторијум Универзитета у Београду унесе моју докторску дисертацију под насловом:

### **Influence of disorder on charge transport in strongly correlated materials near the metal-insulator transition**

која је моје ауторско дело.

Дисертацију са свим прилозима предао/ла сам у електронском формату погодном за трајно архивирање.

Моју докторску дисертацију похрањену у Дигитални репозиторијум Универзитета у Београду могу да користе сви који поштују одредбе садржане у одабраном типу лиценце Креативне заједнице (Creative Commons) за коју сам се одлучио/ла.

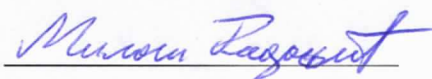
#### 1. Ауторство

- Ауторство - некомерцијално
- Ауторство –некомерцијално –без прераде
- Ауторство –некомерцијално –делити под истим условима
- Ауторство –без прераде
- Ауторство –делити под истим условима

(Молимо да заокружите само једну од шест понуђених лиценци, кратак опис лиценци дат је на полеђини листа).

У Београду, \_\_24.03.2014.\_\_\_\_

Потпис докторанда



1. Ауторство - Дозвољаваате умножавање, дистрибуцију и јавно саопштавање дела, и прераде, ако се наведе име аутора на начин одређен од стране аутора или даваоца лиценце, чак и у комерцијалне сврхе. Ово је најслободнија од свих лиценци.
2. Ауторство – некомерцијално. Дозвољаваате умножавање, дистрибуцију и јавно саопштавање дела, и прераде, ако се наведе име аутора на начин одређен од стране аутора или даваоца лиценце. Ова лиценца не дозвољава комерцијалну употребу дела.
3. Ауторство - некомерцијално – без прераде. Дозвољаваате умножавање, дистрибуцију и јавно саопштавање дела, без промена, преобликовања или употребе дела у свом делу, ако се наведе име аутора на начин одређен од стране аутора или даваоца лиценце. Ова лиценца не дозвољава комерцијалну употребу дела. У односу на све остале лиценце, овом лиценцом се ограничава највећи обим права коришћења дела.
4. Ауторство - некомерцијално – делити под истим условима. Дозвољаваате умножавање, дистрибуцију и јавно саопштавање дела, и прераде, ако се наведе име аутора на начин одређен од стране аутора или даваоца лиценце и ако се прерада дистрибуира под истом или сличном лиценцом. Ова лиценца не дозвољава комерцијалну употребу дела и прерада.
5. Ауторство – без прераде. Дозвољаваате умножавање, дистрибуцију и јавно саопштавање дела, без промена, преобликовања или употребе дела у свом делу, ако се наведе име аутора на начин одређен од стране аутора или даваоца лиценце. Ова лиценца дозвољава комерцијалну употребу дела.
6. Ауторство - делити под истим условима. Дозвољаваате умножавање, дистрибуцију и јавно саопштавање дела, и прераде, ако се наведе име аутора на начин одређен од стране аутора или даваоца лиценце и ако се прерада дистрибуира под истом или сличном лиценцом. Ова лиценца дозвољава комерцијалну употребу дела и прерада. Слична је софтверским лиценцама, односно лиценцама отвореног кода.